Application of Impact Resonance Method for Evaluation of the Dynamic Elastic Properties of Polypropylene Fiber Reinforced Concrete

by

Adham El-Newihy
BASc, American University in Cairo, 2013

A Thesis Submitted in Partial Fulfillment
of the Requirements for the Degree of

Master of Applied Science

in the Department of Mechanical Engineering

Supervisory Committee

Impact Resonance Method for Evaluation of the Dynamic Elastic Properties of Polypropylene Fiber Reinforced Concrete

by

Adham El-Newihy
BASc, American University in Cairo, 2013

Supervisory Committee

Dr. Rishi Gupta, Department of Civil Engineering
Supervisor

Dr. Rodney Herring, Department of Mechanical Engineering
Departmental Member

Abstract

For evaluation and quality control of concrete structures, the impact resonant frequency method is widely accepted for monitoring structure in-service properties and detecting structural damage. Common defects in concrete include consolidation problems during casting and development of micro-cracks during stages of hydration. Monitoring the dynamic characteristics of concrete plays an essential role in detecting real-time and early stages of deterioration. Ample research is focused on detecting large defects, however not much information is available on detection of minor defects of composites like fiber reinforced concrete. Change of elastic behavior when Polypropylene fibers are added as reinforcement is investigated. Destructive tests on structures in-service are not always feasible thus leaving non-destructive condition assessment as the only option. Amongst the various non-destructive tests available, vibrational tests provide a practical method to predict the dynamic moduli of structures (dynamic modulus of elasticity, dynamic modulus of rigidity and dynamic Poisson's ratio). The objective of this research is to assess the dynamic elastic properties of Polypropylene Fiber Reinforced Concrete (PFRC) in correlation with induced cracks and common consolidation defects using a lab developed non-destructive testing method that relies on impulse excitation and stress wave propagation to measure changes in the resonant frequency when polypropylene fibers are added to concrete.

In the experimental program, two fiber sizes, macro and micro, with various volume contents have been used for casting PFRC cylinders and prisms. Fundamental resonant frequencies were measured for all cylinders and prisms in the transverse and longitudinal directions. All measured frequencies are directly related to the low-strain dynamic modulus of elasticity. In addition, PFRC prisms were used to investigate the relationship between the dynamic modulus of elasticity and modulus of rigidity. Several batches of similar mixtures are used to investigate different parameters that affect the resonant frequency of concrete such as the water to cement ratio, curing condition and age. Results indicated a decrease in the resonant frequency and elastic properties with an increase of the fiber content or length. Micro fibers showed higher dynamic elastic moduli when compared to macro fibers of the same mixture under saturated curing conditions. Post-cracked PFRC cylinders and flexural fractured prisms retained some of the resonant frequency with macro fibers exhibiting better elastic recovery when cracked.

Table of contents

List of Figures

List of Tables

List of Acronyms

AASHTO	American Association of State Highway and Transportation Officials
ACI	American Concrete Institute
AEA	Air Entraining Admixture
CV	Coefficient of Variation
FRC	Fiber Reinforced Concrete
FRM	Forced Resonance Method
GU	General Use
IRM	Impact Resonance Method
RFT	Resonant Frequency Testing
PFRC	Polypropylene Fiber Reinforced Concrete
PP	Polypropylene
SCC	Self-Compacting Concrete
SCIJ	Standard Crack Inducing Jig
SCM	Secondary Cementitious Materials
WRA	Water Reducing Admixture
w/c	Water to Cement Ratio

List of Symbols and Units

b	Width (millimeters)
d	Diameter (millimeters)
E_d	Dynamic Modulus of Elasticity (gigapascals)
E_{dt}	Transverse Dynamic Modulus of Elasticity (gigapascals)
E_{dl}	Longitudinal Dynamic Modulus of Elasticity (gigapascals)
E_s	Static Modulus of Elasticity (gigapascals)
f	Fundamental transverse frequency (Hertz)
f'	Fundamental longitudinal frequency (Hertz)
f''	Fundamental torsional frequency (Hertz)
F_c	Compressive Strength (megapascals)
F_r	Modulus of Rupture or Flexure Strength (megapascals)
G	Dynamic Modulus of Rigidity (gigapascals)
GPa	GigaPascal
Hz	Hertz
K	Radius of Gyration (meters)
Kg	Kilogram
kN	KiloNewton
L	Span length (millimeters)
m	Mass (kilograms)
N	Number of samples
MPa	MegaPascal
P	Maximum Load at Failure (newtons)
R	Shape factor
t	thickness at direction of driven wave (millimeters)
T	Correction factor
µm	Micrometer
µs	Microstrain

Dedication

I am grateful for my parents, Mr. Fouad El-Newihy and Dr. Noura Omar, and my dear sister Nadoooda who have provided me with moral and emotional support throughout my thesis and beyond.

To my heart and soul, Kristina Frolova. You have always read me like an open book and always found the best in me.

I dedicate this thesis to my cats, Kitty and Sully.

Acknowledgements

First, I would like to thank my dear Supervisor, Dr. Rishi Gupta, for his guidance throughout my blessed journey. I am very thankful for his continuous motivation and great moments in learning now one of my favorite materials, Concrete.

Also, I would like to thank my Academic advisor, Dr. Rodney Herring, for teaching me innovations in materials and the pure joy behind microscopy.

I am immensely grateful to Dr. Svetlana Brzev and my Academic committee for their comments on an earlier version of this manuscript, yet any errors of my own should not tarnish the reputation of these esteemed persons mentioned above.

To extend, I would like to deeply thank Mechanical Engineering Department Secretary, Ms. Susan Wignall, for her high spirit and continuous support. I also wish to extend my thanks to UVIC's Advance Microscopy Facility manager, Dr. Elaine Humphrey for her thoughtful teachings in the wonders behind microscopy.

Special gratitude goes out to Civil Engineering Technical Support, Dr. Armando Tura and Mr. Matthew Walker for great chats and more exceptional meals. I would also like to thank Civil Engineering Department Secretary Christine Doszecki for making it easier during my questioning days.

I would like to express my gratitude to Mechanical Engineering Faculty Member, Dr. Caterina Valeo, for her kind support during the course of this research. I am also grateful to the following university staff: Mechanical Engineering Staff Mr. Patrick Chang and Mr. Barry Kent, Faculty of Graduate Studies Program Clerk Ms. Karen McKenzie, and University Welcome Center Director Ms. Juanita Shorkey for all their help and continuous support.

I would like to thank all my friends and colleagues of the Faculty of Engineering and the Civil Engineering Research Group. Special thanks go out to my colleagues Pejman Azarsa and Peiman Azarsa for their support in the obstacles of my journey. Moreover, I would like to thank my colleague Chen Yang for fun times in testing concrete.

1 Introduction

1.1 Overview

Concrete, the second most used material in the world, is a composite one with relatively low tensile strength. It exhibits a tendency to fail under a tensile load almost 15% of its attainable compressive strength. This failure can be prevented by using reinforcement having higher toughness and tensile strength properties (Krstulovic-Opara et al., 1994).

Different types of reinforcement are used for specific purposes to provide adequate strength and ductility to the concrete matrix. Concrete structures are usually reinforced by embedding steel rebar in a passive condition before the concrete sets. Reinforcing concrete with steel bars accommodates tensile stresses, minimizes crack propagation and, increases the bond strength with the concrete matrix. Usually, the bars are extruded with a rugged homogeneous surface to provide a stronger bond to the concrete matrix. Deformed steel bars and steel wire meshes are used to compensate the lack of tensile strength that concrete partakes.

As reinforcement bars are embedded in a thick cover of concrete with low permeability, it is likely that steel corrosion will not take place since a passive oxide layer of calcium hydroxide forms protecting the steel surface. While concrete provides an alkaline medium and large cover mass for the steel to avoid corrosion, weakening of the structure can occur due to corrosion happening along the rebar when moisture and chlorides diffuse through generated cracks. Aggressive environments such as marine sites and high chloride areas impact the passive layer and gradually corrode the steel.

When reinforcements corrode, products like iron oxides and iron hydroxides accumulate on the steel surface causing expansive stress due to the space restriction between concrete and steel. Accordingly, corrosion of embedded steel reinforcement is invariably one of the main factors contributing to the deterioration of concrete structures. Hence, parallel alternatives to conventional steel to resolve the inherent crack generation within structures, several researchers investigated integrating fibers to the concrete matrix in order to extend the composite durability, control shrinkage cracking and increase surface toughness (Naaman et al., 1989; Brown et al., 2001; Banthia and Gupta, 2006; Deng and Li, 2007).

According to American Concrete Institute (ACI) Committee 544.3R-08, FRC is “concrete made primarily of hydraulic cements, aggregates and discrete reinforcing fibers” (ACI Committee 544 and American Concrete Institute, 2008). Fibers are commonly distributed randomly within the concrete matrix to contribute to composite toughness and conceal micro-crack propagations. Nowadays, more development in Fiber Reinforced Concrete (FRC) is used for improving the endurance of concrete towards mechanical and environmental influences (Zheng and Feldman, 1995; Kurtz and Balaguru, 2000; Deng and Li, 2007).

As multiscale reinforcement, fibers come in various types and sizes. Originally, the use of glass fibers as reinforcement in cement based materials started in the mid-60’s (Biryukovich et al., 1965). Glass Fiber Reinforced Concrete (GFRC) is composed of short length discrete glass fibers dispersed in fresh plain concrete. Although, glass fibers improve the concrete composite by increasing the tensile and impact strength, a limitation of using these fibers in concrete is fiber embrittlement due to the high alkalinity of cement binder (Ferreira & Branco, 2007). Contemporary materials that are commonly used as fibers in concrete include of steel, glass, natural (wood, fruit, or grass) or synthetic (polypropylene, nylon and polyester) that have a variety of different shapes and sizes per the required purpose. Unlike steel bar

reinforcement, fibers are relatively distributed homogenously throughout the concrete making an effective load distribution. The structural purpose and mechanical properties of fibers, along with their environmental impact, play an important role for selecting the optimum fiber type and quantity. For instance, metallic fibers such as steel enhance concrete ductility, flexure strength, and fracture toughness; however, they are subjected to the same type of corrosion deterioration as steel reinforcement. Consequently, the durability of Steel Fiber Reinforced Concrete (SFRC) is reduced in high sulphate and chloride exposed environments (Mu, et al., 2002). Steel and glass fibers depend on adhesive chemical interaction. However, polymer organic fibers such as polypropylene and nylon rely on an interlocking mechanical mechanism and exhibit hydrophobicity, when added to cementitious medium. (Naaman et al., 1989). The most common type of synthetic fiber reinforcement used in concrete is polypropylene for its high impact resistance, environmental stability, and low production cost. Polypropylene Fiber Reinforced Concrete (PFRC) exhibit a better tensile strength and toughness than regular concrete. However, the increase in strength is not significant since the fibers have a low modulus of elasticity. A disadvantage to polypropylene fibers arises from its hydrophobic nature that can affect the fiber bond with the cement matrix. Although the fibers are not likely to bond chemically with the matrix, chemical admixtures can be used to facilitate bonding.

Typical properties that define concrete's structural integrity are its compressive strength and modulus of elasticity. The elastic modulus of concrete is of great interest as a design factor for structures and a reliable condition indicator of in-service structures. It can be determined through the static and dynamic behavior of structural elements. The static modulus of elasticity of concrete can be measured through quasi-static or uniaxial compressive loading measured according to ASTM C469 (ASTM C469, 2014). The *static modulus of elasticity* (E_s) is obtained from direct loading of specimens to a load lower than the elastic limit of a concrete specimen. On the other hand, the elastic properties of concrete can also be found using vibration resonance according to ASTM C215 (ASTM C215, 2014). The resulting modulus is referred to as the *Dynamic modulus of elasticity* (E_d). Measurement of the dynamic modulus of elasticity will be covered in Section 2.4.

The advantage of using E_d, in monitoring the mechanical properties of concrete over E_s, is that the dynamic modulus is sensitive to changes within the composite such as cracks, mineral admixtures and porosity that provide crucial in-service properties. It is considered more appropriate to assess the dynamic modulus of elasticity in case of dynamically loaded structures since it captures the full cycle of loading and relies fully on non-destructive approaches (Mindess et al., 2003). The non-linear nature of concrete arises from discontinuities within the material such as micro-pores and cracks. Concrete embedded reinforcements and sensors, of different sizes, increase the potential of discontinuities within a concrete structure. These affect the dynamic response of concrete in relation to its microstructure.

Generally, the (E_d) is obtained using sonic vibration techniques that are mainly non-destructive in nature. Some Non-destructive Testing (NDT) methods rely on determining concrete properties using surface hardness or wave propagation properties. Using these methods, the concrete microstructural properties are indirectly determined by means of the measured parameters and empirical relations. Surface hardness methods predict the compressive strength of concrete using compression wave surface rebound properties when concrete is subjected to an impulse load. Similarly, stress wave propagation methods rely on sound, vibrational impulses or low load impacts that provide an evaluation of concrete compressive strength and modulus of elasticity. Both strength and elastic properties are affected by a range of factors including concrete curing conditions, temperature, mixture proportions, water to cement ratio (w/c), aggregate properties, reinforcements, and the presence of cracks. However, E_d is predominantly affected by the coarse aggregate size, type and mineral admixtures used (Noguchi et al., 2009).

Currently, NDTs for measuring the dynamic elastic modulus of concrete depend on methods that entail stress wave propagation properties such as wave velocity and resonant frequency. Regular assessment using non-destructive monitoring of reinforced concrete structures saves restoration time and cost during a maintenance cycle. Vibration parameters are assessed by studying the frequency response of concrete to stress wave propagation. Stress waves can be induced using sound or impact vibration. A review and summary of the NDT techniques used in this study is included in Section 2.3.

Structural damage evaluation using non-destructive resonant frequency testing has reached considerable attention in recent years. The natural frequency is considered a reliable property that indicates the strength and durability of a structure. In addition, it is directly affected by significant deterioration and cracks within the structure. Any change directly related to the mass, stiffness or damping properties of the structure will lead to changes in the dynamic elastic properties such as the resonant frequencies, mode shapes and damping loss factors (He, 1999). Studies show a significant benefit of monitoring the dynamic behavior of a structure using RFT as resonant frequency changes are less susceptible to random error sources such as electronic noise in surrounding circuits and irregular change signal change due to random vibration.(He, 1999).

Vibration is characterized by the mode of testing which predominantly concentrates on the support condition and excitation of concrete specimens. By supporting a concrete specimen in a flexural, longitudinal, and torsional mode, the calculated dynamic moduli of elasticity, modulus of rigidity and Poisson's ratio provide significant information in estimating current strength properties and evaluating the structure's condition in-service. Resonant frequency testing of concrete is further discussed in Section 2.4.Since resonance is generated from the elastic and inertial properties of a material, monitoring the mechanical properties of concrete using vibration test data is achievable. Modification in the resonant frequency, modal shape and damping of an induced vibration can specify possible damage in the composite. This modification is attributed to the location, nature, and severity of the damage. As structural damage modifies the modes of vibration, stress wave propagation methods can be used to monitor the health of concrete structures.

A great number of studies have been conducted on using the RFT method for measuring the dynamic modulus of elasticity of concrete, but few experiments have been conducted on using this technique to measure the dynamic moduli of PFRC considering evaluation of induced cracks and defects. This study gives a broader application of PFRC in construction industry that can help in evaluating structure performance and integrity using RFT. There is a dire demand to develop a cost-effective, reliable, and repeatable technique to measure dynamic elastic property of concrete to provide engineers and researchers a valuable tool to evaluate health of any composite structure in-service and detect signs of deterioration. By knowing the original dynamic elastic properties of a structure, using RFT as a NDT method will allow structural designers to identify the extent of damage and act to avoid the probability of structural failure.

1.2 Proposed Work

Currently, several valuable reports have been established as guidelines for non-destructive testing and resonant frequency measurements to assess the overall dynamic characteristics of concrete (Malhotra and Carino, 2004; Shkolnik, 2005; Lamond and Pielert, 2006; Bungey et al., 2006; Noguchi et al., 2009; Neville and Brooks, 2010). Some laboratory experiments have been conducted to investigate the effect of polypropylene fibers on the resonant frequency of concrete (Manolis et al., 1997; Leung and Balendran,

2002; Leung et al., 2003), however the author recommends to pursue the correlation between PFRC and its reference concrete through the dynamic modulus of elasticity since it accounts for specimen weight, dimensions and geometrical correction factors.

While field examination provides supportive information on the mechanical behavior of concrete structures, it delivers minimal opportunity to assess the constraints surrounding vibrational impulses. Therefore, the main purpose of this study is to investigate the dynamic elastic properties of PFRC in concurrent evaluation of common defects, such as honeycombing or induced cracks, using a non-destructive method, that can be applied in monitoring the integrity of concrete structures. Ultimately, results from this study will contribute in assessing the performance of existing and new PFRC structures to provide guidelines for structural designers and field examiners. This proposed work provides details on fundamental changes in resonant frequency signatures of PFRC when compared to the control concrete matrix while relating the resonant frequency change of PFRC due to induced matrix cracks after concrete hardening using a lab developed NDT. To the author's knowledge, no previous studies in this area were reported.

Studies investigating the dynamic elastic properties of PFRC only considered the resonant frequency without considering mass and size of the tested samples. Hence, to bridge the gap, selected factors such as fiber volume fraction, fiber size, concrete age, and curing conditions of FRC are correlated using the dynamic elastic moduli calculated from the resonant frequency; considering geometrical and density variations of each tested concrete specimen. In addition, this study includes the affect of induced cracks on the dynamic modulus of elasticity of PFRC. Recommendations are given throughout this study by evaluating the repeatability of impact resonant frequency testing. Consequently, the overall objective of this thesis is to bring to light the effects of polypropylene fibers on the dynamic properties of concrete. For fulfilling the study objectives, an experimental program was developed and completed in the Civil Engineering Material Facility at the University of Victoria which will be explained in Section 3.

1.3 Objectives

The fundamental goal of this thesis is to investigate the dynamic elastic properties of polypropylene fiber reinforced concrete using a non-destructive testing method that is reliable, repeatable, and economical. The primary purpose of fiber addition is to improve the mechanical properties of concrete prior and after deterioration occurs.

Objective I *Review the repeatability of the impact resonant frequency method of PFRC*

Objective II *Investigate the effect of increasing fiber volume fraction on PFRC elastic properties*

Objective III *Investigate the effect of curing age on PFRC elastic properties*

Objective IV *Assess the performance of fibers in deterioration and crack bridging*

Scope of Work

Chapter 1 *Introduction*

A brief overview providing the significance of fibers in concrete and the application of resonant frequency testing. Study objectives and proposed work is included in this chapter.

Chapter 2 *Literature Review*

This chapter serves as the backbone of this study for understanding the underlying concepts, advantages and limitations served in throughout this research. The chapter is divided into the following sections: The first section of the chapter describes the benefits of using fibers in concrete and the application of polypropylene fiber in concrete. The second section highlights the significance of non-destructive testing of concrete. The third section provides an overview of resonant frequency testing and its application in concrete including predominant factors that affect the test outcome. The fourth section is literature review of the application of impact resonant frequency testing on polypropylene fiber reinforced concrete.

Chapter 3 Experimental Program

The chapter provides a detailed description of the materials used for developing the PFRC mixtures of this study. Identifying material properties and maintaining a constant source is crucial for having adequate results and not influence the test outcome. Mixture proportioning and sample preparation of PFRC cylinders and prisms of this study were accomplished using three batches. The chart below shows an overview of the selected batches and their purpose. Only the RFT testing samples are included. Supplementary tests such as the compressive strength, flexural strength, induced crack testing is described in this chapter.

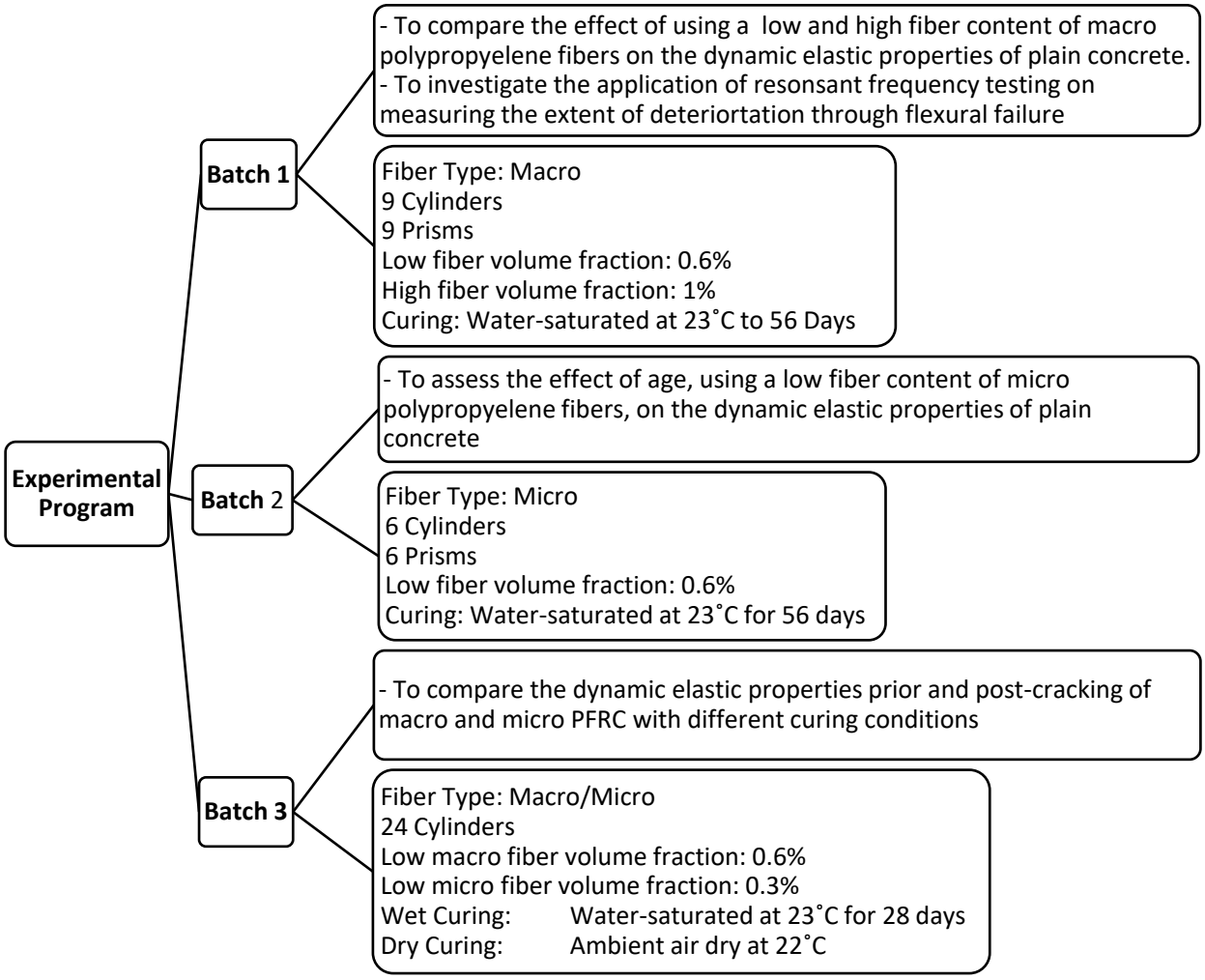

Figure 1-1: Experimental Program Overview

Finally, a repeatability study confirms the optimal connectivity, adhesive attachment, and applied force on the resulting frequency response.

Chapter 4 Results and Discussion

This chapter is divided into three sections. Section 1 covers the standard concrete properties including the PFRC workability, air content, density, and temperature in fresh state. Hardened concrete properties such as the compressive strength, flexural strength and static modulus of elasticity is included. Section 2 covers the repeatability results on selected PFRC samples and validation with a homogenous isotropic material – Aluminum. Section 3 includes the resonant frequency results and dynamic elastic properties of all aforementioned batches.

Chapter 5 Conclusions and Recommendations for Future work

A summary of the results and study highlights are included in this chapter. Recommendation for future work is also provided.

2 Background and Literature Review

2.1 Introduction

Concrete, as a viscoelastic amorphous material at early age of hydration, is relatively brittle under the tensile loading when hardened. Once subjected to the tensile stresses, plain concrete will crack, and eventually fail. Hence, to modify concrete properties in both plastic and hardened stages, it is typically reinforced with steel rebar and various types of fibers. However, dispersed fibers in concrete offer a variety of advantages than steel reinforced concrete as summarized below (Mehta & Monteiro, 2006):

- uniformly distributed fibers in three-dimensions within the concrete matrix, using superplasticizers, perform effective load distribution;
- fiber, typically organic fibers, are less sensitive to corrosion and environmental changes than conventional reinforcing steel bars;
- fibers are more economical and reduce labor cost of steel bar placement.

The concept of using fibers in construction materials has been applied since archaic times when horsehair was mixed into mortars and straw in mud bricks. In 1898, asbestos fibers were introduced to reinforce cement based panels known as the Hatschek process. Later on, (Biryukovich et al., 1965) applied glass fibers for reinforcing cement paste and mortar. Since Fiber Reinforced Concrete (FRC) has become an important construction material, then to result in a more durable one, the type of fiber plays an essential role for defining the structural purpose of FRC. In FRCs, fibers can be selected from a variety of synthetic organic materials such as polypropylene or carbon, synthetic inorganic materials such as glass or steel, natural organic materials such as cellulose or sisal to inorganic asbestos. Based on the concrete application, optimal type of fiber can be determined and directed to its properties such as diameter, specific gravity, Young's modulus, tensile strength, and other mechanical properties.

Polymer fibers generally improve the impact strength and toughness of concrete since they have a low modulus of elasticity. Similarly, natural fibers, like fruit or coir fibers, exhibit properties as polypropylene fibers (Idicula, et al., 2006). Besides, organic fibers minimize the potentials of early age cracking and are less sensitive to corrosion unlike steel fibers. Yet, synthetic fibers like polypropylene can be manufactured in various shapes depending on the required structural service. Therefore, through this work, from the category of synthetic polymeric fibers, Polypropylene has been utilized due to its high toughness and tensile strength.

A considerable amount of research has been conducted to assess the Polypropylene Fiber Reinforced Concrete (PFRC) properties at volume percentage varying from 0.1% - 5.0%. However, PFRC properties are greatly controlled by fiber's size, concentration, and properties while its effectiveness depends on the bond between the fiber and matrix. Though polypropylene fiber is generally known for its low elastic modulus and poor physicochemical bonding with cement paste, the load carrying capacity of a structure under flexural loading may be significantly increased (Brown et al., 2001). The following sections describe general material properties of polypropylene and concrete fiber prerequisites such as size, volume content, and standard guide recommendations.

2.2 Polypropylene Fiber Reinforced Concrete (PFRC)

2.2.1 Polypropylene Fiber

As a thermoplastic material, polypropylene is particularly stiff and changes its failure mechanism to brittle at low temperatures. Polypropylene is a type of Polyolefin (Polyalkane) that exhibits a high melting point and can withstand service temperatures above 105˚C (Maier and Calafut, 1998). As a thermoplastic, polypropylene can be widely modified by softening and extrusion through to the required cross section shape and size. This also contributes to its interlocking with the cement medium in concrete and steadily increasing market share growth rate. Moreover, Polypropylene has the highest shear bond strength between the cement matrix when compared to other synthetic fibers such as Polyacrylic, Polyester, Polyamide (Nylon) and Polyaramid (Kevlar).

Polypropylene fibers are formed through melt spinning processing where molten polypropylene chips are forced through a spinneret. The molten polymer develops as a continuous strand of fiber that is cooled through water quenching or by air cooling and spooled for cutting and storage. The cross-section of the fiber and fiber orientation is aligned by drawing and heating the fibers to a temperature close to the polypropylene melting point, approximately 165 ˚C, before being stretched. Fibers are typically produced in monofilament or multifilament arrangements. Monofilament fibers are produced though a single extruded filament from melt spinning and cooled by water quenching. Through cylindrical monofilaments, fibrillated polypropylene fibers can be produced by expansion of a polymer film which is separated into strips and slit to expand into an open network of fibers. They are categorized by their translucent appearance, negligible absorption capacity and high tensile strength. Multifilament fibers are composed of a single continuous bundle of monofilaments and are categorized by their flexibility and hydrophobic nature.

Polypropylene fiber surpasses other fiber materials due to its low density, manufacturing, and recyclability cost. Polypropylene fibers provide concrete with improved durability and high resistance to plastic shrinkage since they are more uniformly dispersed in the concrete matrix than traditional reinforcement methods. Moreover, macro fibers promote concrete's fracture toughness by demonstrating greater post-cracking resistance than plain concrete and when compared to micro fibers (Beaudoin, 1990). Unlike steel fibers, polypropylene fibers are environmental stable due to their non-corrosive nature and are easier to place and finish in concrete.

Polypropylene shows a moderate to no increase in strength; however, it provides an extensive increase in ductility, decrease in plastic shrinkage and resistance to impact (Banthia et al., 1987; Mindess and Vondran, 1988; Barragan et al., 2012). According to ASTM C1116, Polypropylene (Type III Synesthetic Fiber Reinforced Concrete) is known to be durable and chemically stable within concrete (ASTM C1116, 2015). The fibers come in macro and micro sizes per fiber denier and length that is discussed in depth through (ASTM D7508, 2015). Polypropylene fibers are the most used synthetic fibers in reinforcing concrete for their flexibility in sizes and shapes.

For the mechanical properties of PFRC, polypropylene fibers do not contribute much to the improvement of the composite tensile strength however it significantly improves the flexure strength, toughness and ductility. The primary use of fibers in concrete is to improve concrete's tensile response post cracking and to control crack propagation (Shah and Rangan, 1971). Like most fibers when mixed with concrete, polypropylene fiber length, shape, aspect ratio and more importantly volume content affect both the microstructure of PFRC and its mechanical response to applied stress (Shah and Rangan, 1971).

2.2.2 PFRC Properties

2.2.2.1 Fiber Volume fraction

Any addition of fibers into a plain concrete mixture affects its properties in both fresh mixture and hardened composite. The binder to fiber volume fraction and fiber aspect ratio affect the workability of fresh mixture FRC. Studies show that increase in fiber content decreases the workability of the composite due to high specific surface area of fibers (Zhang and Li, 2013). Hence, the smaller the fibers, the lower the workability. A fiber content above 1% requires a change in the concrete binder content to maintain adequate workability. This affects fiber dispersion which can lead to unfavourable effects in the performance of FRC and therefore preventing the competence of the fibers in the matrix (Mehta and Monteiro, 2006).

A volume content between 0.1-0.5% of fibers is added to concrete mainly to reduce early age shrinkage cracking when concrete hardens (Banthia and Gupta, 2006). These fractions of fiber are added to large surface exposed concrete structures that commonly have a high tendency to shrinkage cracking. As the percentage of fibers added increases, the relative toughness and composite strength correspondingly increase when compared to plain concrete (Mehta and Monteiro, 2006). Like toughness, polypropylene fiber reinforcement showed that the fibers decrease the overall composite crack sensitivity even in poor curing conditions (Yew et al., 2015).

Usually, low volume fraction of polypropylene fibers (<0.3%) are used for overlays, pavements, slabs, flooring, crash barricades and reservoirs (Zheng and Feldman, 1995). These fibers are advantageous in being environmentally stable as they are chemically inert, hydrophobic, passive when encountered by water or high chloride environments, and are non-reactive with the concrete alkaline medium (Deng and Li, 2007).

2.2.2.2 Fiber Size

Fibers prevent bundling and coagulation from occurring during fresh concrete mixing. Fibers added to concrete are categorized in two types: Macro or Micro fibers. Macro fibers (length at least 20 mm) promote crack bridging and offer structural support to hardened concrete matrix. On the other hand, micro fibers (length up to 15 mm) help improve concrete's response to early crack development arising from drying and plastic shrinkage. Microfibers have a larger aspect ratio and exhibit low dispersion due to intermolecular Van der Waal interactions. Although these attractive forces are considered weak when compared to ionic, metallic, or covalent bonds, micro fibers show lower dispersion and agglomerate during concrete mixing when compared to macro fibers. Thus, superplasticisers are used to promote a consistent concrete mixture. Moreover, fiber separation and mixing techniques are recommended by ACI 544 to ensure homogeneous distribution of fibers throughout the mixing process (ACI Committee 544 and American Concrete Institute, 2008). Short fibers have a high aspect ratio promoting crack bridging capabilities in concrete, which is a great advantage for strengthening at a small crack resolution.

2.2.3 Application of Polypropylene Fiber in Concrete

This section reports various researches that assess the performance of FRC integrated polypropylene fiber in the composite. The effect of polypropylene fibers on shrinkage and cracking of concretes, evaluated by (Aly et al., 2008), showed that increasing dosages of polypropylene fibers with different volume fractions ranging from 0.05%-0.5% resulted in small but consistent increases of the overall total shrinkage strain of concrete. Even though, the increase in shrinkage are considerable in specimens without any curing (exposed only 1-day), the differences are not notable in 7-days moist curing samples. Incorporating 15% and 30% fly ash into PFRC specimen also reduced drying shrinkage of the mix, regardless separately or together (Karahan and Atiş, 2011).

Freeze-thaw resistance of polypropylene fiber concrete, as a factor defining the durability of PFRC was studied by (Karahan and Atiş, 2011; Zhang and Li, 2013). Both studies indicated that freeze-thaw

resistance of PFRC containing silica fume and fly-ash slightly increased in comparison to plain concrete. Investigation on fire resistance of polypropylene and steel fibers in High Strength Concrete (HSC), conducted by (Kodur et al., 2003), showed an improvement in the ductility of HSC samples and also reduction in spalling; while promoting the composite fire resistance.

Pullout behaviour of 50 × 1.25 × 0.2 mm polypropylene fibers from cementitious matrix was studied by (Singh et al., 2004). In their work, it was concluded that fiber abrasion effect becomes dominant by increasing in its embedded length which eventually causes an increase in pullout load in the fractional sliding zone of the pullout. Once mechanical indentation of the fiber surface is applied, the authors stated that the bond strength between polypropylene fibers and cement matrix increased by a factor of three with optimum level of dent modification.

Polypropylene fiber reinforced silica fume concrete was also studied by (Toutanji et al., 1998) to measure its chloride permeability and impact resistance. Using different length and volume fraction of the fibrillated polypropylene fibers, it was deduced that incorporating polypropylene fiber in the matrix led to an increase in the permeability of concrete samples containing no silica fume. Also, the permeability of plain and silica fume reduced in this study when fiber length decreased from 19 to 12.5 mm, with an equivalent volume fraction. Adding polypropylene fibers into silica fume concrete improved the impact resistance.

Using aggregate fibers like polypropylene, of moderate to low strength and elastic modulus, can be valuable in conserving the integrity of concrete. A lower modulus of aggregates allows for compressibility when encountered with volumetric change due to swelling or thermal stresses. Therefore, aggregate compressibility reduces stress concentrations within the concrete unlike rigid aggregates that promote crack development (Neville and Brooks, 2010).

In recent years, several researchers conducted experimental studies to examine the effect of various fibers on dynamic mechanical properties of concrete elements. However, to the author's knowledge, only limited studies have been completed on investigating the dynamic modulus of elasticity of polypropylene fibers in the concrete elements. Finding the true material properties, especially using polypropylene fibers, is a challenging task as there are limitations arising from prerequisite conditions and dimensions for testing. However, using NDT methods on concrete increase the confidence levels of results. Therefore, this study is mainly focused on testing the dynamic elastic properties of PFRC by means of a reliable and repeatable NDT method discussed in Section 2.3.

2.3 Significance of Non-destructive Testing (NDT)

Nowadays, civil engineering applications call for the ability to predict and monitor existing structural properties and their durability using non-invasive testing techniques. Direct determination of concrete properties requires loading representative or core samples to failure. This may delay concrete evaluation of existing structures. Hence, using a variety of standardized Non-Destructive Testing (NDT) methods can be applied to any existing concrete structure being reliable, comprehensive, and cost effective. NDT implies that testing is carried out without damaging or altering the structure being tested. Effective NDTs should integrate flexible testing, according to the location and size of structures.

The advantages of NDTs of direct core testing are summarized as follows: 1) Reduction in labor consumption 2) Reduction in time for test preparation 3) Examining concrete structures where direct testing is not applicable 4) Minimizing structural impact for testing 5) Cost effective method for testing existing structures. However, finding true material properties using NDTs is challenging as there are limitations arising from the prerequisite conditions and dimensions for testing. Hence, NDT methods are frequently used concurrently with sample direct testing to obtain higher confidence intervals.

Application of NDTs in concrete is focused on quality control of pre-cast structures, eliminating uncertainties of apparent noncomplying material specification, as summarized in Table 2-1. For monitoring the strength development of structures from initial casting conditions, NDTs provide the opportunity to locate cracks or embedded reinforcement. Since concrete's response to quasi-static and dynamic loading is nonlinear, multiple factors determine its stress-strain response predominantly focusing on the microstructure of concrete and materials embedded within it. Testing concrete mechanical properties using NDTs is divided into two types - The first type involves NDTs that are used for estimating strength properties, represented by surface hardness and results of penetration tests. The second type applies stress wave propagation methods that utilize sonic vibrations and pulse velocities to determine mechanical properties of concrete.

Table 2-1: Typical NDT ASTM Standards used for Construction and Cementitious Materials

ASTM Standards	Standard Test Method for
C215	Fundamental Transverse, Longitudinal, and Torsional Resonant Frequencies of Concrete Specimens
C597	Pulse Velocity through Concrete
C803	Penetration Resistance of Hardened Concrete
C805	Rebound Number of Hardened Concrete
C900	Pullout Strength of Hardened Concrete
C1074	Estimating Concrete Strength by the Maturity Method
C1383	Measuring the P-Wave and the Thickness of Concrete Plates using the Impact Echo Method
C1740	Evaluating the Condition of Concrete Plates using the Impulse-Response Method

NDT explores material and mechanical properties without affecting the serviceability of the part or system (Workman & Moore, 2012). The motive behind concrete NDT is driven by an economic advantage and safe construction optimization, as well as overall aid in structure maintenance. Factors, such as acquisition resolution, signal to noise ratio and information about the tested structure, are required for having an optimal, reliable, sensitive, and assessable NDT method (McCann & Forde, 2001). For carrying out a successful NDT, it is essential to understand the physical nature and dimensional discontinuities within a property. Additionally, understanding the fundamental process and limitations are critical for choosing an economic, environmental, and reliable NDT method (Shull, 2002). The following section outlines the Resonant Frequency Testing (RFT), as the chosen NDT method, applied in determining the dynamic elastic properties of concrete using a linear stress wave propagation.

2.4 Resonant Frequency Testing

The resonant frequency of vibration is an important parameter in defining the dynamic elastic response of concrete. The free vibration of a structure at a particular frequency of oscillation is the natural frequency of the system. The natural or resonant frequency of material vibration is an intrinsic property for any material with elastic properties and mass. Concrete's natural frequency is proportionally related to its

modulus of elasticity. Measuring the resonant frequency of concrete NDT methods can be used for classification of strength and durability. These methods use empirical equations to predict the dynamic elastic properties of concrete. The dynamic elastic properties of concrete can be determined numerically using the static elastic modulus, compressive strength, and density.

2.4.1 Modulus of Elasticity of Concrete

For designing fiber reinforced concrete structures, the Young's modulus of elasticity (E) provides vital information for assessing structural design and durability. The elastic modulus of concrete is a fundamental factor for evaluating structural deformation. It is important for defining the stress to strain relationship in design of structural members subjected to compressive, flexure and tensile loads (ACI Committee 318 and American Concrete Institute, 2014). The modulus of elasticity is expressed as the ratio of axial stress to strain for a material subject to uniaxial loading (Neville & Brooks, 1987).

Since concrete is a composite made primarily of aggregates and cement, both elements contribute to most of the elastic modulus of concrete. Aggregates usually provide a large percentage of the modulus of elasticity of concrete. Thus, concrete's stress/strain curve is positioned between the aggregate and cement stress/strain curve. Since concrete modulus of elasticity is lower, when compared to that of its aggregate modulus, the actual stress at the interface of each aggregate within the concrete is larger compared to that of the applied nominal compressive stress (Neville and Brooks, 2010). There are no standard guidelines for testing the aggregate modulus of elasticity; however, the aggregate size, type, shape and aggregate-cement bond dominates concrete's elastic modulus. The difference between the aggregate and hydrated cement paste modulus of elasticity adversely affects microcrack development and propagation between the cement-aggregate interface hence, the incompatibility is advantageous to the global concrete properties (Neville and Brooks, 2010).

Globally, development of microcracks and other consolidation issues in concrete decrease the modulus of elasticity. In addition, the rate and amount of loading provides the type of moduli being verified. Consequently, three types of modulus of elasticity can be deduced from the compressive strength vs strain of concrete: (1) the secant modulus (2) the initial modulus, (3) the tangential modulus and shown in Figure 2-1.

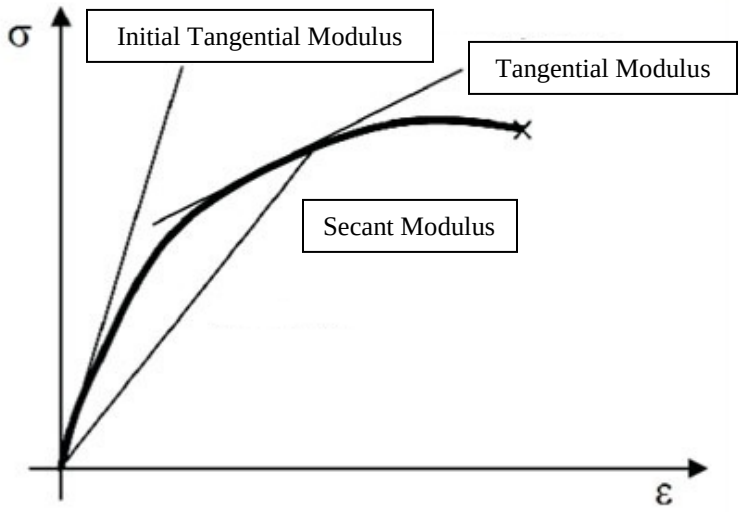

Figure 2-1: Stress-Strain diagram of concrete with modulus of elasticity types

The *secant modulus of elasticity* is obtained from the gradient between any two points in the stress-strain diagram. Usually, this modulus is experimentally provided by quasi-static loading of concrete samples to stresses ranging 15-50% of the ultimate strength for failure. Similar to secant modulus, the *chord modulus* (Static) line is drawn starting from 50 με to 40% of the ultimate compressive strength, unlike the secant modulus which starts from the origin (Neville and Brooks, 2010). However, in a compression testing machine, a small stress or strain is applied to position the concrete specimen in a steady state. The static modulus of elasticity (E_s) is inherently applied to the linear portion of the loading cycle of concrete. The common stress-strain response of concrete can be described as linear when lower than 40% in stress and 1000 μ_ε in strain (Lamond and Pielert, 2006).

The *initial tangential modulus of elasticity* (Dynamic) is defined by the tangent line inclination from the origin of the stress-strain diagram. This modulus can be used to define concrete deflection exposed to low stress levels. Hence, the modulus can be defined as the sonic modulus or dynamic modulus of elasticity. The tangent modulus of elasticity can be provided at any given stress. This line can be used to relate different loading and unloading stages for in-service structures. If small changes of loading are considered, a *tangential modulus of elasticity* can be used at any point on the stress/strain curve (Neville and Brooks, 2010).

Usually, for testing modulus of elasticity concrete, the secant modulus and initial tangential modulus are used to define the deformation nature of concrete to express the 1) Static Modulus of Elasticity (E_s) and 2) Dynamic Modulus of Elasticity (E_d) respectively. These moduli are differentiated by the strain-rate of the applied load (Bischoff and Perry, 1991). This difference is related to the rate at which load is applied and is primarily dependent on the strength and w/c ratio of the concrete (Sharma and Gupta, 1960). The inconsistency between the moduli in concrete is recognized by 1) nonlinearities in the moduli between unconfined compression testing with axial loading (static) and unconstrained impact excitation by determining the compression wave velocity (dynamic) 2) difficulty in measuring the static moduli at a similar strain range as used in dynamic testing 3) confusion about which type of moduli is measured during dynamic testing (Whitehurst, 1967). In addition, factors such as cyclic fatigue, creep and micro-cracking during axial loading differentiate the static modulus from the dynamic modulus of elasticity (Neville and Brooks, 2010). Accordingly, resonant frequency testing, used for calculating the dynamic modulus of elasticity, subjects concrete to low strain loads at a higher strain rate therefore, the testing method is considered as non-destructive.

2.4.2 Principles of Resonant Frequency Testing

Determining the modulus of elasticity from wave propagations was first reported by Rayleigh in 1877 (Rayleigh and Lindsay, 1945). Using the velocity of sound moving through a material with a known resonant frequency, Rayleigh developed a mathematical model to determine the dynamic modulus of elasticity from the wave velocity passing a specimen and the specimen's resonant frequency. This model was modified to provide an upper bound estimation of the natural resonant frequency (Rayleigh and Lindsay, 1945). According to this model, the total energy of the closed system remains unchanged. Therefore, it is based on the kinetic and potential energies of a closed system to be equal. Equations developed by Rayleigh were determined as perfectly elastic, homogenous, and isotropic systems such that the material composition and density are uniform. Such a system is known as a conservative system.

As a composite material, concrete is heterogenous and appears to exhibit some inelastic strain prior to failure under compression. Typically, the stain at fracture is 2×10^{-9}. Therefore, in practice, concrete designers treat concrete as an inelastic material and do not recommend it for structures that are subjected to high impact loads unless the concrete is reinforced with steel bars or fiber reinforced polymer bars (Mehta and Monteiro, 2006). The property for a material that defines the decrease in amplitude of free vibration is known as damping or wave attenuation. Although damping for any given vibration occurs, it can be negligible when compared to the total system energy. However, damping in concrete occurs due to

scattering and absorption of compression waves from aggregate particles and the presence of cracks and pores in concrete. Hence, a significant increase in damping can indicate the presence of pores, defects, or weakness in the interfacial transition zone between the aggregates and cement.

Later, during the 1940s, Powers first established measuring the natural resonant frequency by matching the tone of a hammer struck concrete specimen to a musical tone of a frequency calibrated orchestra bell (Powers, 1938). Although there is an apparent error when using this method, it gave a start to developing methods that are more refined. Later, the resonant frequency method was distinguished using electronic circuitry by Hornibrook for measuring the freeze-thaw resistance of concrete (Hornibrook, 1939). Hornibrook's work is considered as the groundwork for optimization of measuring the resonant frequency by exciting concrete prisms to their fundamental resonant frequency (Thomson, 1940; Stanton, 1944). Measuring the resonant frequency of concrete is found using a constant vibration and low amplitude or an impulse vibration with a low strain. Thus, these measurement practices are distinguished as 1) Forced resonance method (FRM) and the 2) Impact resonance method (IRM) which are covered in Section 2.4.4.

Stress wave propagation methods for concrete rely on exciting a dense medium for a short period to respond in linear and angular accelerations. (Mehta & Monteiro, 2006). Stress waves propagate in a solid, through compression waves and shear waves, and on the solid surface through particle motion. Any external transient stress pulse on concrete travels through the structure through dilatational, distortional, and surface waves known as Raleigh waves. Compression waves are longitudinal modes of wave vibration where wave particles pulsate back and forth parallel in the direction of wave propagation. As the particles travel, the compressive volume change causes the particle to rapidly propagate; hence terming them as Primary waves (P waves). On the other hand, shear wave particles move transverse (or vertical) to the direction of wave propagation. Unlike P waves, shear waves create no volume change during wave propagation and are slower than P waves, thus termed as Secondary Waves (S waves). P waves and S waves propagate through a structure and are reflected by internal defects such as voids or cracks and through the external boundary of the structure. These waves can be used to provide the elastic properties of a concrete medium through wave velocity and resonant frequency.

2.4.3 Theoretical Background

Evaluating the dynamic elastic moduli of concrete specimens are based on a unidimensional wave propagating theory (Timoshenko, 1970). Consider a wave signal sampled at a rate of f_s in Hz for a total number of samples (N), the time between each sample is given by

$$\Delta t = \frac{1}{f_s} \qquad \text{Eq. 2.4.3-1}$$

For analyzing the input waveform, a Fast Fourier Transform (FFT) matrix is used to obtain an amplitude-frequency domain output from the time domain signal. For given time-domain signal, an FFT can convert and measure the frequency content outputting the signal in frequency-domain. FFT is used to measure the frequency and phase information of an input signal. It provides both the signal magnitude and phase. The output frequency domain provides discrete frequencies at which the impact energy is concentrated. Through a set of filters using the FFT, the signal energy is divided between several frequency bands. Peak energy frequency bands provide the structural modes of vibration. The first peak has the highest acceleration amplitude and defines the first mode of vibration. The given amplitude and number of samples in the signal are denoted by x[i] sampled from $0 \leq i \leq N-1$. Using a Discrete Fourier Transform (DFT) algorithm, the magnitude of the frequency X[k] is given by

$$X[k] = \sum_{i=0}^{N-1} x_i \, e^{\frac{-i2\pi fk}{N}} \qquad \text{Eq. 2.4.3-2}$$

for $0 \leq k \leq N - 1$. For the output frequency domain, the frequency (Δf) resolution is given by

$$\Delta f = \frac{1}{N\Delta t} = \frac{f_s}{N} \qquad \text{Eq. 2.4.3-3}$$

To discretize the required analog signal, the collected signal using the accelerometer is converted from time-domain to frequency-domain using a defined sampling rate (f_s) and number (N); giving the FFT. Digital filter and FFT techniques are used to provide bandwidth and vibrational decay measurements from measured modal resonant frequencies. A comparison between digital filter and FFT methods shows that FFT techniques provide a higher resolution for determining the bandwidth and have no limitation regarding low damping. However, as damping increases, the transfer rate of the spectra is limited (Gade and Herlufsen, 1994). The FFT function is a reliable tool for determining and analyzing signals collected via data acquisition (DAQ) devices.

For a given single spectrum signal input, the FFT output is a two-sided spectrum in complex form having real positive and imaginary negative numeric sequences. The complex form should be scaled and converted to polar form to obtain the signal magnitude and phase. In actual frequency analysis, testing instruments display only the positive half of the frequency spectrum since the input signal spectrum is symmetrical around the divide between the frequency spectrums. Therefore, the negative frequency information is redundant. For a two-sided frequency spectrum, the energy is divided equally between the positive and negative spectrums. Therefore, for having a single frequency spectrum, disregard half of the output spectrum and multiply every sample magnitude point by 2 except the initial magnitude where the imaginary factor equals 0.

The Nyquist frequency (f_n) is translated as half the Sampling Frequency (f_s). Approximately double the sampling rate is required for the FFT in consequence to the Nyquist theorem. It outlines that for the highest frequency of a continuous time signal, the highest frequency in a discrete-time sequence is almost half that of the signal. Accordingly, a signal should be sampled twice as fast to capture resonance. Therefore, the periodicity of the discrete transform is between 0 and f_s.

Frequency resolution (Δf), also known as digital step, should be compensated with the number of discrete values (N) compiled. Consequently, the following equations give the frequency resolution and Nyquist maximum obtainable frequency. The signal length can be maximized until f_n reaches the highest required frequency for a given number of samples.

$$f_n = \frac{1}{2\Delta t} = \frac{1}{2} f_s \qquad \text{Eq. 2.4.3-4}$$

The larger the sampling frequency, the better the frequency resolution for a given number of samples. It is important to have a higher` sampling rate for determining the true resonant frequency of a structure. Oversampling is noted as having a sampling rate almost double the Nyquist frequency and is usually preferred since signals are not perfectly filtered and often contain higher frequency components. For obtaining the Nyquist frequency, the output frequency domain is divided by the sampling frequency of the system. This will give an output frequency spectrum from zero to one, where one is the Nyquist ratio.

Some important features are used to limit the length of the time history. This ensures to filter out discretization approximations that may lead to errors. A phenomenon known as aliasing occurs if the Nyquist theorem condition is not met. Aliasing occurs from under-sampling below f_n and is considered a false lower frequency component. To prevent aliasing inside the spectrum of interest, the input signal is monitored to confirm that the resonant frequency is excited based on the desired frequency resolution and sampling rate. Another problem, known as leakage, can arise if the discrete time of the signal does not coincide with the assumed periodicity. Spectral lines close to the true frequency are introduced with signal energy leakage. This can be corrected by the following:

Windowing: This filtering process involves multiplying a time function to the input signal prior to FFT. This allows any values outside the sampling rate to be zero thus avoiding leakage. There are several windowing time functions used depending on the input signal. Hanning, Hamming or rectangular windows are typically used for continuous time signals. For short period signals, exponential windows are more applicable.

Averaging: Typically, it is essential to ensure that the output frequency domain lies within a confidence interval. The number of averages used on a signal depends on any external noise removal from the signal and the statistical consistency to improve coherence.

The resonant frequency of a structure can be expressed in certain modes of vibration. These modes of vibration are described by a particular modal frequency and a mode shape. The following principles cover the free vibration of a prismatic and cylindrical bar typically used for assessing the elastic properties of concrete structures. These equations are adapted from (ASTM C215, 2014).

Transverse Mode of Vibration

(Goens, 1931) determined the modulus of elasticity for bars of different cross-section through (Timoshenko, 1922) equations for free-flexural vibration of bars with different cross-sections. By simplifying Goen's solution, (Pickett, 1945) expressed the modulus of elasticity (E) in GPa through the material mass (m) in Kg and first mode flexural frequency (f) in Hz and shape factor (C) by

$$E_{dt} = Cmf^2 \qquad \text{Eq. 2.4.3-5}$$

Where shape factor (C) in Ns^2kgm^2 is defined by the prism/cylinder length (l), gravitational constant (g), second moment of inertia (I), and dimensionless geometric correction factor (T_1) of a bar cross-section. Therefore, for the transverse fundamental mode of vibration, the shape factor can be given as

$$C = \frac{4\pi^2 l^3 T_1}{gI(4.73)^4} \qquad \text{Eq. 2.4.3-6}$$

For Eq. 2.4.3-6, the dimensionless geometric constant (T_1) is dependent on the radius of gyration of a beam cross-section, beam length and material Poisson's ratio. Further research for the shape factor from (T_1) was established by (Dickson and Wachtman, 1971) following (Spinner et al., 1960; Spinner and Tefft, 1961) for developing the equations for the *transverse modulus of elasticity* of prisms and cylinders. Since only the fundamental resonant frequency is measured (1st mode), the subscript for (T_1) is dropped. The correction factor depends on the ratio (*K/L)* between the radius of gyration of a bar (*K)* in meters and length, while having an expected Poisson's ratio (μ).

- For a prismatic length (L) in meters, cross-section with a width (b) in meters, thickness at which compression wave is driven (t) in meters and first mode flexural resonant frequency *(f)* the transverse shape factor (C) in Ns^2Kgm^2 and dynamic modulus of elasticity (E_{dt}) can be given as

$$C_{Prismatic} = 0.9464\frac{L^3T}{bt^3} \qquad \text{Eq. 2.4.3-7}$$

$$E_{dt} = 0.9464mf^2T(\frac{L^3}{bt^3}) \qquad \text{Eq. 2.4.3-8}$$

- For a cylindrical cross-section with a diameter (d) in meters, the transverse shape factor and dynamic modulus of elasticity in GPa are given as

$$C_{Cylindrical} = 1.6067\frac{L^3T}{d^4}$$ Eq. 2.4.3-9

$$E_{dt} = 1.6067mf^2T(\frac{L^3}{d^4})$$ Eq. 2.4.3-10

Longitudinal Mode of Vibration

As a longitudinal axial force is applied to a center-supported bar, the bar vibrates through free supported longitudinal displacement. Through the measured longitudinal frequency, the dynamic modulus of elasticity is given as

$$E_{dl} = Dm(f')^2$$ Eq. 2.4.3-11

- For a prismatic cross-section with a width (b) in meters, wave driven thickness (t) in meters and first mode longitudinal resonant frequency *(f')* in Hz, the longitudinal shape factor (*D*) and dynamic modulus of elasticity (E_{dl}) can be given as

$$D_{Prismatic} = 4\frac{L}{bt}$$ Eq. 2.4.3-12

$$E_{dl} = 4mf^2(\frac{L}{bt})$$ Eq. 2.4.3-13

- For a cylindrical cross-section with a diameter (d) in meters, the longitudinal dimension factor and dynamic modulus of elasticity (E_{dl}) in GPa are given as

$$D_{Cylindrical} = 5.093\frac{L}{d^2}$$ Eq. 2.4.3-14

$$E_{dl} = 5.093m(f')^2(\frac{L}{d^2})$$ Eq. 2.4.3-15

Torsional Mode of Vibration

Vibration of a bar in torsional mode produces a shear-twisting wave along the longitudinal axis. The shear modulus can be measured by applying a force to excite the bar through a torsional frequency.

$$G = Bm(f'')^2$$ Eq. 2.4.3-16

- For a prismatic cross-section (*A*) in m^2 with a width (b) in meters, thickness at which compression wave is driven (t) in meters and cylindrical cross-section (*A*) in m^2 with a diameter (d) in meters, first mode torsional resonant frequency *(f'')* in Hz, longitudinal dimension factor (*B*) in $Ns^2/kg{\cdot}m^2$, where the shape factor (*R*), *R*=1 for circular cross-section and *R*=1.183 square cross-section, the dynamic modulus of rigidity (G) in GPa can be given as

$$B = 4\frac{LR}{A} \quad \text{Eq. 2.4.3-17}$$

$$G = 4m(f'')^2(\frac{LR}{A}) \quad \text{Eq. 2.4.3-18}$$

Poisson's Ratio

Considering concrete as an isotropic solid, the ratio of lateral to longitudinal strain (ν) can be given using E_{dl} and G as follows

$$\nu = \left(\frac{E_{dl}}{2G}\right) - 1 \quad \text{Eq. 2.4.3-19}$$

As recommended by ASTM C215, the dynamic Poisson's ratio (ν) may vary between 0.10 – 0.25 for dry and saturated specimens respectively. Since concrete is more saturated at early age, higher values of ν are expected (ASTM C215, 2014).

Determination of the resonant frequency equations were derived from experimental analysis of different concrete sections with different size, age, and composition. RFT can be applied to concrete given that the test specimen is large with respect to its constituent materials for free vibration to occur (Malhotra and Carino, 2004).

2.4.4 Resonance Frequency Testing Techniques

Methods of defining the modulus of elasticity in concrete can be divided into direct, contact or non-contact tests. First, direct measurement of stress and strain relies on mechanical compressing of a concrete cylinder to obtain concrete deflection until 40% of the applied compression force. The static modulus of elasticity can be obtained via direct testing and is calculated using the equations adapted from (ASTM C469, 2014). Contact methods are non-destructive techniques that rely on wave propagation and resonance methods. Resonant Frequency Testing (RFT) adopted from (ASTM C215, 2014) and Impact-echo testing (IE) are predominant methods used for damage detection or location respectively. These methods depend on contact vibration, using a pulse vibrator or impact hammer, to measure the dynamic modulus of elasticity via the reflected wave velocity, resonant frequency, density, and geometry of a concrete specimen.

Non-contact methods to analyze the dynamic elastic properties of concrete include sonic or laser vibrometer techniques. When a sonic speaker or laser is applied on a concrete surface, the reflective wave properties frequency and wave velocity can be used to determine the in-situ dynamic modulus of elasticity. Using Ultrasonic Pulse Velocity (UPV) testing adopted from ASTM C597 is mainly focused on contact and non-contact vibration, using a speaker or ultrasonic transducer, to obtain the velocity of the wave passing through concrete which is related to dynamic modulus of elasticity (ASTM C597, 2016).

(Popovics, 2008) investigated and reported the difference between the dynamic and static moduli of elasticity. The authors compared the static and dynamic moduli via ASTM C469 and ASTM C215 respectively. The results showed that the dynamic elastic modulus is always greater than the static modulus relying on the composite nature of concrete rather than the nonlinear behavior to applied strain rates. This was confirmed by preparing two phase concrete samples indicating the influence of the composite. Moreover, the author highlighted that the relation between static and dynamic moduli is affected mostly by the dynamic modulus. In addition, the author indicated that the measured elastic moduli using UPV has shown to overestimate the modulus. Similarly, (Lee et al., 2015) determined the dynamic elastic moduli of concrete cylinders using UPV and RFT. The authors determined that the coefficient of variation (CV) using

UPV is higher than that of RFT. In addition, the authors instigated that it is inappropriate to predict the static elastic modulus using UPV values for having considerably large error.

This study only focuses on measuring the dynamic elastic properties using the resonant frequency testing as the primary testing method for the dynamic modulus of elasticity. Resonant Frequency Testing (RFT) methods for concrete are measured through two alternate procedures:

- Resonant frequency by constant vibration known as the *Forced* resonance method
- Resonant frequency through impulse vibration known as the *Impact* resonance method

2.4.4.1 Forced Resonance Method (FRM)

All early investigations of measuring the resonant frequency of concrete used a constant contact vibration known as the *forced resonant frequency* method. It consists of two phases – the first part is vibration induction using sinusoidal excitation and the second part senses that vibration. This method states that the resonant frequency is determined when vibrations, induced in concrete specimens, result in a maximum response amplitude. Concrete prisms and cylinders are tested according to ASTM C215 Section 8 for forced resonance testing (ASTM C215, 2014).

This method implies a constant vibrational input to determine the resonant frequency of concrete. Figure 2-2 shows the components required for forced resonance testing. Vibration is generated using an electronic audio-frequency oscillator. Ideal mechanical vibration is adjusted by amplifying the oscillator. The vibration is collected using a pick-up transducer located at specific areas on a concrete specimen. The pick-up circuit consists of a piezoelectric transducer unit, an amplifier and signal indicator that converts the mechanical vibration to electrical AC voltage output. To find the resonant frequency, the rate of vibration is altered until its amplitude reaches its maximum and the resonant frequency is read from a variable driving audio-oscillator. The oscillator, vibrator and pickup are compiled in a testing unit known as a Sonometer. The driving oscillator consists of a variable frequency audio oscillator, an amplifier unit and a driving unit. The driver should be calibrated for a resolution of ± 2%. For detecting the natural frequency, the driving vibration frequency is increased until the maximum potential deflection is shown on the signal indicator reading the natural resonant frequency. The fundamental modes of vibration can be observed from the cathode-ray oscilloscope (Malhotra and Carino, 2004).

For a hardware check, the pickup is placed at both ends of the vibrating specimen and at the support nodes. Support and position of transducers for forced resonance are given in Section 8 of ASTM C215 and Figure 2-3 in this study (ASTM C215, 2014). At the vibrating end, the oscilloscope reaches a maximum amplitude shown while at the support nodes, a horizontal line is displayed on the oscilloscope indicating no vibration. Several authors have widely used it, however, since the oscillator has large surface area compared to general concrete lab samples, it is difficult to vibrate curved, thin or irregular specimens in their fundamental modes.

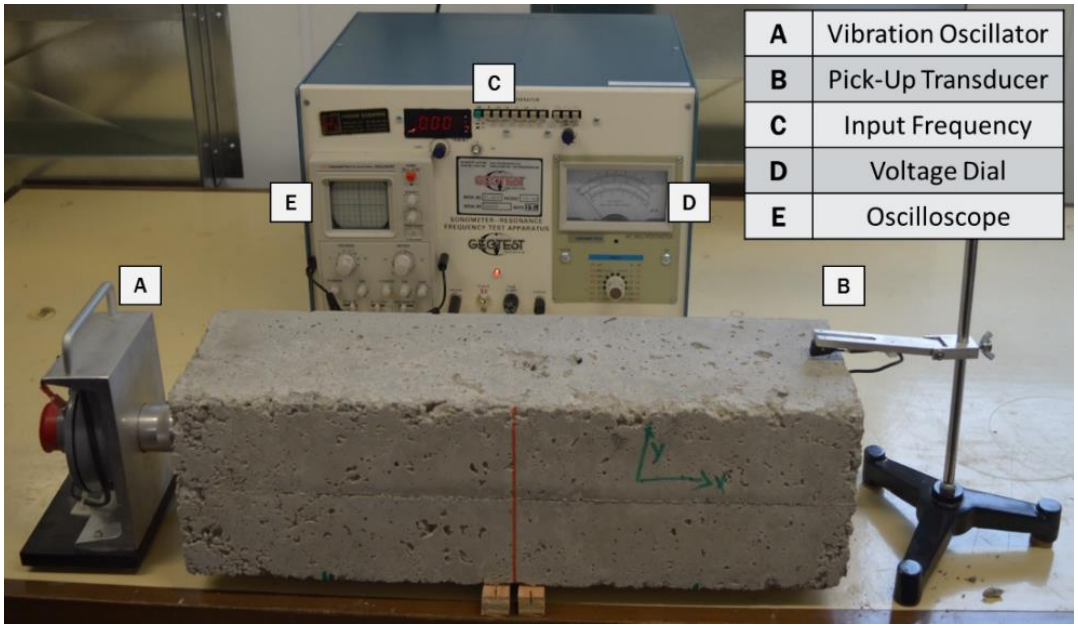

Figure 2-2: Forced Resonance Method

2.4.4.2 Impact Resonance Method (IRM)

An *impact resonant frequency* approach proposed by (Gaidis and Rosenburg, 1986) relies on impacting the test specimen with a ball-tip hammer rather than using a forced vibration to induce a stress wave. The stress wave is picked up by an accelerometer set at different locations on the test specimen that define the transverse, longitudinal and torsional modes of testing. Accelerometer data is collected in time domain and then converted to a defined frequency domain using the FFT function to determine the natural resonant frequency for a given vibration. The highest peak in an amplitude-frequency graph defines the resonant frequency of the tested concrete. This method, along with the standards developed, only applied to laboratory sized specimens like cylinders and beams. Currently, a standardized method for larger sized or irregular specimens is unavailable. The representative impact resonant frequency data acquisition setup is shown in Figure 2-3.

Specimen support is vital for assuring that the measured frequency is the natural resonant frequency. For transverse vibration, the support nodes are located at a distance equal to 0.224 times the length of the specimen (L) away from the ends of the specimen. Vibrations in transverse mode are zero at the two nodal points and maximum at the ends of the specimen. For the longitudinal and torsional modes, the vibration node is zero at the center and maximum at the ends. The support should enable the specimen to vibrate freely by aligning the support with the zero vibration nodes of the specimen. Balance is maintained during testing by measuring the length of each specimen prior to testing and adjust the supports correspondingly.

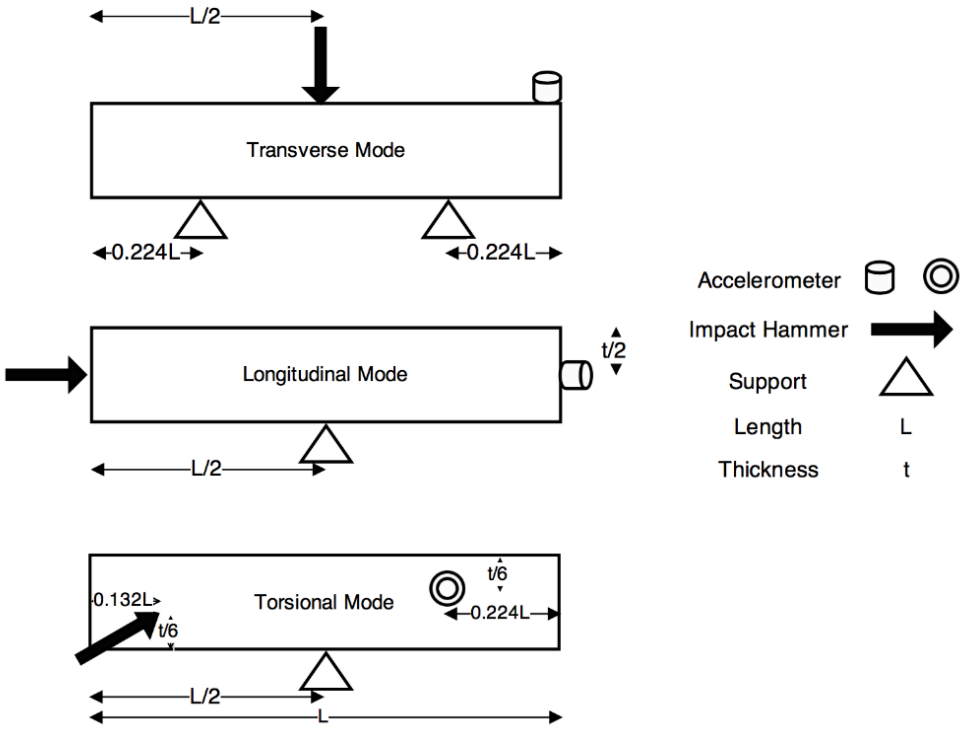

Figure 2-3: Specimen setup for Transverse, Longitudinal and Torsional modes of testing (Adapted from ASTM C215)

Proficiency is essential to determine the required frequency since some resonant frequencies can be attained corresponding to different modes of vibration. An approximate range of frequencies is summarized in Table 2-2 adopted from (Balendran, 1993; Jones, 1969). Concrete specimens with a large length to transverse thickness ratio (L/t) are also difficult to excite to in the fundamental natural resonant mode of transverse vibration. As recommended by ASTM C215, the L/t ratio should be between 3 and 5 (ASTM C215, 2014). This ensures that vibration modes occur along the required axis of testing.

Table 2-2: Approximate Range of Frequencies for Concrete Specimens Adapted from (Balendran, 1993; Jones, 1969)

Size *Length : Width : Height* *Diameter : Height* (mm)	**Shape**	**Approximate Resonant Frequency Range** (Hz)		
		Transverse	**Longitudinal**	**Torsional**
150 : 150 : 750	Prism	550 – 1050	1700 – 3200	1050 – 1150
100 : 100 : 750	Prism	400 – 750	1700 – 3000	1150 – 1800
100 : 100 : 500	Prism	900 – 1500	2500 – 4500	1800 – 2700
100 : 100 : 300	Prism	2500 – 4500	5000 – 7000	3000 – 4200
150 : 300	Cylinder	2500 – 4500	5000 – 7000	3000 – 4200

2.4.5 Influencing Parameters on RFT Measurements

Concrete is a heterogenous material where the localized stress to strain ratio can be dissimilar from the nominal applied stress to strain. As concrete hardens from the initial casting, its resonant frequency

increases at a high rate during the initial 3 days of curing and increases at a low rate during the remaining time of curing. The high rate increase is caused by a decrease in porosity as the reaction products, Calcium-Silicate-Hydrate (C-S-H) and Calcium Hydroxide ($CaOH_2$), of concrete enlarge when hardened.

Like the compressive strength of concrete, the modulus of elasticity increases as hydration is continued. Both strength and elastic properties of concrete are affected by a range of factors including aggregate properties, curing conditions, temperature, mixture proportions, water to cement ratio (*w/c*), and the presence of reinforcement and internal microcracks within the composite (Bungey et al., 2006). Other important factors include concrete age and coarse aggregate type (Malhotra and Carino, 2004). The following section focuses on several influential factors pertaining to the dynamic modulus of elasticity and fundamental frequency of concrete.

2.4.5.1 Mixture Proportions and Admixtures

One of the factors, influencing the concrete dynamic modulus of elasticity, is the basic moduli of its ingredients and their relative proportions. Although concrete is a composite material primarily made of aggregates and cement binder, its characteristics do not follow the rule of mixtures (Mehta and Monteiro, 2006). For example, under compressive loading both the aggregates and cement binder, when individually tested, would fail elastically. However, concrete itself exhibits inelastic behavior prior to fracture. Moreover, concrete strength is lower than the individual strength of its components. Such irregularities can be explained on the basis of its microstructure predominantly defined through the interfacial transition zone between the coarse aggregates and the cement binder (Mehta and Monteiro, 2006).

In (Jones, 1969) and reported by (Malhotra and Carino, 2004), it is evaluated that the elastic modulus of hardened concrete increases for a given cement paste composition having the same *w/c* ratio, as the total aggregate percentage increases. However, a reduction in the dynamic modulus of elasticity has been observed once the water content and volume of entrapped air increases. Also, in an unpublished study conducted by Canada Center for Mineral and Energy Technology (CANMET), it is stated that the values of static and dynamic moduli were comparatively higher than concrete strength for concretes containing high volume of low-calcium fly ashes. They believed that the higher value mostly resulted from the un-hydrated fly ash particles behaving as fine filler in the matrix.

The advantage of having polypropylene fibrous concrete with fly ash was report by (Karahan and Atiş, 2011). The authors used a fly ash content of 0%, 15% and 25% by mass with fiber volume fractions of 0%, 0.05, 0.1, and 0.2% by volume. By monitoring the compressive strength, static elastic modulus, porosity and water absorption of PFRC, the authors concluded that addition of polypropylene and fly ash in concrete will reduce the overall composite unit weight. Moreover, polypropylene fibers reduce the workability of concrete while the addition of fly ash improves it. The presence of polypropylene fibers and fly ash was also found to increase the freeze-thaw resistance of PFRC having fly ash as the more dominant enhancer.

(Chavan and Vyawahare, 2015) also experimentally attempted to compare the static and dynamic modulus of elasticity in Self-Compacting Concrete (SCC) incorporating silica fume and fly ash. Since the SCC has uniform consistence than normally vibrated concrete, it was observed the values of static and dynamic modulus are strongly correlated. The average static elastic modulus was about 4 GPa lower than the dynamic modulus. SCC however has a uniform consistency when compared to normal compact of concrete. With better cement matrix distribution in concrete, the modulus of elasticity is consistent since the regular amorphous microstructure is not present. Adding cement binder replacements, such as fly ash and Silica Fume, affect the resonant frequency of PFRC. At early age curing, fly ash alters the reaction rate of calcium silicates and calcium aluminate.

A previous study conducted by the author was used to investigate the influence of matrix strength between standard cast plain concrete and defect cast plain concrete due to honeycombing from consolidation errors (Gupta and El-Newihy, 2015). All specimens were cast for 32 MPa concrete. The dynamic elastic properties for 150×150×550 mm plain concrete prisms and 100×200 cylinders were tested. The results showed a substantial decrease in elasticity of honeycombed specimens when compared to normal cast beams of the same mixture. However, the longitudinal modulus showed more consistency throughout testing when compared to the transverse modulus. Porosity of the honeycombed structure is the main factor affecting the elastic properties along with a slight mass difference from porosity when compared to the reference concrete. From resonant frequency testing, wave propagation increasingly disperses with the presence of cavities in the composite producing a lower resonant frequency; hence, the elastic moduli decrease.

2.4.5.2 Specimen Size

The value of the dynamic modulus is affected by variation in size of concrete specimens. According to (Obert and Duvall, 1941) study, the specimens with larger dimensions, and thus more weight, have lower resonant frequency.(Kesler and Higuchi, 1945) perceived that longer beams resonating at lower frequencies showed higher elastic moduli compared to proportionally smaller beams while as reported (Jones, 1969), little change in the moduli for various samples having a frequency range 70 to 10,000 Hz. As it is described in (Malhotra and Carino, 2004) by (Thorton and Alexander, 1987), the resonant frequency of the fundamental flexural mode increases with the increase in thickness or decrease in length of the sample even if other parameters are kept constant.

In a recent experimental study, conducted by (Lee et al., 2015) on investigating the effects of cylinder size (150×300 mm and 100×200 mm) on empirical relation of static and dynamic modulus of elasticity and compressive strength of concrete, it was concluded that the different cylinder sizes do not have an effect on concrete moduli for normal strength concrete (≤40 MPa). However, for high strength concrete greater than 40 MPa, they pointed out that the size of sample become critical. Therefore, special care is required for comparison between static and dynamic moduli of high strength concrete for samples with different dimensions. Correlation of the static and dynamic modulus of elasticity of conventional concrete is not affected by *w/c* ratio and aggregate content (Zhou et al., 2015). Aggregate content and water to cement ratio are the two dominant factors that affect static and dynamic moduli as their relationship is mainly controlled by the aggregate in plain concrete (Zhou et al., 2015).

2.4.5.3 Curing Condition

Although the dependency of the dynamic modulus of elasticity on the moisture content has been recognised (Obert and Duvall, 1941), the study found small changes in the elastic modulus with age after 3-4 days of drying. Moreover, according to their study, a large reduction in the value of dynamic moduli takes place within the first 48 hours of oven drying, although, the subsequent change is rather small. As low a temperature as 34˚C in oven drying curing even leads to an irreversible reduction of the elastic modulus. This reduction can be explained by micro-cracking of paste from shrinkage phenomena which causes the subsequent decrease in its stiffness, and thus influencesthe dynamic moduli. It was also found in (Kesler and Higuchi, 1945) that the dynamic modulus of elasticity increases as the strength increases for the same curing conditions and it rises with age if concrete is kept moist. However, other studies on large blocks incorporating Secondary Cementitious Materials (SCM) have identified that longer periods of air-drying do not have any detrimental influences on both static and dynamic moduli of elasticity. Due to slow pozzolanic reaction of SCMs, it is concluded that strength obtained in these concrete specimens over a longer period seems to lead to higher elastic moduli.

(Zhou et al., 2015) study reported that curing temperature affects the development of both the static and dynamic moduli of elasticity while it did not influence the correlation between both moduli. Furthermore, the dynamic elastic modulus of air-cured concrete may slightly decrease due to continuing moisture loss of concrete through time. The elastic modulus of saturated (water cured) concrete can be up to 5% greater than that of air-dried concrete (Bungey et al., 2006). A study performed by (Graft-Johnson and Bawa, 1969) showed a decrease of the damping coefficient with increase in age, aggregate-to-cement ratio, density and compressive strength. It was also noted that air-cured samples gave much higher values possibly due to evaporation changing the rigidity of the cement.

(Jones, 1969) study on beam specimens, moist-cured for 25 days and afterward air-cured for 150 days, showed significant changes in the elastic moduli readings taken from flexural and longitudinal resonance tests. The author believed that the difference in modulus, resulted from the moisture loss, mainly consequence in gradients for moisture content, elastic modulus, and density in each dimension of the beam which eventually affect the flexural and dynamic moduli. Hence, curing conditions have critical effects on the resonance frequency and dynamic moduli and it is recommended to test specimens in water-saturated or saturated-surface-dry (SSD) conditions.

2.4.5.4 Age

The modulus of elasticity of concrete varies under loading and with age (Graft-Johnson and Bawa, 1969). As concrete hardens from the initial casting, its resonant frequency increases at a high rate during the initial 3 days of curing and increases at a low rate during the remaining time of curing. The high rate increase is caused by a decrease in porosity as the reaction products, Calcium Silicate Hydrate and Calcium Hydroxide, of concrete develop. A study by on plain concrete specimens yet confirmed that age and curing condition both affects the internal structure and density of concrete and thus potentially could have an influence on the modulus, especially through development of hydration product and internal cracking. Plachy's study also evaluated the static Young's moduli which later compared with dynamic moduli (Plachy et al., 2009). According to their study during one year monitoring of concrete specimens, there were no significance variations in the value of dynamic and also static modulus in time. (Han and Kim, 2004) found no major correlation between sample age and the relationship between the moduli, but all samples were tested up to 28 days of age.

2.4.5.5 Temperature

(Bahr et al., 2013) studied the effect of high temperature on the modulus of elasticity of concrete to determine the concrete's fire resistance through temperature dependent factor. Using an impulse excitation technique, the authors investigated the elastic properties of fire exposed concrete and found a degradation trend in the elastic modulus with an increase in temperature. Subsequently, the authors proposed a new temperature dependent model.

Several studies have used this technique for studying the defects in lab specimen, however, limited information is available in correlating the influence of polypropylene fibers along with the effect of consolidation and induced defects on the dynamic elastic modulus of plain concrete.

2.5 Application of Impact Resonance Method on Polypropylene Fiber Reinforced Concrete

Various studies have been conducted to measure mechanical properties of FRC such as flexure strength, fiber pullout strength, abrasion resistivity. However, there is limited research evidence regarding the assessment of the dynamic elastic properties of PFRC using different size fibers and concrete specimens.

Typically, the resonant frequency of PFRC decreases in both air and moisture curing conditions. This can be related to the lower density of the polypropylene fibers when compared to that of other aggregates used. This section includes a review of previous literature conducted on resonant frequency testing of FRC focusing on the use of polypropylene fiber. Other research pertaining to the evaluation of dynamic properties of concrete using RFT are also considered.

The dynamic properties of PFRC disc slabs were determined by (Manolis et al., 1997). In their experiment, 19 mm fibrillated polypropylene fibers with three volume fractions, 0 %, 0.1 % and 0.5 % of the same mixture, were cast in a circular slab 20 cm thick. They reported that polypropylene fiber content did not have a significant influence on first natural frequency, yet it enhanced the impact resistance of concrete specimens, especially for these specimens containing 0.5% polypropylene fiber. It was recommended to investigate the effects of fiber length or utilize various mix designs to maximize the fibers' contribution to strength development.

An initial study, conducted by (Leung and Balendran, 2002), showed that the resonant frequency of PFRC is can be affected by the presence of polypropylene fibers, curing condition and the partial replacement of cement by mineral admixtures such as silica fume and fly ash. The authors used 0.2% polypropylene fibers by volume of concrete for all mixtures. The results showed a slight decrease in the resonant frequency when adding polypropylene fibers. Moreover, the addition of fly ash with the fibers decreases the resonant frequency of the concrete at early age (3 Days and 7 Days), however, the resonant frequency tends to increase with age (28 Days and 91 Days) (Leung and Balendran, 2002). Yet, the benefits of polypropylene fibers show come into effect after cracking occurs and play a role in crack width control and abrasion resistance. To expand the comparison, specimens could be assessed though their dynamic elastic properties. This ensures that most variables, including variation in concrete density and geometry, are considered when comparing samples of the same mixture.

(Ward et al., 2008) evaluated the effect of fatigue and thermal cycling on carbon fiber reinforced polymer (CFRP) beams using the impact resonance method. The authors experimented 1.2m long reinforced beams subjected to thermal cycling between 23˚C and -18 ˚C. Moreover, they evaluated fatigue loading cycled between high and low stress levels to study IRM in damage detection. The FFT frequency spectrum, modal fundamental frequency and dynamic properties were used to asses the damage of the beams. The authors summarized that the IRM for thermal cycling was inconclusive. However, for fatigue cycling, the dynamic elastic moduli showed a decrease in stiffness from the measured fundamental frequency. The largest decrease was observed for the longitudinal frequency as about54% less than the original dynamic moduli and about 32% less than the original P-wave velocity. Moreover, the authors indicated a that CFRP strengthened beams retained a higher stiffness from both elastic and P-wave velocities under loading when compared to un-strengthened beams.

(Zhang and Li, 2013) investigated the effect of polypropylene fibers on the freeze-thaw resistance of concrete using four different fiber volume fractions (0.06%, 0.08%, 0.1% and 0.12%). Addition of polypropylene fibers greatly improved the durability of concrete containing fly ash and silica fume and slightly increased the freeze-thaw resistance when compared to plain concrete. RFT can be used to determine changes in dynamic properties of concrete undergoing freeze-thaw cycles. (Hamoush, 2011) studied the effect of freeze-thaw cycles of Very High Strength Concrete (VHSC). By determining the dynamic moduli and Poisson's ratio, the authors showed that both above mentioned factors increase at 40 cycles of freeze-thaw while the modulus of elasticity decreases with more freeze-thaw cycles as cracks initiate and develop.

(Ali et al., 2012) studied the relation between the static and dynamic elastic moduli of coconut fiber reinforced concrete beams based on resonant frequency and damping ratio. Their results show that concrete exhibited a high damping ratio and a lower modulus when coconut fibers are added. The authors concluded that the elastic properties improve when the fiber volume fraction reaches 5% and length of 50 mm.

The effect of the steel fiber (0.5% and 1%) and carbon fiber (0.5%) on mechanical properties of concrete incorporating 10% silica fume has been experimentally investigated in (Giner et al., 2012). For each mix design, three prismatic (100×100×400 mm) specimens for evaluation of their fundamental longitudinal, transverse, and torsional resonant frequencies and three cylindrical (Ø150×300 mm) samples for measuring their compressive strength were cast in this study. Out of the three modes of vibration, it was concluded that the addition of carbon fibers relatively increase the resonant frequencies of concrete samples. In contrast, resonant frequency values tend to decrease as the steel fiber content increases. Although the modulus of elasticity of concrete is expected to increase with an increase in steel fiber content, the authors indicate that the decrease in resonant frequency values can be related to the increase of porosity and air content that is produced by the addition of more fibers. A similar trend has been observed for the dynamic elastic properties. It is reported that the static elastic modulus shows lower values compared to their dynamic counterparts for all mixes.

2.6 Summary

Reinforcing concrete with polypropylene fibers has been proven to provide an economical and efficient method to promote better environmental stability and higher impact and shrinkage resistance of concrete. The local mechanical properties of PFRC are affected by fiber length, volume fraction and type of fiber used. Global factors include the concrete age, water/cement ratio, mixture proportions, temperature, curing conditions and aggregate size/type. Yet the effect of polypropylene fibers on the compressive strength and elastic modulus properties of concrete is unclear. Some cases showed a slight increase in both properties when polypropylene fibers are added. Still, polypropylene fibers are known to be dominantly significant in increasing impact resistance, promoting toughness and controlling plastic shrinkage of concrete. Furthermore, polypropylene fibers offer extensive crack bridging and slow down crack propagation.

Based on the literature review, it can be concluded that the resonant frequency method is practical for determining dynamic properties of concrete. Moreover, it is repeatable, convenient, and reliable for correlating the dynamic elastic and shear moduli of different concrete mixtures. The lab developed NDT method presented in this thesis has been applied to a limited number of PFRC samples with different dimensions. The impact resonance method shows a potential for viable assessment of concrete dynamic properties using selected specimens of different sizes and reinforcements.

3 Experimental Program

This section comprises the materials, mixture composition, casting, curing conditions and preparation of specimens including the testing procedures that are investigated during this study. The specimens are divided into three batches with the following specifications:

- Batch 1: To study the effects of macro fibers on Polypropylene Fiber Reinforced Concrete (PFRC) using low and high fiber quantities, when compared to unreinforced (plain) concrete of the same mixture. To review the dynamic elastic modulus of flexure cracked PFRC beams.
- Batch 2: To evaluate the effects of micro fibers on the dynamic properties of PFRC monitored from Day 1 (after casting) to 56 Days when compared to plain concrete of the same mixture.
- Batch 3: To evaluate the dynamic properties of macro and micro PFRC cylinders, prior to cracking and post-cracking, accounting for saturated and dry curing conditions.

Currently, there are normalized standard procedures for determining the dynamic elastic properties of concrete using stress wave propagation techniques in accordance to the American Society for Testing and Materials (ASTM), British Standard Institute (BSI) and Deutscher Ausschaussfur Stahlbeton (DAS). All standard associations have a similar testing procedure; however, there are dimensional correction factors in defining the dynamic modulus of elasticity differs. Through this study, testing of fresh and hardened concrete properties was performed according to ASTM standards. *ASTM C215 – Standard Test Method for the Transverse, Longitudinal and Torsional Resonant Frequency of Concrete (*ASTM C215, 2014) has been the primary focus of this study to investigate the dynamic elastic properties of concrete specimens.

3.1 Materials

3.1.1 Cement

Portland cement Type GU was used for all concrete batches. Appendix A.A shows the used cement type in accordance with ASTM C150 – Type 1 general use.

3.1.2 Fly Ash

Fly ash used was obtained from Centralia power plant, located in Centralia, Washington, USA. The fly ash is classified as Class F per ASTM C618.

3.1.3 Aggregates

Natural gravel with a nominal size of 12.5 mm containing a small amount of partially crushed material was used as coarse aggregates for all mixtures. Sand collected from Sechelt Pit was also used as fine aggregate. Table 3-1 includes the properties of the used aggregates. Appendix A includes the sieve analysis of the coarse and fine aggregates along with other properties.

Table 3-1: Coarse and fine aggregate properties

Aggregate	Coarse	Fine
Maximum Size (mm)	12.5	4.75
Specific Gravity	2.8	2.7
Water Absorption (%)	0.45	1.2
Fineness	-	2.61

3.1.4 Fibers

Two different polypropylene fibers were considered in this study developed by (Propex Operating Company, 2016). Type 1 (*Enduro® 600*) is a macro-monofilament fiber with a patented sinusoidal

deformation. Type 2 (*FiberMesh® 150)* is a 100% virgin polypropylene micro fiber. Table 3-2 includes the fiber material properties. Type A and Type B fibers used in this study are shown in Figure 3-1. Types A and B from here on in this study refer to designations for the macro and micro fibers respectively.

Table 3-2: Polypropylene Fiber Properties

Mechanical Property	Unit	Type A PP - Macro Fiber	Type B PP - Micro Fiber
Fiber Length	mm	50	12
Equivalent Diameter	mm	0.5	0.018
Specific Gravity	-	0.91	0.9
Aspect Ratio	%	0.5	0.5
Elastic Modulus	GPa	7.5	7
Tensile Strength	MPa	550	300-450
Water Absorption	%	0	0
Melting Point	°C	164	162
Thermal Conductivity	W/mK	Low	N/A
Density	Kg/m^3	910	900

Figure 3-1: Macro (left) and micro (right) polypropylene fibers

3.1.5 Water

Potable clean tap water at 15˚C was used for all concrete mixtures.

3.1.6 Admixtures

Water-Reducing-Admixture (WRA)

MasterPozzolith 210 provided by BASF® was used as the superplasticizer for mixtures. WRA was added to allow easier workability when adding fibers. The volume per $1m^3$ of WRA used for each batch is shown in Table 3-4: Mixture Proportions for Concrete. A summary of the physical and chemical properties of WRA is provided in Table 3-3.

Air-Entraining-Admixtures (AEA)

DAREX ED provided by Grace Canada, Inc. was used as for active air-entrainment during fresh concrete mixing. The admixture is an Alkyl Sulphate liquid composed essentially of Tall oil. Tall oil is a by-product of chemical pulping of coniferous trees, like Pine trees, and is fundamentally made of fatty acids and other alkyl hydrocarbon derivates. AEA was added to supply concrete with microscopic air bubbles that protect the concrete through freeze-thaw cycles. A summary of the physical and chemical properties of AEA is included in Table 3-3.

Table 3-3: Summary of admixture properties

Item	**WRA**	**AEA**
Supplier	BASF Canada, Inc.	Grace Canada, Inc
Trade Name	POZZOLITH 210	DAREX AEA ED
MSDS ID	30605620/SDS_GEN_CA/EN	D-07092
Form	Liquid	Liquid, Oil based
Color	Dark brown	Light brown
pH	6 - 11	11
Density (Kg/m^3)	1125 - 1155	1000
Solubility in water	Completely soluble	
Solubility in other solvents		

3.2 Mixture Proportions

The following mixture proportions were applicable for moderate to high strength concrete 31 – 45 MPa. According to AASHTO-AGC-ARTBA Joint Committee, it is advised to increase the mortar fraction and reduce the coarse aggregate content to accommodate the increase in surface area due to polypropylene fiber addition (AASHTO-AGC-ARTBA Joint Cooperation Committee, 2001).

Three separate batches of PFRC were prepared by modifying some variables between each batch. The mixture proportions are given in Table 3-4. CC designates the control concrete mixture of Batch 1 and Batch 2. A higher fiber content of 1% is indicated by *H* in Batch 1. FRC comprises polypropylene fiber reinforced concrete with macro and micro fibers designated as *A* and *B* correspondingly for all batches.

The total cementitious unit weight used for mixing is the same for each batch; however, for Batch 1 and Batch 2, 20% of the total cement weight was substituted with Fly Ash. Fiber mixtures were regulated by modifying the quantity of WRA used while all AEA volumes remained constant between each batch. WRA dosages were adjusted to accommodate for low workability of fiber mixtures and maintain slump between all batches. A w/c ratio of 0.5 was chosen for Batch 2 to investigate the effect of increasing the water content on the dynamic elastic properties of PFRC. No fly ash was used as a mineral admixture for Batch 3 to highlight the effect of substituting finely pulverized fly ash into the cementitious mixture. Moreover, Batch 3 focuses on testing concrete cylinders

Table 3-4: Mixture Proportions for Concrete

Batch							
Concrete Type	1			2		3	
	0% Fiber	0.6 % Macro PP	1% Macro PP	0% Fiber	0.3% Micro PP	0.6 % Macro PP	0.3% Micro PP
Mixture ID	CC1	FRC-A	HFRC-A	CC2	FRC-B	FRC-A	FRC-B
W/C	0.43	0.43	0.43	0.5	0.5	0.41	0.41
Materials (Kg/m^3)							
Cement	276	276	276	276	276	345	345
Fly Ash	69	69	69	69	69	-	-
Sand	815	815	815	820	820	815	815
Aggregate	1045	1045	1045	1100	1100	1045	1045
Water	148	148	148	170	170	145	145
Fibers (%)	-	0.6	0.6	-	0.3	0.6	0.3
WRA	1.883	1.883	2.389	-	-	1.225	1.225
AEA	0.123	0.123	0.123	0.123	0.123	0.123	0.123

3.3 Specimen Preparation

The cylinders and prisms are cast according to (ASTM C192, 2015). The moisture content for the aggregates and water content were adjusted by drying the aggregates in an oven for 24-hrs set at a 110±5 ˚C. Using a vertical drum type concrete mixer, 50 Liters in volume, each batch was cast separately not exceeding 30 L to avoid any overflow. Primarily, fine sand and coarse aggregates are dry mixed for 30 seconds to ensure a consistent distribution of the aggregates. Next, cement mixed with the predetermined amount of fly ash is added and mixed for 30 seconds to coat the aggregate mixture. By rule of mixing, the WRA and AEA chemical admixtures are added to the water prior to hydrating the dry mixture. When all materials are added, the mixture runs for 3 minutes undisturbed, followed by 2 minutes resting time and then a final round of mixing for 3 minutes. The concrete mixture was allowed to rest for a couple of minutes and then poured into a wheelbarrow for easier handling. The workability, air content, density and temperature are subsequently tested and discussed in Section 3.4.1.

Each of the cylindrical and prismatic molds were cast in two layers. The molds were filled to half their volume and placed on a vibrating table. The total vibration time for cylinders and beams was 8 seconds and 10 seconds per layer, respectively. After consolidation, all specimens were surfaced and finished with a fine foam trowel. Promptly after the casting, the all specimens were sealed with a plastic sheet to maintain moisture for 24 hours at room temperature during concrete hardening. An overview of the size and number of specimens selected for each batch is included in Table 3-5. After 24 hours of hardening, prisms and cylinders were removed from the molds and saturated in a water bath set at 23 ± 2°C for 28 days of curing (ASTM C192, 2015). For dry curing conditions, samples were kept uncovered at ambient room temperature of 22 ±2˚C at relative humidity of 50%.

Table 3-5: Specimen Testing Breakdown

Batch	Mixture ID	Concrete Type	Prism[1]	Cylinder[2]	
			Dynamic Moduli[3]		Compression[4]
1 (w/c = 0.43)	CC1	Plain Concrete	3[A]	3	3
	FRC - A	0.6% Macro PFRC	3[A]	3	3
	HFRC - A	1% Macro PFRC	3[A]	3	3
2 (w/c = 0.5)	CC2	Plain Concrete	3	3	3
	FRC - B	0.3% Macro PFRC	3	3	3
3 (w/c = 0.43)	FRC - A	0.6% Macro PFRC	-	12[B]	6[C]
	FRC - B	0.3% Micro PFRC	-	12[B]	6[C]

[1] *Size: 100×100×350 mm & 150×150×550 mm*
[2] *Size: 100x200 mm*
[3] *According to ASTM C215*
[4] *According to ASTM C39 at 28 days*
[A] *Additional prisms were tested for modulus of rupture according to ASTM C1609*
[B] *Same set are tested after cracking*
[C] *Additional three cylinders were tested for compressive strength at 14 days*

3.4 Testing

3.4.1 Standard Concrete Testing

3.4.1.1 Fresh Concrete Properties

Workability

Workability of fresh concrete was measured using a slump test in accordance with (ASTM C143, 2015). Slump is measured by the change in height (mm) of compacted concrete undergoing a normal viscous reaction to gravity when the cone is pulled upwards releasing the fresh concrete. For optimal results, the test should go uninterrupted, from start of filling the mold to removing the cone, in an elapsed time of 2.5 minutes relating to ASTM C143 procedures. All mixtures were tested using the same apparatus and results are averaged to the nearest 5 mm.

Air Content

Air content is defined by the percentage of air present in a fresh concrete mixture. From ASTM C231, a Type B air meter was used for testing the percentage air in both plain concrete and FRC mixtures as concrete the mixtures consist of relatively dense aggregates (ASTM C231, 2014). The mechanism behind the apparatus starts by air being pumped into a pressure cap air chamber that is sealed air tight with a constant volume base. The air meter is calibrated to initial pressure. As the air is released from the pressure cap air chamber to the base, the percentage is the resulting air content of the concrete mixture. Air content testing was repeated twice to ensure consistent values.

Density

Density of the concrete is can be regulated on the stage of fresh mixture preparation through the average density of composed materials. The density of a fresh concrete batch is measured in accordance

with ASTM C138 and it is theoretically defined as the mass to volume ratio (ASTM C138, 2014). For measuring fresh mixture density, a container of known volume and weight is filled to the brim with the freshly prepared concrete mixture. The fresh mixture was rodded to compensate the possibility of excessive loss in entrained air (ASTM C138, 2014).

Temperature

Temperature of fresh concrete mixture was measured in accordance with (ASTM C1064, 2012). The standard defines the types and precision of temperature measurement devices required to use. using a standard glass thermometer or resistance thermometers, to the nearest 0.5°C. Moreover, the size of the sample plays a role in overall temperature change. According to ASTM C1064, the smaller the sample, the greater the temperature loss or gain from the surrounding (ASTM C1064, 2014). Concrete mixture sample should be large enough to allow a minimum depth of 75 mm to surround the thermometer. Any aggregate size 12.5 mm or greater might cause the thermometer to obtain an equilibrium reading at a longer period. A thermometer was placed in different location of the mixture after the mixing process is complete and average reading of the temperature is reported.

3.4.1.2 Hardened Concrete Properties

Compressive Strength

Compressive strength of concrete can be defined as the maximum compressive strength a concrete specimen withstands when loaded to failure. In this study, cylindrical specimens Ø100x200 mm are compressed along their longitudinal axis. Each cylinder side was surface ground using a diamond grit grinding disc having about2mm cut-off per side. This ensures even distribution of the load applied on the cylinder surface. The cylinders were saturated surface dry before each test. An average of 3-cylinder compression tests are used to define the structures compressive strength at 28 days from casting (ASTM C39, 2016). The compressive strength (F_c) of the cylinder is calculated using the following equation:

$$F_c = \frac{P}{\pi r^2} \qquad \text{Eq. 3.4.1-1}$$

Where F_c in N/mm^2 is the compressive strength, P in Newtons is the failure load and r is radius of the cylinder in mm.

All cylinders were tested according to *ASTM C39 Standard Test Method for Compressive Strength of Cylindrical Concrete Specimens* (ASTM C39, 2016). The compression machine, shown in below Figure 3-2, has a maximum capacity of 3000KN with an applied loading rate maintained at 0.25 MPa/s for every test. At 7 days from curing, some cylinders were used to assess the compressive strength of each mixture.

Figure 3-2: Forney Compression Machine Used for Determination of Compressive Strength

Flexural strength

Flexural strength (F_t) of the specimens was determined using (ASTM C1609, 2012). The maximum flexure strength of a concrete prism is determined through the first peak load facture of the concrete prism. The test comprises a 100×100×350 mm simply supported concrete beam under third-point loading as shown in Figure 3-3.

$$F_t = \frac{PL}{bd^2} \qquad \text{Eq. 3.4.1-2}$$

Where F_t is the flexure strength in MPa, P is the applied force in Newtons, L is the effective span length in meters, and b and d are the prism width and effective depth in millimetres.

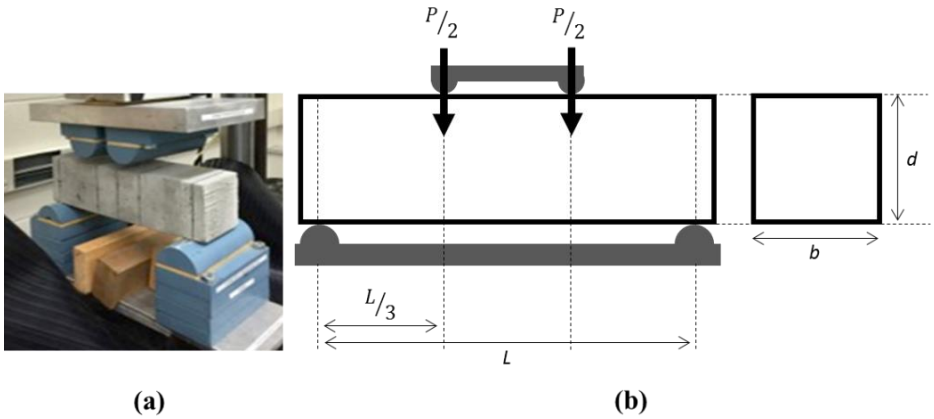

Figure 3-3: a) Third point loading test setup b) Flexure loading schematic (adapted from ASTM C1609)

3.4.2 Resonant Frequency Testing

Impact resonant frequency testing was performed in accordance with *ASTM C215 Standard test method for fundamental transverse, longitudinal and torsional resonant frequencies of concrete specimens* Figure 3-4. Although ASTM C215 states that this technique is for concrete specimens, the testing procedure could be carried out on paste and mortar specimens correspondingly. All prismatic concrete specimens were tested in transverse, longitudinal and torsional modes while the cylindrical specimens were tested in transverse and longitudinal modes. Although it is achievable to test the torsional mode of a cylinder with a 90˚ tab to align the accelerometer perpendicular to the curved surface, the curved surface of the cylinder and small aspect ratio makes it complicated to separate the torsional fundamental frequency from the transverse mode of excitation.

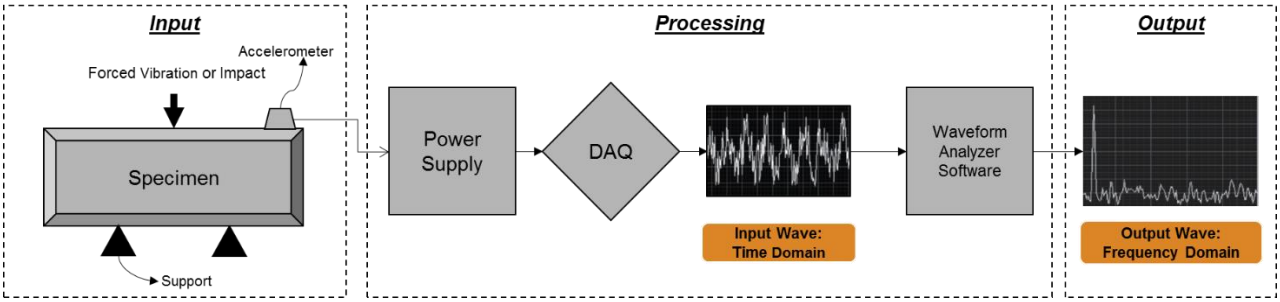

Figure 3-4: Resonant Frequency Testing using Impact Method

Throughout transverse mode excitation, the specimen were supported at their defined nodes along the fundamental flexural bending mode positioned 0.224 multiplied by the length (L) of the specimen from both the sides of the specimen. The impact is released at center of the sample parallel to the accelerometer placed on the same surface to simulate a simply supported bar. Longitudinal and torsional modes were setup by applying the specimens at a center node support ($0.5L$) with the accelerometer being perpendicular to the impact. For nodal support, neoprene bars 150x25x8 mm length, width, and thickness respectively were position as shown in Figure 2-3. Figure 3-5 shows the prismatic and cylinderical setup for each mode of vibration.

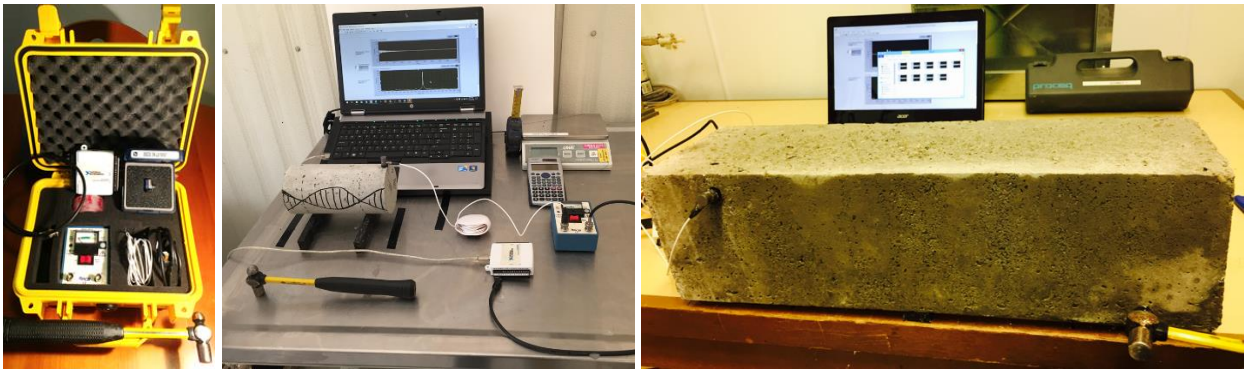

(a) **(b)** **(c)**

Figure 3-5: (a) Resonance Frequency Testing Equipment (b) Setup for cylindrical specimen (Transverse mode) and (c) Setup for prismatic specimen (Torsional mode)

Primarily, a PCB Integrated Circuit Piezoelectric (ICP©) accelerometer, with a pickup sensitivity of 102.2 mV/g (10.2 mV/ms^{-2}), and frequency range of 0.3 – 15 kHz, is attached to the concrete surface using microcrystalline adhesive wax. The accelerometer Model 352C33 was manufactured by PCB electronics. The attained time domain signal was amplified and passed through a low pass filter cut-off

frequency at 10 kHz. Table 3-6 shows the properties of the uniaxial accelerometer used for this study. The input compression wave voltage is collected using a 4 channel NI USB6009 DAQ with a built in Analog to Digital Convertor (ADC). After attaching the accelerometer and positioning the concrete samples to the required mode of testing, a standard ball tip hammer weighing 110 ± 2 grams with a tip diameter of 10 mm, is used to strike the surface at precise locations on the samples being tested.

Table 3-6: Accelerometer Specifications

Type	**PCB - ICP©**
Model	352C33
Height	15.7 mm
Weight	5.8 g
Sensitivity	10.2 mV/(m/s^2)
Frequency Range	0.3 – 15000 Hz
Non-linearity	<1 %
Transverse Sensitivity	<5 %
Temperature Range	-54 to 93℃

The FFT requirements are modeled in a visual instrument (VI) program using National Instrument's LabVIEW 2014 (NI LabVIEW). The program was exclusively developed for this study considering (ASTM C215, 2014) for acquisition requirements. Exponential windowing and averaging, along with a discrete frequency domain, were examined to ensure output noise reduction and coherence. All waveform acceleration responses were digitized in the time domain to 1024 samples at a sampling acquisition rate of 20 kHz. The sampling rate of a data acquisition system should be large enough for determining the highest predicted frequency to fulfill the Nyquist frequency. This led to a signal response time of 51.2 ms along with a sample interval (SI) of 25 μs. The spectral line spacing in the frequency domain, or digital step, is 19.5 Hz and the Nyquist frequency for the response is 10 kHz.

From the output amplitude-frequency graph, the first amplitude peak value verifies the natural resonant frequency according to the tested mode of vibration. The RFT tests were performed three times and averaged for all modes of vibration for each specimen. Any results deviating 10% from the mean frequency are disregarded and the test was repeated. Dynamic elastic and shear moduli are calculated according to the equations described in Section 2.4.3 for impact resonant frequency testing.

For all cases, the specimen orientation was kept constant during testing to ensure that any changes observed in the specimen vibration response would not arise from changing the testing setup. Transverse vibration was carried out parallel to the direction of casting for all concrete prisms and perpendicular for all concrete cylinders. This was maintained to ensure that the dominant vibrational thickness is accounted for in the transverse vibration of prisms and longitudinal vibration of cylinders. When testing concrete through multiple impacts, the surface may crumble. For reliable practice suggested by (Malhotra and Carino, 2004), consecutive readings are measured at the same contact location of the hammer on the concrete surface and omitting the first two readings from the measured set to remove anomalies. The mode of vibration and equivalent resonant frequency for each mode are reported to nearest 10 Hz while the dynamic modulus of elasticity and dynamic modulus of rigidity are calculated to the nearest 0.5 GPa. In addition, the dynamic Poisson's ratio is reported to the nearest 0.01 ratio.

3.4.3 Induced Crack RFT Testing

Figure 3-6 shows the *Standard Crack Inducing Jig* (SCIJ) developed by (Gupta and Biparva, 2015). This jig houses a Ø100x200 mm cylinder between v-shaped cutting edges that act as stress concentrators. Ideally, the SCIJ develops cracks ranging 0.1 – 0.5 mm in width. For achieving a consistent crack, the authors recommended that the ideal age to induce cracks is between 2-3 days of curing. This is due to the fact that that at earlier age (E.g. 1 day of curing), the concrete fractures in a ductile manner. While at later ages (E.g. 28 days of curing), the crack fracture behaves in a brittle manner. However, it is recommended by the authors to investigate the cracking of each mixture on sample cylinders to ensure a consistent crack width. Hence, the aim of Batch 3 is to investigate the recovered dynamic moduli of macro and micro PFRC during two curing regimes prior to crack induction. For constant testing, the uniaxial tension is terminated as the concrete cylinder cracks for maintaining a constant crack width. With pilot investigation of the suggested cracks for the concrete mixture of this study, cylinders were cracked at 14 days.

The crack generated by the SCIJ should be measured from each face of the concrete cylinder. An average of five readings of the crack width were taken for each sample. After cracking the cylinder, the RFT was carried out again, in Transverse mode, having the impulse direction perpendicular to the indentation line to capture the full plane of cracking. Subsequently, the cracked PFRC cylinder was tested in the longitudinal mode as shown in Figure 3-6 (c). Since the crack area is along the longitudinal dimension of the cylinders, the expected longitudinal vibration may be inconsistent to interpret in the frequency domain. By that, the longitudinal frequency variation may not indicate a notable change. All cracked cylinders are positioned in the same orientation for transverse and longitudinal testing. During testing, signal variations can occur due to external vibration, insecurely supported cables, or by disturbance in the accelerometer. Any frequency measurements that deviated by 10% from the average value were disregarded and the test was repeated.

(a) **(b)** **(c)**

Figure 3-6: Setup for cracking (a) SCIJ Front view (b) cylinder held in SCIJ Isometric view (c) Longitudinal Impulse Direction Setup

3.4.4 Microscopic observation

Microscopic imaging in this study followed the procedures as outlined in ASTM C856 '*Standard Practice for Petrographic Examination of Hardened Concrete*' (ASTM C856, 2017). During concrete repair, rubble and concrete shattered pieces are considered useful for petrographic examination of concrete mixtures. Yet, as recommended by ASTM C856, imaging concrete at from its original state of unaltered deterioration, similar to cracks developed in this study, clearly demonstrate the nature of crack propagation. Cracks developed in this study are imaged as discussed in Section 3.4.3. Images were captured from a concrete surface area (78.55 cm^2) when compared to the crack size distribution (4.1 cm^2) of the same surface. When handling the cylinders, no forceps or external tools were used to handle the cylinders after crack induction.

For petrographic imaging, a Firefly® GT800 digital microscope was used to observe and locate the bridging mechanism of macro and micro polypropylene fibers after cracking. The microscope is equipped with a 2-megapixel camera having a maximum working distance of 200 mm along with an optical magnification up to 160X and 500x digital magnification). The handheld microscope allows for cracks to be imaged from the PFRC surface as shown in Figure 3-7 that were cracked using the setup shown in Figure 3-6. For locating fibers with active crack bridging, images were captured at a working distance of 14 mm having a field of view of 5.4 mm × 4.1 mm. The cylinders were surface ground prior to cracking for an attempt to locate polypropylene fiber bridging in the depth of the crack. Images were captured using a standard video imaging software and the microscope was calibrated using a universal calibration slide.

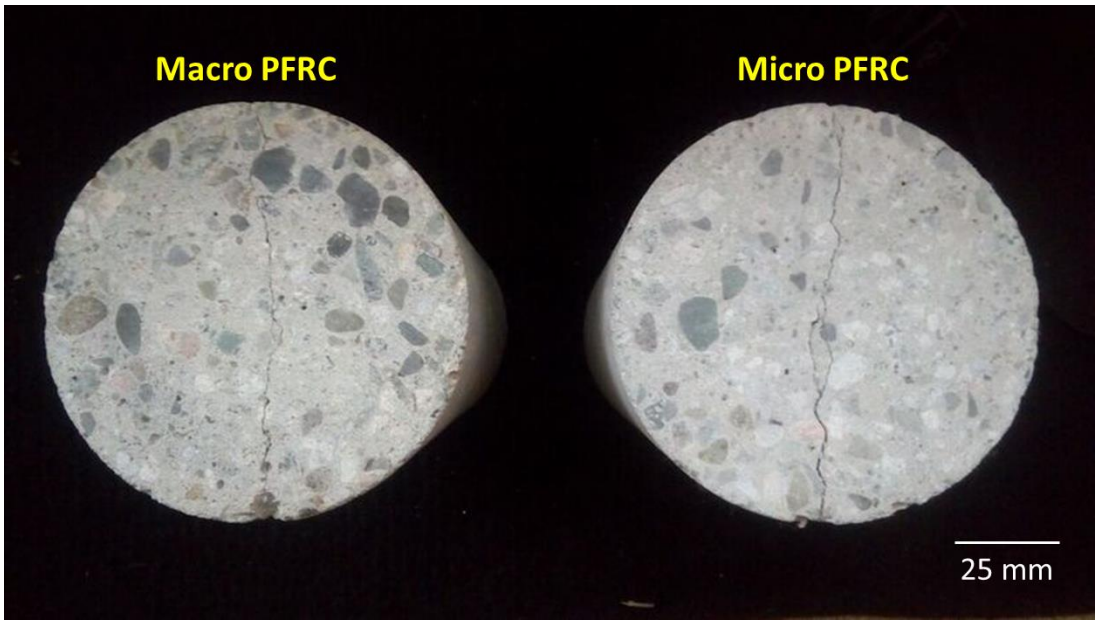

Figure 3-7: Typical crack propagation for macro and micro PFRC

3.5 Repeatability and Validation

The resonant frequency method has been used by several researchers as a reliable method for monitoring changes in concrete properties and for carrying out repeatable tests using the same concrete specimen (Kolluru et al., 2000; Malhotra and Carino, 2004; Li and Yang, 2007; Ward et al., 2008; Popovics,

2008; Noguchi et al., 2009; Giner et al., 2012; Lee et al., 2015). For consistently determining the resonant frequencies, several measurements have been performed throughout this study to inspect and validate the repeatability of impact testing. The transverse mode of vibration was investigated in this section using a cylindrical (Ø100x200 mm) plain concrete specimen as the representative sample. Reference aluminum cylinders were tested for evaluating the transverse and longitudinal resonant frequencies in comparison with the predicted elastic modulus. Since aluminum is an isotropic homogenous material when compared to concrete's true heterogenous and anisotropic nature, a comparison between the experimental and theoretical value of aluminum is expected to indicate the reliability of the experimentally determined elastic moduli. All tests were conducted at an ambient temperature of 21 ± 2 ˚C. The findings from these measurements are intended to enable a practical implementation of IRM.

3.5.1 Effect of Impact Force Variation

For this study, the effect of varying the impact force was used to investigate any variation in the resonant frequency and force amplitude determined from a frequency response function. Force variation was applied by noting three light impacts, three medium impacts and three hard impacts with a load approximately <0.5V, <1V and >2V (Volts) respectively as shown in Figure 3-8. For harder impacts, the compression wave experiences more forced vibration when compared to light and medium impacts. Therefore, a wave delay can occur as shown in Figure 3-8. This can arise from the brittle nature of the concrete surface during the impact and from the pick up voltage range of -5V to 5V. An average of the frequency response function is determined for each impact. The representative cylinder is setup in transverse mode as presented in Figure 2-3. For reliability, the accelerometer was carefully positioned and attached without being removed during the force variation testing. A similar repeatability study was published by (Gudmarsson, 2014) on disc-shaped asphalt concrete considering force variation, accelerometer reattachment, accelerometer position and equipment operator as repeatability parameters on the same specimen.

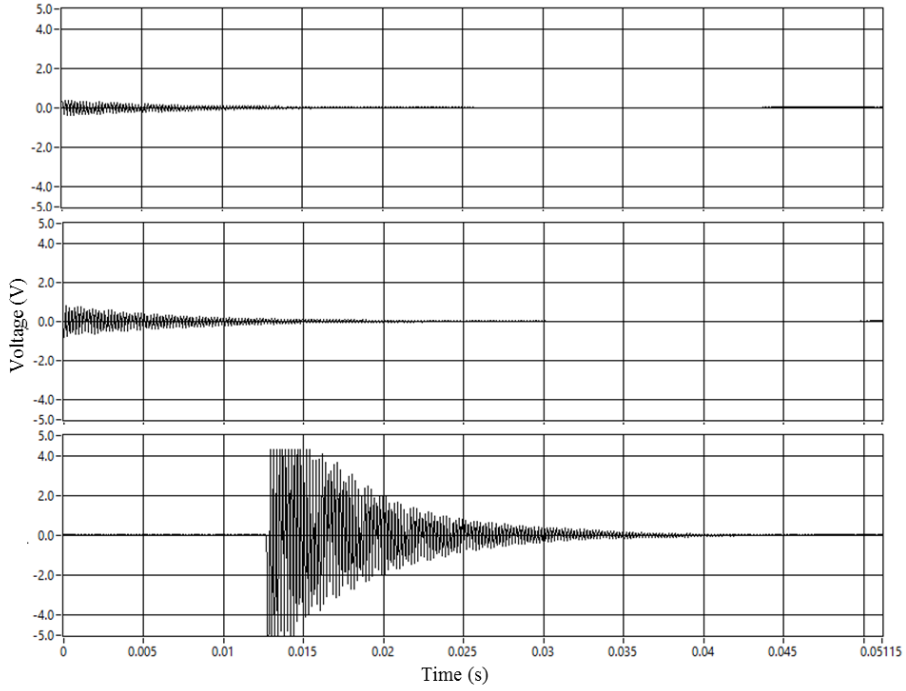

Figure 3-8: Representative light (top), medium and hard (bottom) impacts

3.5.2 Effect of Accelerometer Attachment Variation

Connection Type

Different types of adhesives to attach the accelerometer were investigated in this study. The types of attachments used are adhesive wax, double-sided tape, superglue and melted wax.

Attachment/Reattachment

The process of attaching and reattaching the accelerometer on the same concrete cylinder was investigated. Using the recommended connection type, adhesive wax, this test was carried out to ensure that the processed frequency response is the same. The test was conducted on four consequential trials. Each attachment was properly secured and the surface was cleaned from any wax residue prior to reattachment.

Location

Modal testing of the same cylindrical specimen was conducted on four different locations 90˚ apart on both sides of the cylinder. Differences that can be inferred from this test is that possible inhomogeneity with in the PFRC cylinder and variation in geometry due to casting may introduce differences in both the detected wave acceleration and resonant frequency. The accelerometer position scheme is shown in Figure 3-9. Impacts for transverse vibration are similarly induced in the center of the specimen coincident to the location of the accelerometer in transverse mode as shown in Figure 2-3.

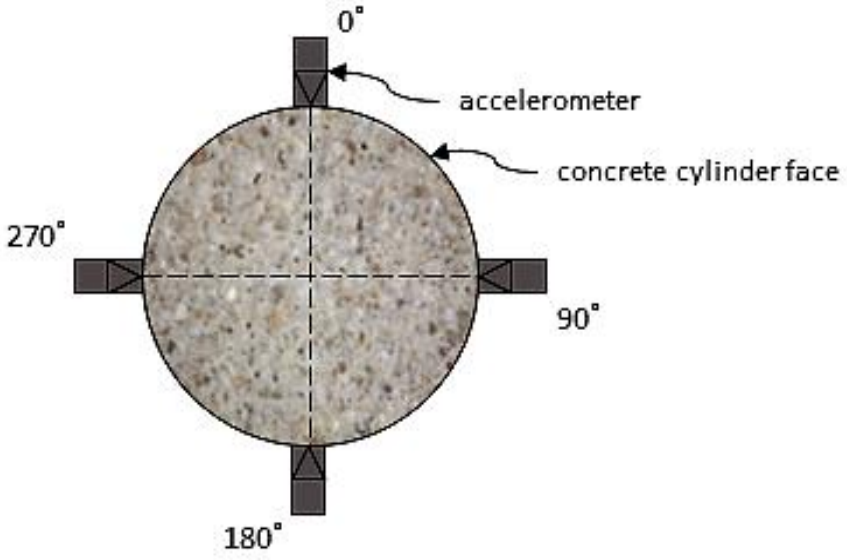

Figure 3-9: Accelerometer location on concrete cylinder

3.5.3 Validation with Isotropic Material

Two aluminum solid 6061-T6 cylinders with the same dimensions as the concrete cylinders used in this study (Ø100x200mm) were used to determine any discrepancies when testing the frequency response of the concrete. The aluminum cylinders differed in length by 3 mm. Researchers conducted several tests of concrete's resonant frequency by correlating the properties with a nominally linear elastic and isotropic material (Kolluru et al., 2000; Malhotra and Carino, 2004; Popovics, 2008). Manufacturing of the aluminum cylinders is in accordance to ASTM B221 specification of extruded aluminum bars (ASTM B221, 2014). Figure 3-10 shows the control aluminum cylinders and a representative concrete cylinder. Appendix A includes the aluminum cylinder material properties.

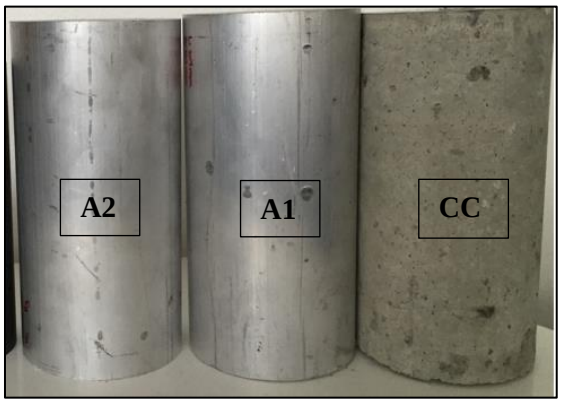

Figure 3-10: Validation of Testing with Isotropic Specimens

The aluminum cylinders were tested in transverse and longitudinal modes as shown in Figure 2-3. A precursor test to identify if the aluminum resonant frequencies showed that aluminum (100x200 mm) cylinders experience a first mode longitudinal resonant frequency outside the Nyquist range of 10 kHz. Thus, the sampling rate and number of samples taken (N) were adjusted to 40 kHz and 2048 samples respectively to maintain a consistent frequency resolution.

3.5.4 Validation with Existing Models

For designing concrete structures, usually concrete compressive strength (f_c), and static modulus of elasticity (E_s) are recommended by design codes. Yet, for field measurement, structure condition and concrete quality assessment, the dynamic modulus of elasticity (E_d) is commonly used. Some models have been developed by (Balendran, 1993; Han and Kim, 2004; Popovics, 2008; Neville, 2012; Zhou et al., 2015) which provide a relationship between the pre-mentioned moduli based on multiple design parameters such as *w/c* ratio, curing condition and aggregate size and volume.

The static modulus of elasticity can be estimated from its compressive strength. The relationship between f_c and E_s is recommended by numerous standardized guidelines shown in Table 3-7. These models are used along with linear E_d estimation from E_s to assess the experimental E_d longitudinal moduli and compressive strength.

Table 3-7: Existing models based on the relationship between the compressive strength, static and dynamic moduli of elasticity of concrete

Reference	Equation	Units
ACI 318	$E_s = 4700\sqrt{f_c}$	E_s: MPa f_c:MPa
ACI 363	$E_s = 3300\sqrt{f_c} + 6900$	E_s: MPa f_c:MPa
CSA A23.3	$E_s = 4500\sqrt{f_c}$	E_s: MPa f_c:MPa
EC-2	$E_s = 22(\frac{f_c}{10})^{0.3}$	E_s: GPa f_c:MPa
(Noguchi et al., 2009)	$E_s = 3.35\times10^4(k_1.k_2)\left(\frac{\rho}{2400}\right)^2(\frac{f_c}{60})^{\frac{1}{3}}$	E_s: GPa f_c:MPa k_1 & k_2: experimental constants
(Neville, 2012)	$E_s = 1.25E_d - 19$	E_s: GPa E_d:GPa
(Balendran, 1993)	$E_s = 0.83E_d$	E_s: GPa E_d:GPa
(Popovics, 2008)	$E_s = \frac{446.09{E_d}^{1.4}}{\rho}$	E_s: GPa E_d:GPa ρ: kg/m^3
(Jin and Li, 2001)	$E_d = 7.077(f_c)^{0.4467}$	E_d: GPa f_c:MPa

These models estimate (E_s) using empirical equations and the experimental dynamic modulus of elasticity results. They also define the static modulus of elasticity (E_s), using the compressive strength, density, and/or dynamic elastic modulus properties of concrete. The models were chosen for their practical reliability for comparison of concrete specimens however, empirical equations may be inaccurate when compared to direct measurement values. Some codes may have an error of estimation up to 60% with low strength concrete (Yildirim, 2011).

The ratio of the static to dynamic modulus of elasticity increases with higher concrete strength (Popovics, 2008). Popovics proposed the best prediction of the dynamic modulus of elastic of high strength concrete (Popovics, 2008). Also, the method advised by (Swamy and Rigby, 1971) provides a relation between the static (E_s) and dynamic (E_d) elastic modulus of concrete (Neville, 2012). Currently, the equation is addressed in the British Testing Standard – BS 1992-1-1:2004 (British Standard BS EN 1992-1-1, 2004). This equation does not apply for lightweight concrete and concrete having more than 500 Kg/ m^3 of cement (Neville, 2012; Popovics, 2008).

(Noguchi et al., 2009) model estimates the elastic modulus of concrete by statistically analyzing more than 3000 datasets from various types of concrete considering the types of coarse aggregates, mineral admixtures, and density of concrete. The authors defined a correction factor, K_1, in their equation considering the effect of different types of coarse aggregates on the modulus of elasticity of concrete, as reported in Table 3-8.

Table 3-8: K_1 values (Noguchi et al., 2009)

Lithological Type of Coarse Aggregate	K_1
Crushed limestone, calcined bauxite	1.20
Crushed quartzitic aggregate, crushed andesite, crushed basalt, crushed clayslate, crushed cobblestone	0.95
Other	1.00

In addition, (Noguchi et al., 2009) added admixtures for the second correction factor (K_2). Table 3-9 presents the practical corrections factors for K_2 of mineral admixtures.

Table 3-9: K_2 values (Noguchi et al., 2009)

Mineral Admixture	K_2
Silica Fume, Ground Granulated Blasted Furnace Slag, fly ash fume	0.95
Fly ash	1.10
Other	1

Different empirical relations in defining properties of a specified concrete type do not usually agree with each other. In fact, values of the dynamic modulus of elasticity fluctuate significantly according the size, type and testing methods of specimens (Popovics, 2008). According to ASTM C215, different values of the dynamic modulus of elasticity may result from a variety of factors including specimen mode of vibration, resonant frequencies, shapes and sizes. Hence, it is not suitable to equate results from different specimen vibration modes and geometry (ASTM C215, 2014). Therefore, it is challenging to select the optimum equation with the least errors for prediction of the modulus of elasticity of concrete with different specimens and dynamic tests.

3.6 Summary

This chapter reflects the tests carried out on polypropylene fiber reinforced concrete, specifically prismatic and cylindrical specimens. The purpose of the performed experiments was to assess the changes in the dynamic modulus of elasticity using resonant frequency testing, when two types of polypropylene (macro and micro) fibers are added to concrete. The tests were divided into three batches: Batch 1 examines the effect of changing the volume content of macro fibers on concrete. Batch 2 examines the effect of micro fibers on concrete based on the age of curing. Batch 3 examines the effect of induced cracks on the resonant frequency of polypropylene fiber reinforced concrete. For Batch 3, microscopic imaging was conducted to observe macro and micro fiber bridging after cracking.

Furthermore, a repeatability study is included taking into account the effect of impact force variation, accelerometer position, reattachment and attachment type. For validating the experimental results, a homogenous material (aluminum) was chosen to account for variations when testing the heterogenous composite (concrete). Other experiments in this chapter were conducted to obtain an overview of the effect of polypropylene fibers on the static modulus of elasticity and flexural strength. For numerical validation of the elastic moduli, existing models are used, considering concrete density, compressive strength, aggregate type and mineral admixtures. Additional tests are required to obtain more comprehensive information on the effect of polypropylene fibers in the relationship between the static and dynamic modulus of elasticity and on the performance of polypropylene fibers in concrete when using fly ash or other SCMs. Results of the experimental program are presented in the following chapter.

4 Results and Discussion

The following chapter is divided into three categories. Section 4.1 covers the standard concrete properties of each of concrete mixture which include the fresh properties: workability, air content, concrete density, fresh mix temperature and properties of hardened concrete: compressive and flexure strength. Section 4.2 covers the repeatability and validation testing of IRM. Section 4.3 covers the resonant frequency properties of all mixtures discussed in Section 2.4.2 including the calculated dynamic elastic properties of PFRC prisms and cylinders.

4.1 Standard Concrete Properties

4.1.1 Fresh Concrete Properties

Workability

Workability of all concrete mixtures are defined using the slump test according to (ASTM C143, 2015). Table 4-1 shows the slump values calculated for Batch 1, Batch 2, and Batch 3. All plain and fiber reinforced concretes are within the required slump range 120 ± 40mm. For all mixtures with added fibers, the slump decreased significantly when added to concrete during mixing. As the fiber volume increases, the deformability of a fresh FRC mixture decreases irrespective of the type. A low slump value is common for FRC, when compared to plain concrete mixtures of the same mixture having the volume fraction of fibers as the dominant variable (Kakooei et al., 2012). Nevertheless, macro fibers used in Batch 1 and Batch 3 exhibited a higher slump than micro fibers. This arises from compensation of lost fluidity, of the mixture from fiber addition, when WRA was added.

Fresh FRC mixtures with polypropylene micro fibers exhibited a lower slump than that of macro fibers. When added to a fresh concrete mixture, microfibers decreased the water content of the binder thus decreasing the workability. Microfibers decreases concretes workability due the large surface area available for retaining water and the fiber's hydrophobic nature. Hence, a percentage of 0.3% micro fiber was used, when compared to 0.6% macro fibers. On the other hand, polypropylene macro fibers were harder to consolidate and finish within the molds. As practiced in industry, adjusted WRA values were increased as the fiber content increases to maintain regular workability. For Batch 2 micro fibers, no WRA was used showing the subsequent affect on the workability of FRC. Batch 3 macro and micro fibers showed an average slump value of 110 ± 5 mm where the adjust WRA content was used in Table 4-1.

Air Content

The air content was measured as an approach to detect any unbalanced air distribution. Improper air distribution in the mixture could result in production stage errors or defects during service period. The resulting air content of all batches are between 3-7% in accordance with (ASTM C231, 2014). In Table 4-1, for Batch 1, CC1 mixture may have higher air content due to the mixer reaching its maximum capacity. Yet, the higher air content did not show any effect on the measured workability of the concrete, resulting in homogenous air distribution.

Density

Density values are within the standard range of normal-weight concrete ~2,300 Kg/m^3 in accordance with (ASTM C138, 2014). All concrete mixtures are within normal range between 2,200 and 2,450 kg/m^3. However, an increase in the air content decreased the concrete density when fibers were added. This can be explained by the increase in porosity when fibers were added.

Temperature

Mixture temperature for all batches is tested in accordance to (ASTM C1064, 2012). Batch 1 and Batch 3 temperature measurements were taken in Winter, while Batch 2 measurements were taken in Summer.

Table 4-1: Fresh Concrete Properties

Batch	**1**			**2**		**3**	
Mixture ID	CC1	FRC-A	HFRC-A	CC2	FRC-B	FRC-A	FRC-B
Concrete Type	0% Fiber	0.6 % Macro PP	1% Macro PP	0% Fiber	0.3% Micro PP	0.6 % Macro PP	0.3% Micro PP
Slump (mm)	110	130	135	110	90	120	110
Air Content (%)	6.8	4.2	4.6	6.5	4.5	6.6	5.8
Density (kg/m^3)	2432	2408	2407	2294	2239	2216	2267
Temperature (˚C)	5.3	5.5	5.2	15.3	15	9.2	9.8
WRA (kg/m^3)	1.883	1.883	2.389	-	-	1.225	1.225

4.1.2 Hardened Concrete Properties

Compressive Strength

Compressive strength of concrete cylinders from each mixture were measured according to ASTM C39 (ASTM C39, 2016). Inclusion of both macro and micro polypropylene fibers has no substantial effect on concrete compressive strength. Addition of fibers marginally decrease the compressive strength compared to the control concrete CC1 and CC2. The reduction furthers when the volume fraction of fibers increases as noted from Batch 1. Table 4-2 outlines the average compressive strength of each mixture at 28 days from casting. Compressive strengths are relatively equal for all batches except Batch 2 where the w/c ratio was deliberately kept higher to observe the change in strength and elastic modulus. This would enable studying mixtures with two different strengths. An overview of specimen tested for compression is provided in Appendix B.

Static Modulus of Elasticity

Static elastic modulus results of Batch 1 are found in accordance with (ASTM C469, 2014). The results show a notable decrease in the static elastic modulus when fiber content increases from 0% – 1%. The gain in the ultimate compressive stress over strain, of plain concrete, decreases with an increase of fiber content. It should be noted that the static modulus of elasticity and flexural strength testing of Batch 2 and Batch 3 are not carried out since Batch 1 satisfies the scope of the study. In this study, it is assumed that the static modulus of elasticity is considered in this study to be a constant value as shown in Table 4-2.

Flexural Strength

Concrete specimens (100×100×350 mm) were used to measure flexural strength. Fractures occurred in the middle third of the span length during flexural testing. Addition of polypropylene fibers did not significantly change the compressive strength however, the flexural strength of PFRC prisms measured in accordance to ASTM C1609, increased by 5% and 16% when using 0.6% and 1% of macro fibers respectively. The increase in flexural strength is primarily due to the fibers intersecting and bridging the cracks. Figure 4-1 shows the axial deflection against the applied loaded for flexural bending. While the reference plain concrete specimen fractured to splitting, no sustain load was observed after fracture. By using 1% polypropylene fiber in concrete, PFRC fractured about the same load as when using 0.6% polypropylene fibers however, increasing the fiber percentage sustained more deflection before failure. Polypropylene fibers expand by stretching to accommodate cracks hence absorbing additional energy generated in the vicinity of the crack tips. Frequency testing was performed on these specimens prior to

fracturing the prisms. Residual strength, toughness and other flexure parameters are not addressed in this study.

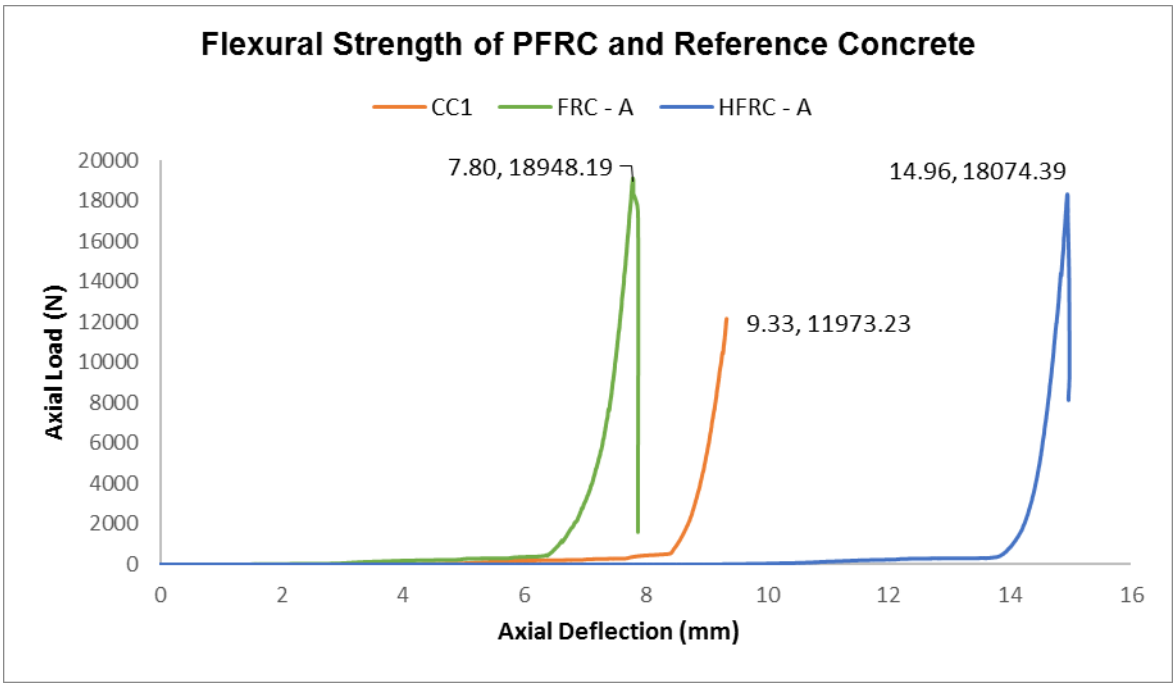

Figure 4-1: Batch 1 - Flexural strength of 0%, 0.6% and 1% PFRC

Table 4-2: Hardened Concrete Properties

Batch	**1**			**2**		**3**	
Concrete Type	0% Fiber	0.6 % Macro PP	1% Macro PP	0% Fiber	0.3% Micro PP	0.6 % Macro PP	0.3% Micro PP
Average Compressive Strength (MPa)	33.21	32.67	30.33	30.34	33.40	31.55	34.91
Static Modulus of Elasticity (MPa)	27957	21075	18245				
Flexural Strength (MPa)	4.19	6.63	6.32				

Microscopic Imaging

Microscopic imaging was conducted as described in Section 3.4.4.. Figure 4-2 shows a hairline crack with an average width of 300 µm imaged at 100X magnification. The images show micro fibers during active crack bridging after uniaxial tension was applied. Fibers imaged from the surface of the crack showed no tearing indicating active bridging up to 300 µm wide cracks.

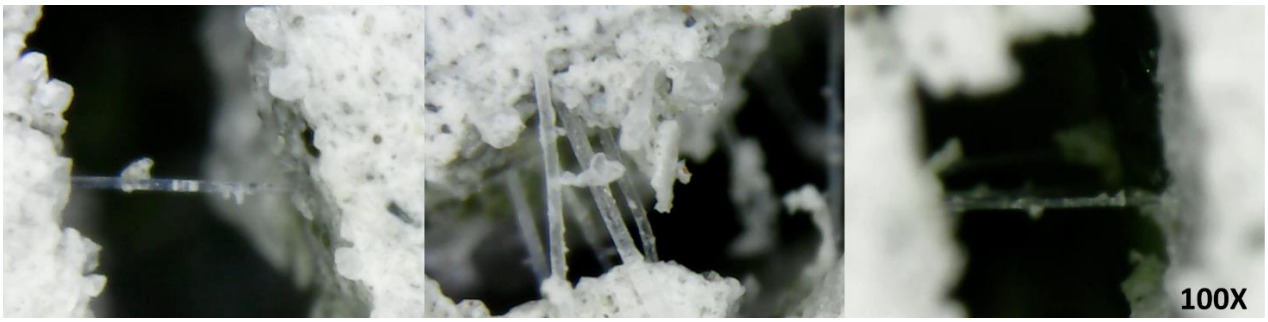

Figure 4-2: Micro fiber crack bridging observed using optical microscopy

Figure 4-3 shows the crack bridging response of macro polypropylene fibers. With an equivalent diameter of 0.5 mm, the macro polypropylene fibers show active crack bridging. When imaging the crack surface, the fibers showed twisting with some tearing observed at wider openings (>500 µm). However, macro fibers showed narrower crack widths when compared to micro fiber. Comparatively, macro fibers show effective crack bridging as the crack width increases.

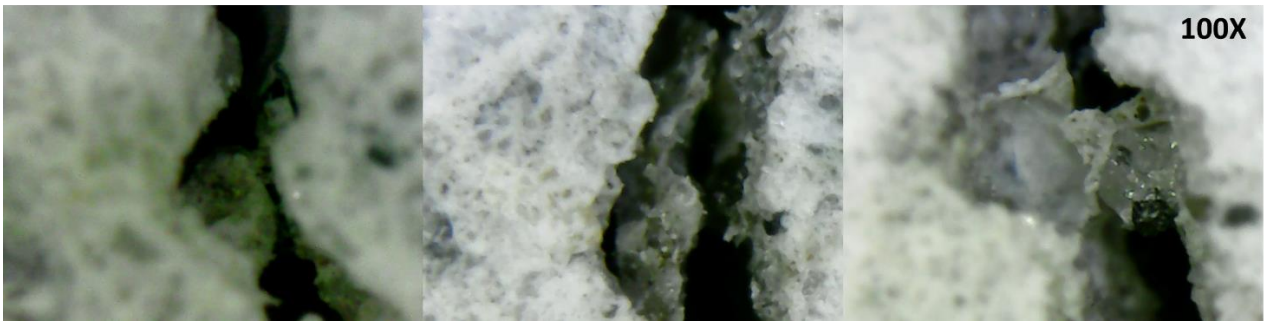

Figure 4-3: Macro fiber nature observed through crack using optical microscopy

4.2 Repeatability

4.2.1 Effect of Force Variation

A series of three hard, three medium and three light impacts were applied to a sample concrete cylinder as discussed in Section 3.5.1. Figure 4-4 shows the resultant frequency response of the impact forces. Response amplitude varied significantly showing a descending trend from high to low impacts. However, the resonant frequency presented clear independence from the applied load averaging at 5265 ± 10Hz. The frequency dispersion of the impacts given by the Coefficient of Variation (CV) is 1.8%. A statistical overview is presented in Appendix D.

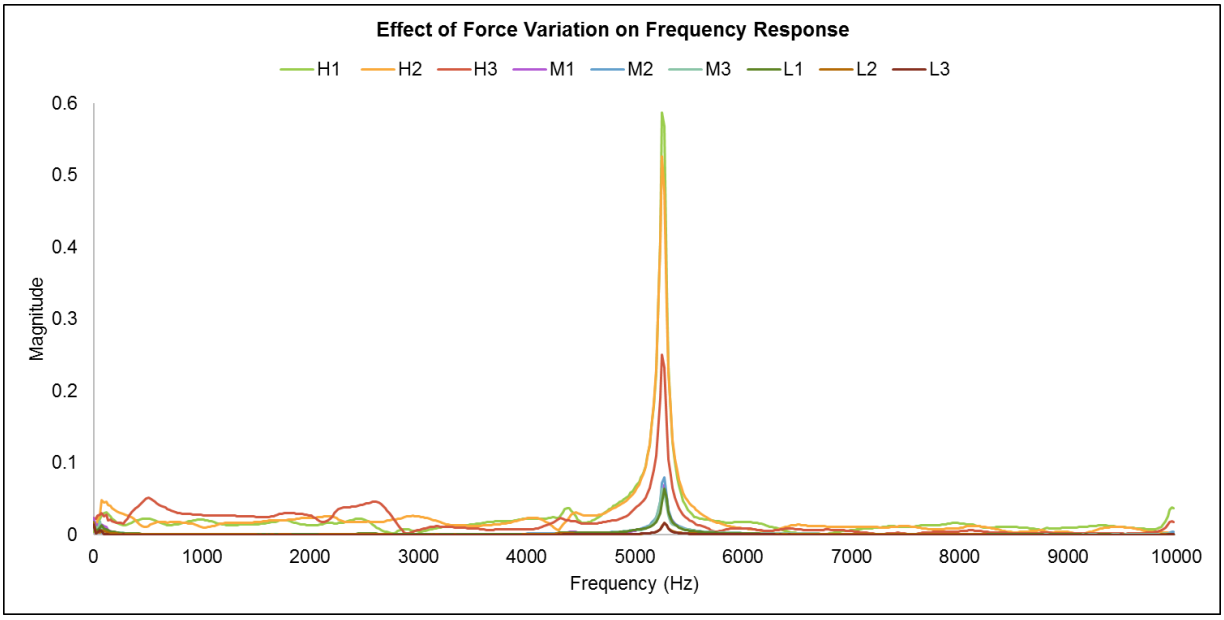

Figure 4-4: Effect of force variation on frequency response

From Table 4-3, the results show that high load impacts resulted in a slightly lower frequency (~20 Hz) than both medium and low load impacts. As high impacts exhibit a higher damping rate, the sampling window may not have captured the full extent of the wave attenuation thus, lowering the detected frequency of the full wave. Note that the frequency resolution of 19.5 Hz is the shift between the lower and higher impact frequencies. The shift will decrease as the resolution is refined. For refining the resolution, the sampling frequency (20 kHz) should be halved (10kHz) while having the same number of samples. Note that by doing this, the required Nyquist frequency domain is also halved (5 kHz). This will affect the result through frequency aliasing and will not detect the true resonant frequency. A sampling rate of 80 kHz can be used with 2048 number of samples; however, the accelerometer is limited to a maximum frequency of 15 kHz.

Table 4-3: Resonant frequency response of high, medium, and low impacts

Impact	High			Medium			Low		
Designation	H1	H2	H3	M1	M2	M3	L1	L2	L3
Magnitude	0.59	0.53	0.25	0.07	0.08	0.06	0.05	0.02	0.02
Frequency (Hz)	5253.91	5253.91	5253.91	5273.44	5273.44	5253.91	5273.44	5273.44	5273.44

4.2.2 Effect of Accelerometer Attachment

Connection Type

Figure 4-5 shows the frequency response by the first mode transverse vibration of a concrete cylinder. Table 4-4 outlines that using adhesive wax, melted wax and superglue indicated the same frequency of 5312.5 Hz while the double-side tape result in a frequency of 5136.7 Hz. This deviation can arise from the curved nature of the concrete cylinder and the minimal contact surface area of the accelerometer stub on the cylinder surface when using the tape. Additionally, the double-side tape exhibited more vibration damping than the other attachments. Consequently, it is important to use a material with reliable adherence and to check for proper accelerometer attachment before testing. A statistical overview is presented in Appendix D.

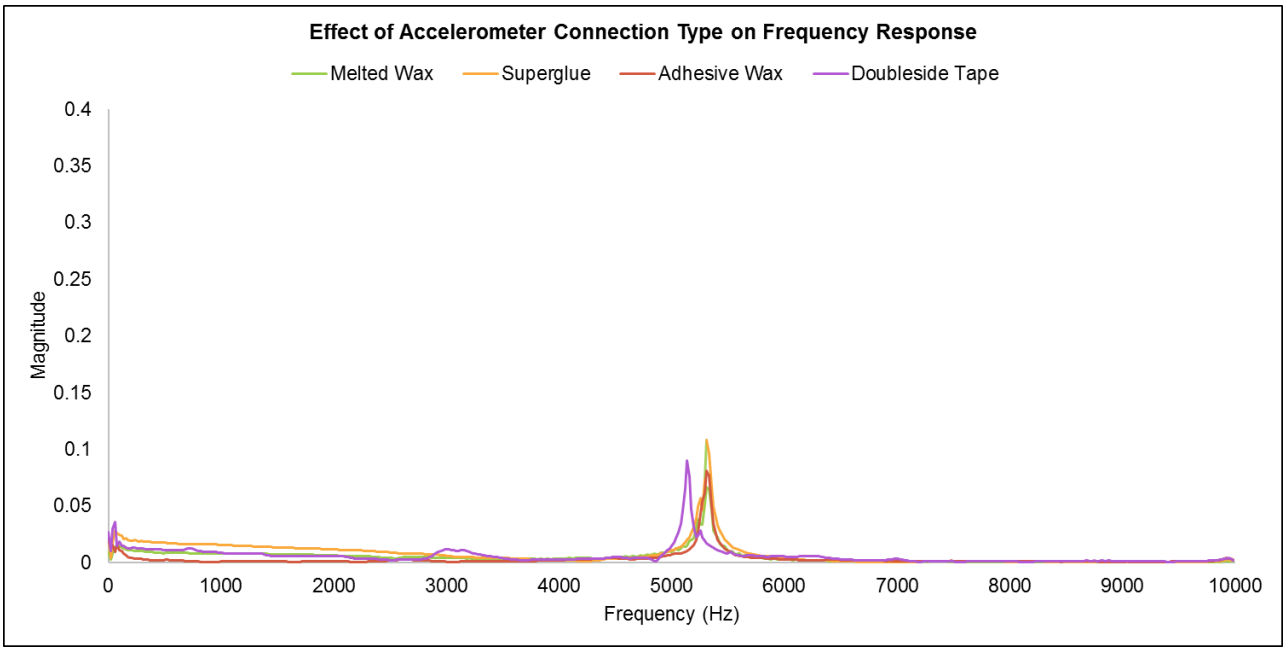

Figure 4-5: Effect of connection type of accelerometer on frequency response

From a perspective of optimal connection with irregular surfaces, using adhesive wax show a strong alignment on concrete surfaces, whether curved or irregular from surface aggregates. This can be indicated by the presences of other indicated frequencies as shown in Figure 4-5.

Table 4-4: Resonant frequency response using different adhesives

Connection Type	Melted Wax	Superglue	Adhesive Wax	Double-side Tape
Magnitude	0.07	0.11	0.08	0.09
Frequency (Hz)	5312.50	5312.50	5312.50	5136.72

Attachment/reattachment

Figure 4-6 shows the effect of attaching, removing and reattaching the accelerometer using adhesive wax as the same adherent connection. The result of for consecutive impacts indicates no deviation for the standard frequency of 5234.4 Hz. Difference between the trials is bound to the frequency resolution. Hence, a finer resolution <19.5 Hz will identify higher deviations.

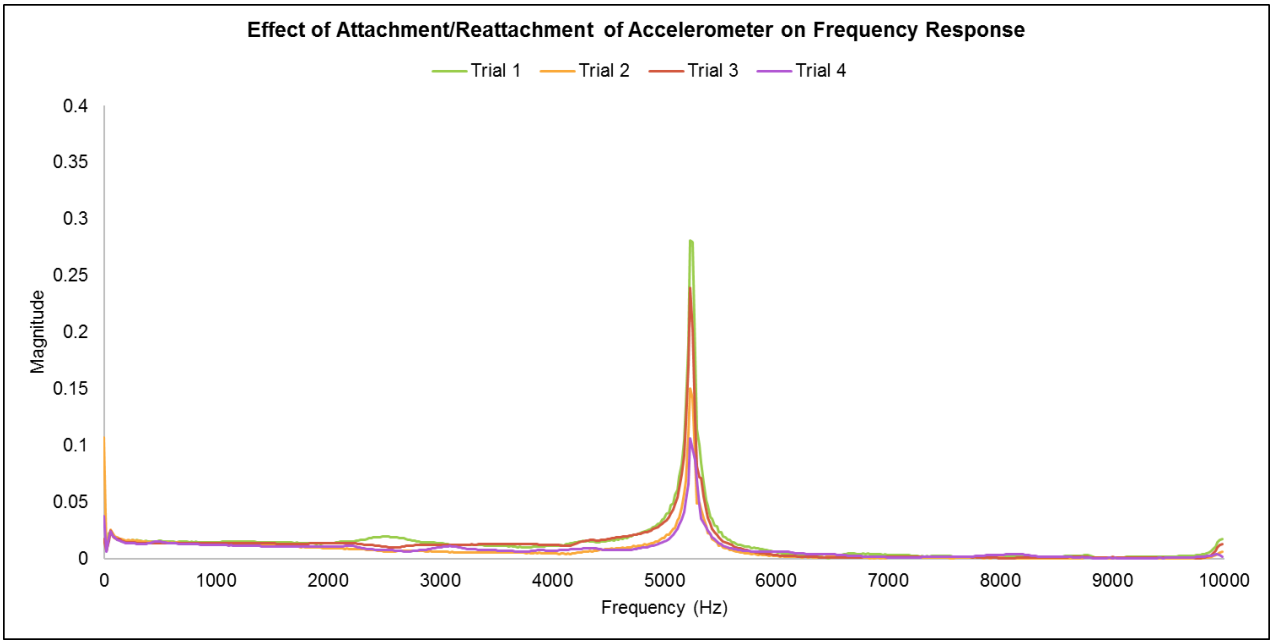

Figure 4-6: Effect of attachment/reattachment of accelerometer on frequency response

Location

Figure 4-7 shows the frequency response of transverse excitation at eight different nodes (four per cylinder side) around a concrete cylinder as described in Section 3.5.2. The magnitude of the frequency response varied significantly for each node. This can result from both the difference in impact load, orientation of accelerometer and differential density in the specimen at the location testing. The average resonant frequency obtained for the nodes is 5288 ± 25Hz for the frequency values shown for each rotation angle in Table 4-5. Difference in the frequency can arise from the composite nature of concrete whereby any difference in specific gravity will cause a shift in the resonant frequency.

Table 4-5: Resonant frequency response by changing accelerometer position

Location around cylinder	0˚	90˚	180˚	270˚
Magnitude	0.08	0.29	0.11	0.31
Frequency (Hz)	5273.44	5312.50	5253.91	5312.50

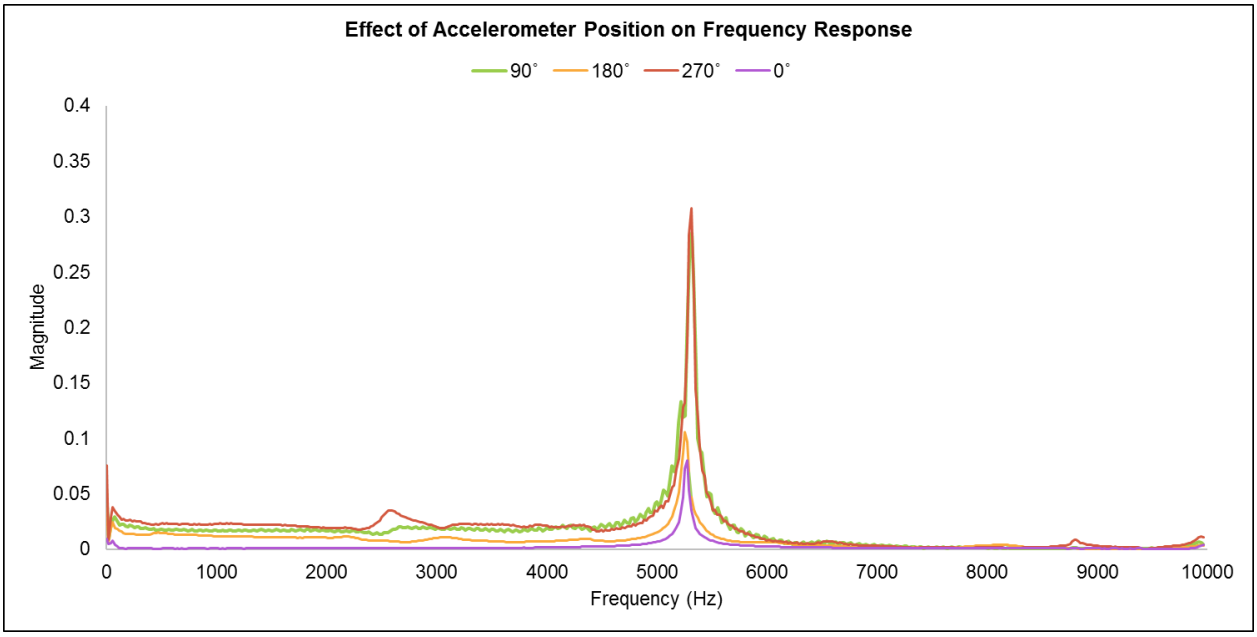

Figure 4-7: Effect of accelerometer position on frequency response

4.2.3 Validation with Isotropic Material

For calibrating vibration measurements, the impact resonant frequency method was applied to a homogenous material (aluminum) with defined material properties. The aluminum 6061-T6 cylinders are geometric replicates of the concrete samples. The transverse and longitudinal modes of vibration are used for measuring the first mode resonant frequency of the cylinders supported according to Figure 2-3. Figure 4-8 shows the resulting frequency response for both modes. Table 4-6 highlights the measured resonant frequencies and calculated dynamic moduli of aluminum cylinders according to (ASTM C215, 2014).

By having a larger vibrating mass, the resonant frequency decreases. The results obtained highlight the frequency drift between two homogenous isotropic materials with slightly different lengths evaluated using the IRM. Thus, correlation between the same concrete mixture should include the dynamic modulus of elasticity as the leading variable since dimensional factors are considered. However, for reliable assessment and a lower variance in frequency, the longitudinal frequency should be primarily used for frequency correlation of composites with of same mixture.

The transverse frequency relies on estimating the Poisson's ratio prior to calculating the elastic modulus. A Poisson's ratio of 0.33 was assumed for aluminum cylinders tested in this study.

Table 4-6: Resonant frequency response and calculated elastic moduli for aluminum cylinders

Aluminum	Length (mm)	Diameter (mm)	Mass (Kg)	L/r ratio	E (GPa)	μ	F_t (Hz)	F_l (Hz)	E_{dt} (GPa)	E_{dl} (GPa)
A1	207	102	4.45	4.06	68±1	0.33	7640	12290	72.16	68.11
A2	204	102	4	4			7660	12460	68.65	68.22

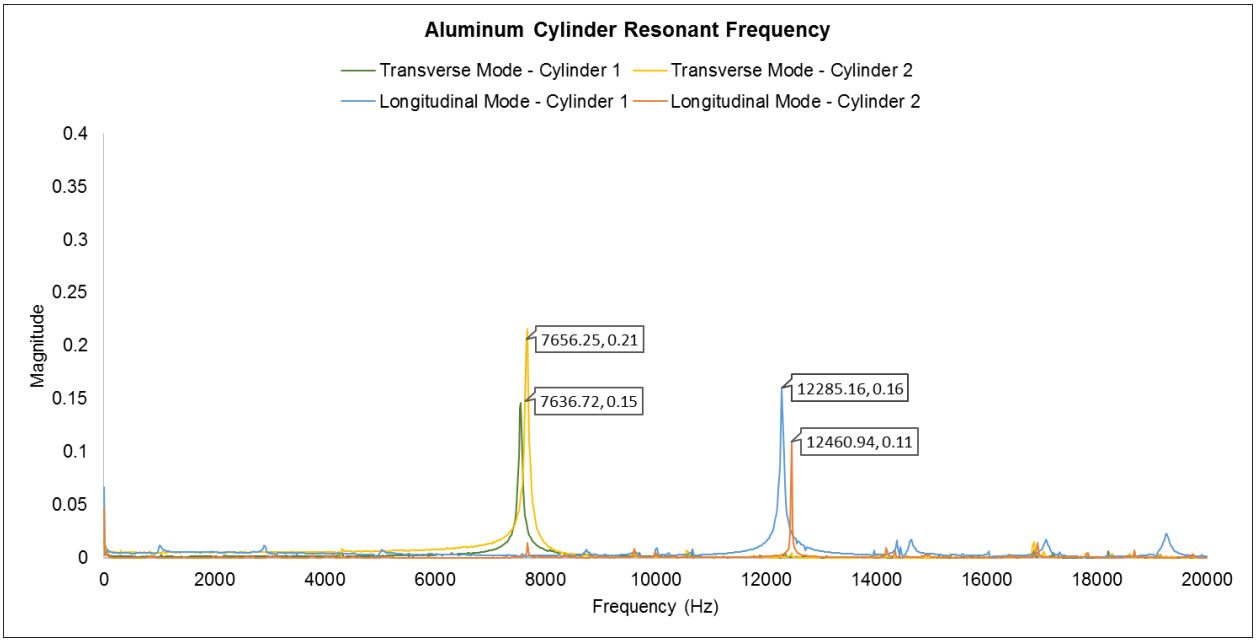

Figure 4-8: Transverse and Longitudinal Frequency Response of Aluminum Cylinders

Both aluminum cylinders exhibit similar properties in the first mode resonant frequencies in the transverse and longitudinal modes of vibration. The difference between the cylinders for the transverse frequencies is 20 Hz while the longitudinal is 175 Hz. Since A1 is almost 3 mm longer than A2, for the same diameter, the elastic modulus increases as the overall mass increases. Amplitudes for the frequency response rely on the impact force applied during testing. The elastic moduli calculated from Section 2.4.3 are proportional to the detected frequencies. Comparing the transverse elastic modulus between A1 and A2 is dependent on the correction factor (T) and therefore shows an over estimation as formerly studied (Popovics, 2008). The transverse modulus using ASTM C215 showed an over estimation of ~2GPa when the L/D ratio was modified. Yet, the longitudinal moduli seemed to be more consistent regarding the ratio. Hence. the L/D ratio is important to consider for comparing the two moduli of the same material.

4.2.4 Summary

The repeatability studies outline several factors to consider when performing IRM. The type of material used for attaching the accelerometer, adherent contact and position may affect the resulting frequency response; hence, affecting the proportional dynamic modulus of elasticity. However, the effect is more prominent on the viscous component of vibration or amplitude. The amplitude is more sensitive to the applied load, accelerometer position and attachment. To maintain controlled resonant frequency testing, the latter should be considered for consistent results. Although, the maximum percentage change in transverse and longitudinal frequencies are 0.69% and 0.13% respectively. Nevertheless, this would result in a percentage change in the transverse and longitudinal elastic modulus of 2.49% and 0.08% respectively. However, it is important to consider that the sample mass and length had a slight difference as noted in Table 4-6. The resulting dynamic elastic values are reliably acceptable given the typical %CV in various concrete related tests.

4.3 Dynamic Elastic Properties of Concrete

This section is divided between the experimentally tested resonant frequency of all batches and the calculated dynamic elastic properties considering concrete mass and dimensional variation. A full layout of the results is provided in Appendix C.

4.3.1 Resonant Frequency

The resonant frequencies for concrete prisms and cylinders of three batches were evaluated using the IRM discussed in Section 2.4.4.2. Tests were conducted according to (ASTM C215, 2014). Resonant frequency results were measured to the nearest 10 Hz as per the standard. In general, the results show that both macro (Type A) and micro (Type B) polypropylene fibers decrease the resonant frequency of PFRC when compared to plain concrete of the same mixture. Moreover, for the same type of concrete, as the specimen size increases, the resonant frequency decreases. Although this study includes lab developed samples that are studied using low impact excitation at higher frequencies, the recognition of frequency variation for any given sample is achievable. Some limitations arise from both averaging and resolution of frequency since there is a finite number of samples, or bins, to generate the frequency domain.

Table 4-7 shows the first mode fundamental resonant frequencies of prismatic specimens in this study. For Batch 1 (100×100×350) and Batch 2 (150×150×550) prisms, the transverse, longitudinal and torsional mode of vibration were tested at 28 days. The results indicate the increase in resonant frequencies with a decrease of the specimen size. Variation in frequency between samples of the same mixture can be a product of difference in a length and frequency resolution. Only prisms were used to measure the resonant frequencies in the torsional direction since cylinder testing exhibits complex support requirements that affect the results.

Table 4-7: Transverse, longitudinal and torsional resonant frequency of PFRC specimens

Batch	ID	Resonant Frequency (Hz)		
		Transverse	Longitudinal	Torsional
Prisms: B1 (100×100×350 mm)/**B2** (150×150×550 mm)				
1	CC1	2823±47	6177±25	3573±35
	FRC - A	2850±105	6100±53	3537±25
	HFRC - A	2703±55	6000±36	3360±72
2	CC2	1650±26	3583±25	2070±0
	FRC - B	1600±26	3440±40	2000±20
Cylinders: (Ø100×200 mm)				
1	CC1	6017±15	9827±231	
	FRC - A	5927±6	9717±146	
	HFRC - A	5577±15	9317±15	
2	CC2	6086±71	9750±53	
	FRC - B	5780±26	9303±80	
3	FRC - A	5760±35	9407±37	
	FRC - B	5943±24	9747± 9	

Batch 1: concrete mixture was used to investigate the effect of adding polypropylene synthetic fiber on the frequency response of concrete by increasing macro fiber volume fraction. No significant

variation in the resonant frequency results were observed for the samples of the same concrete mixture. This is a good indicator for having consistent measurement for each mixture. This is specified by the coefficient of variation (CV), for plain concrete (CC1) <0.02%; yet slightly higher for NFRC and PFRC <0.04%. Figure 4-9 and Figure 4-10 show the resonant frequency measured for control plain concrete (CC1), 0.6% polypropylene fiber reinforced concrete (NFRC) and 1% polypropylene fiber reinforced concrete (HFRC).

From Figure 4-9 and Figure 4-10, addition of 0.6% and 1% fiber slightly decreased the resonant frequency of PFRC. However, this is not the same for CC1 and NFRC prisms as shown in Table 4-7. The resonant frequency average of NFRC is slightly higher than CC1. This is due to fact that the resonant frequency depends on the vibration mode and density of the concrete samples. In addition, the density of polypropylene is lower than that of the aggregates and cement matrix. This agrees with the work of (Leung and Balendran, 2002) discussed previously in Section 2.5. Also, these results add to identifying more prominent changes of PFRC when the volume percentage is altered.

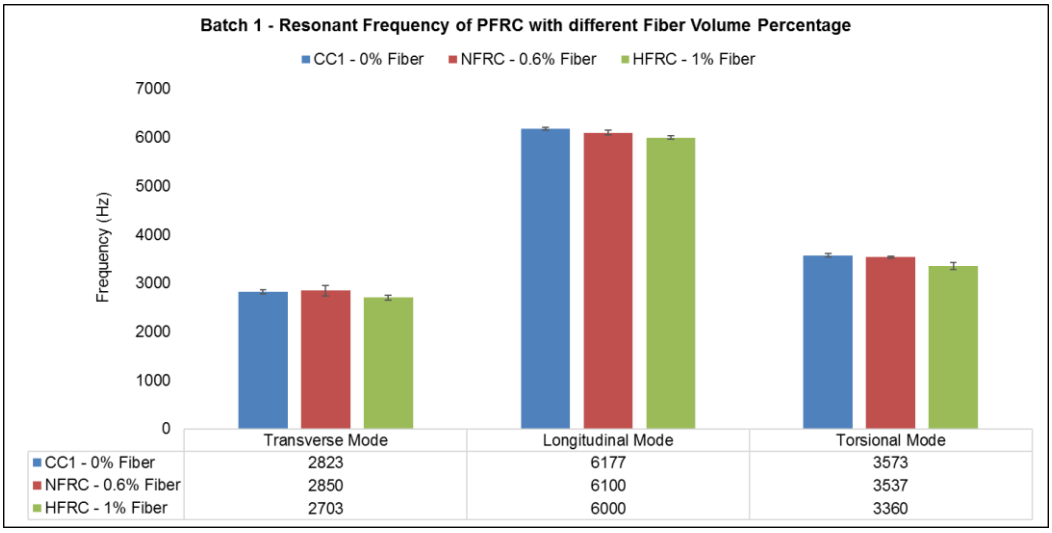

Figure 4-9: Batch 1 - Resonant Frequency of PFRC prisms with 0%, 0.6% and 1% macro PP fiber

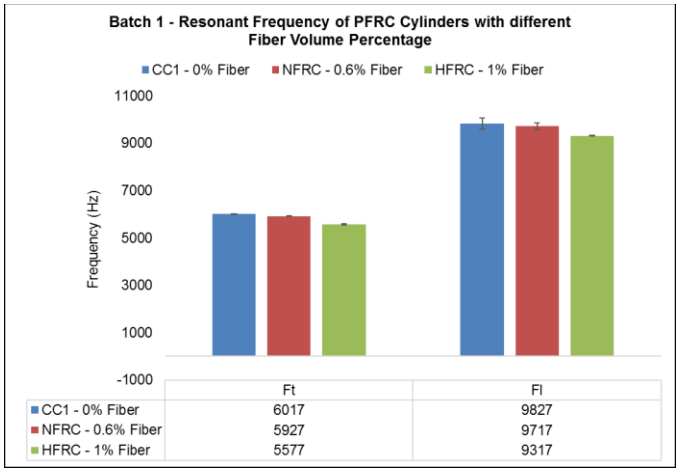

Figure 4-10: Batch 1 - Resonant Frequency of PFRC cylinders with 0%, 0.6% and 1% macro PP fiber

From this batch, selected 100×100×350 mm prisms considered for flexural failure were tested to determined the recovered resonant frequency when fibers are added. It was impossible to test the control concrete since the prisms split after flexure loading. As concrete is considered an orthotropic material when cracking and deterioration occurs, the linear dynamic modulus of elasticity calculation is nullified. The results from Table 4-8 show the average frequency determined from three consecutive impacts in the transverse longitudinal and torsional mode.

Table 4-8: Transverse, longitudinal and torsional resonant frequencies of selected PFRC prisms

Mixture ID		**Mass** (Kg)	**Original frequency response** (Hz)			**Flexural failure frequency response** (Hz)		
CC1		8.94	2770	6150	3540	n/a		
FRC – A	4*	9.98	2840	6120	3510	540	1400	820
HFRC – A	3*	8.64	2640	6030	3280	1570	3630	2330

**Average crack width bottom span of prism in millimeters*

Representative frequency responses of impacts in the transverse, longitudinal and torsional modes of vibration are shown in Figure 4-11, Figure 4-12 and Figure 4-13 for 0.6% macro polypropylene fiber and Figure 4-14, Figure 4-15 and Figure 4-16 for 1% macro polypropylene fiber in PFRC prisms. From the graphs, the original PFRC prism frequencies drift to a lower frequency. Other peaks appear when compared to the original dominant first mode peak of the original prism. This indicates that polypropylene macro fibers maintained some frequency parameters. In addition, the increase of resonance peak widths shows a sign of an increase in modal damping consequently indicating damage. Addition of 1% macro polypropylene fibers showed an improved frequency response when compared to using 0.6% macro polypropylene fibers. By increasing the amount of fibers in PFRC to 1%, more fibers are allocated at the center-span flexure crack. These fibers sustain wave propagation through the composite subsequently improving impulse responses post cracking.

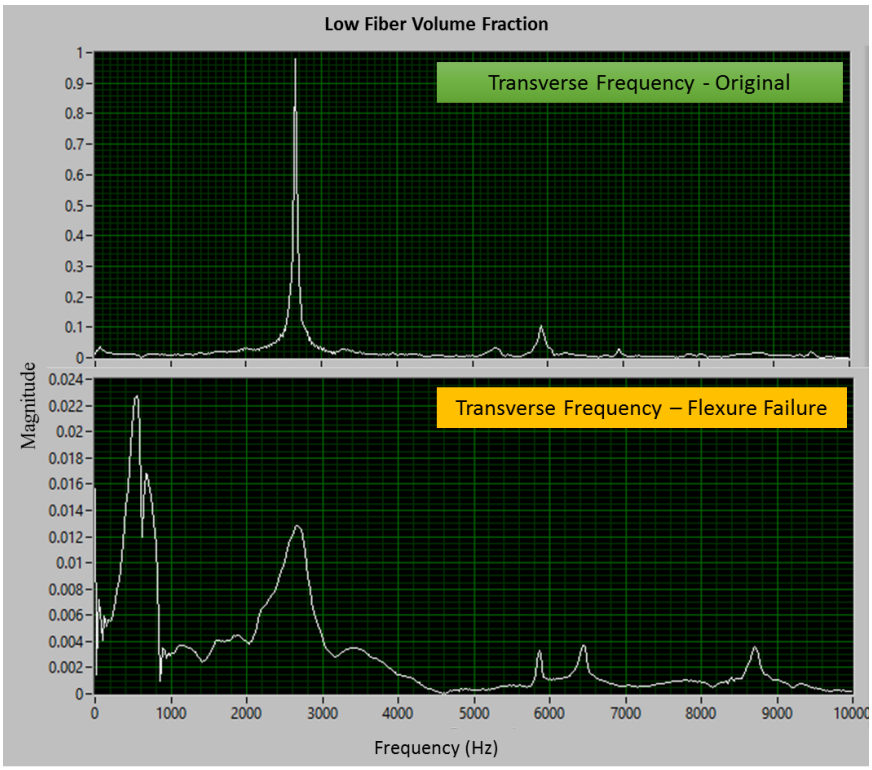

Figure 4-11: Batch 1 – Transverse frequency drift of PFRC prism (low fiber volume fraction)

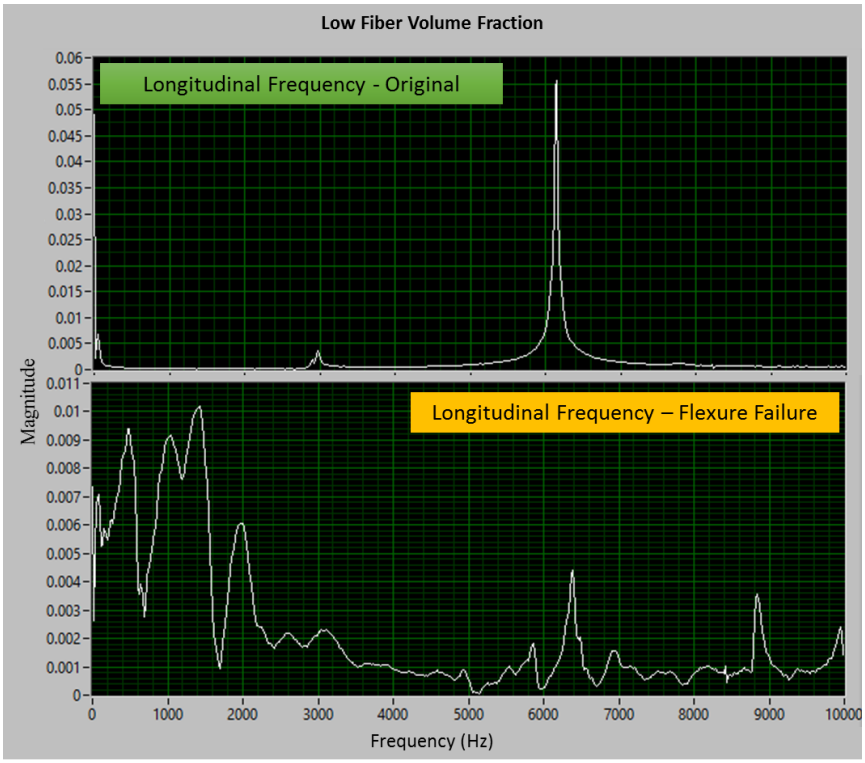

Figure 4-12: Batch 1 – Longitudinal frequency drift of PFRC prism (low fiber volume fraction)

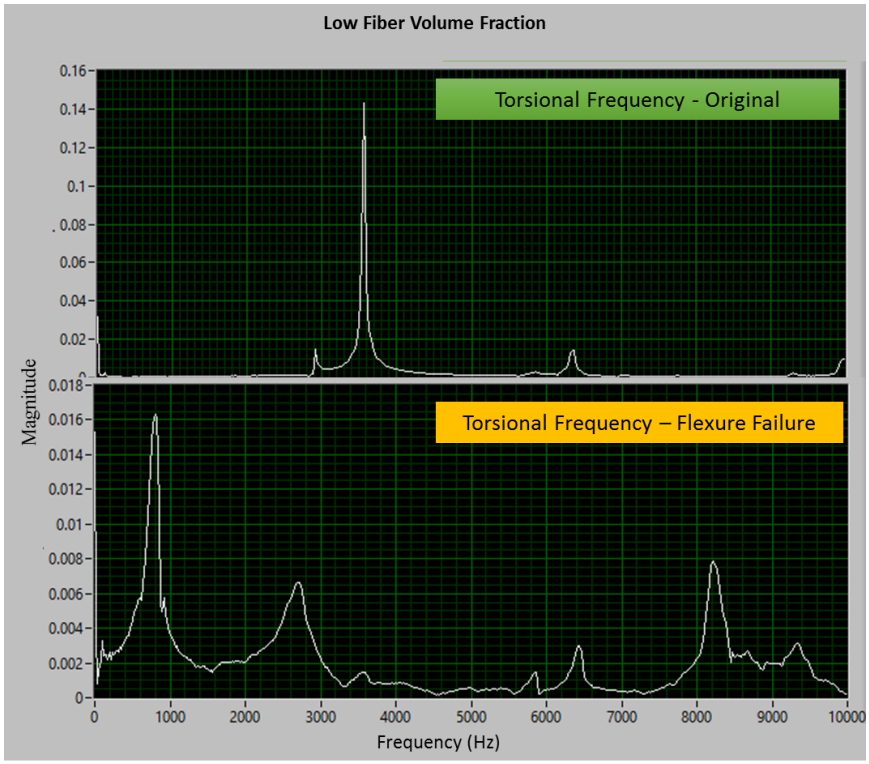

Figure 4-13: Batch 1 – Torsional frequency drift of PFRC prism (low fiber volume fraction)

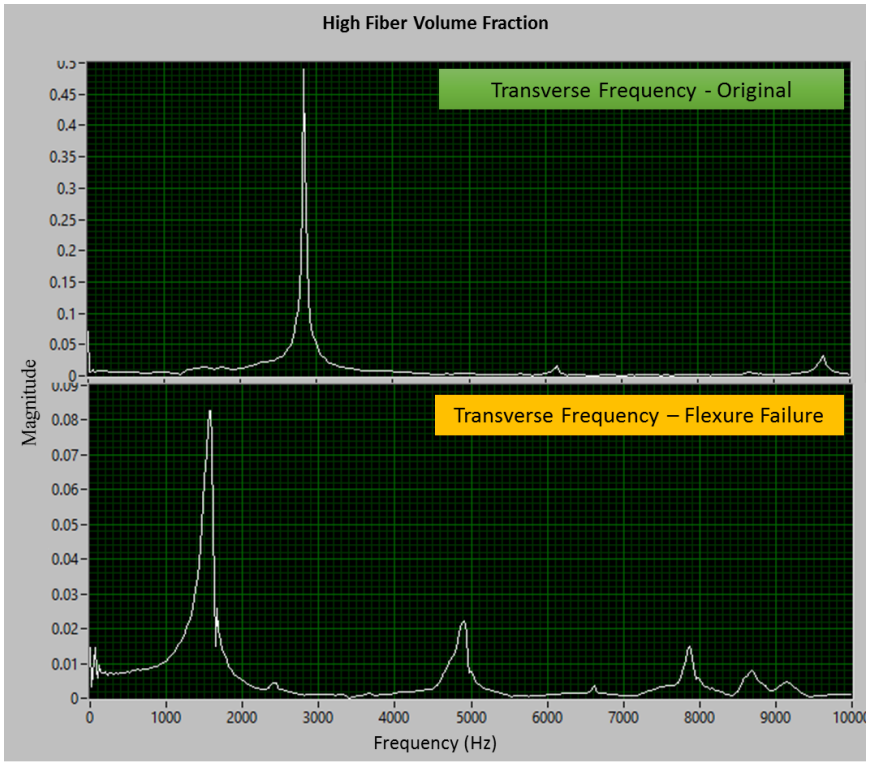

Figure 4-14: Batch 1 – Transverse frequency drift of PFRC prism (high fiber volume fraction)

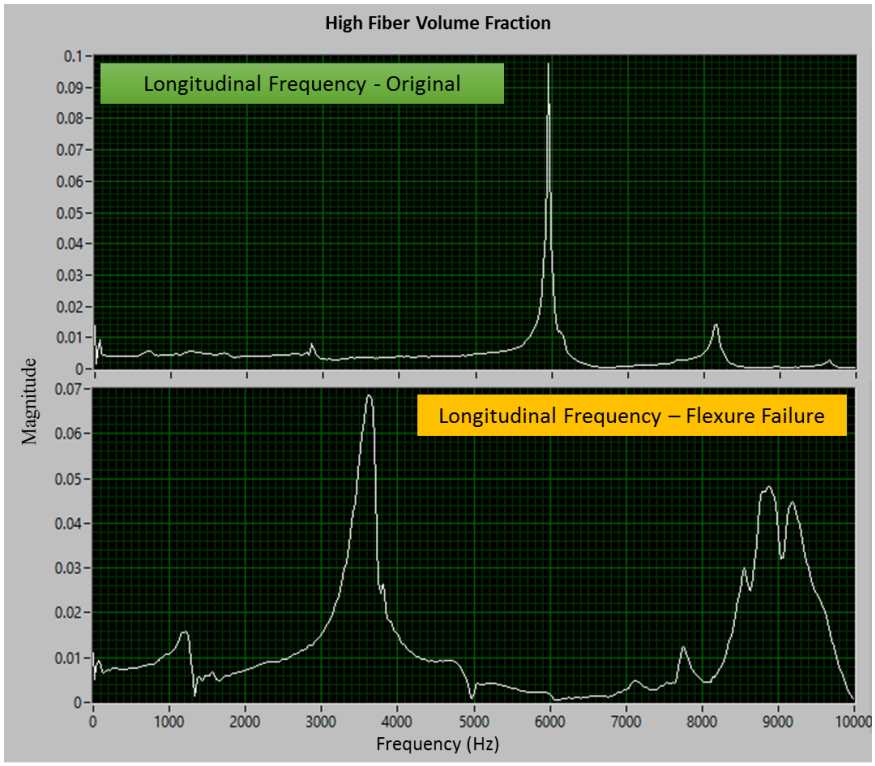

Figure 4-15: Batch 1 – Transverse frequency drift of PFRC prism (high fiber volume fraction)

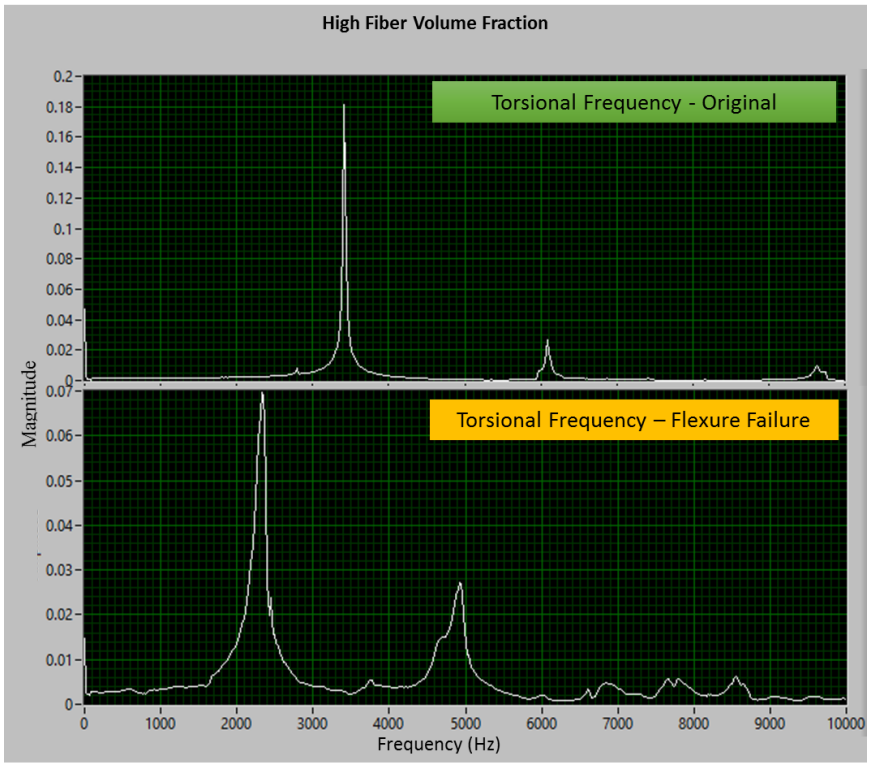

Figure 4-16: Batch 1 – Torsional frequency drift of PFRC prism (high fiber volume fraction)

Batch 2: This concrete mixture was used to investigate the effect of adding polypropylene micro fiber on the frequency response of concrete with age. Based on the analysed results, there is no noticeable variation in the resonant frequency results for the samples of the same concrete mixture. For plain concrete (CC2), the coefficient of variation (CV) is <0.011%; yet it is slightly lower for micro fibers <0.008%. Figure 4-17 and Figure 4-18 show the resonant frequency measured in various ages for control plain concrete (CC1) and micro polypropylene fiber reinforced concrete (FRC-B).

Figure 4-17 and Figure 4-18 provides an overview of the experimental results obtained. As concrete specimens aged, the resonant frequency for both CC2 and FRC-B samples increased because of on-going hydration, however, beyond 14-days of age, the increase in values are minimal. Still, incorporating polypropylene micro fibers into concrete resulted in lower resonant frequency for all modes when compared to plain concrete.

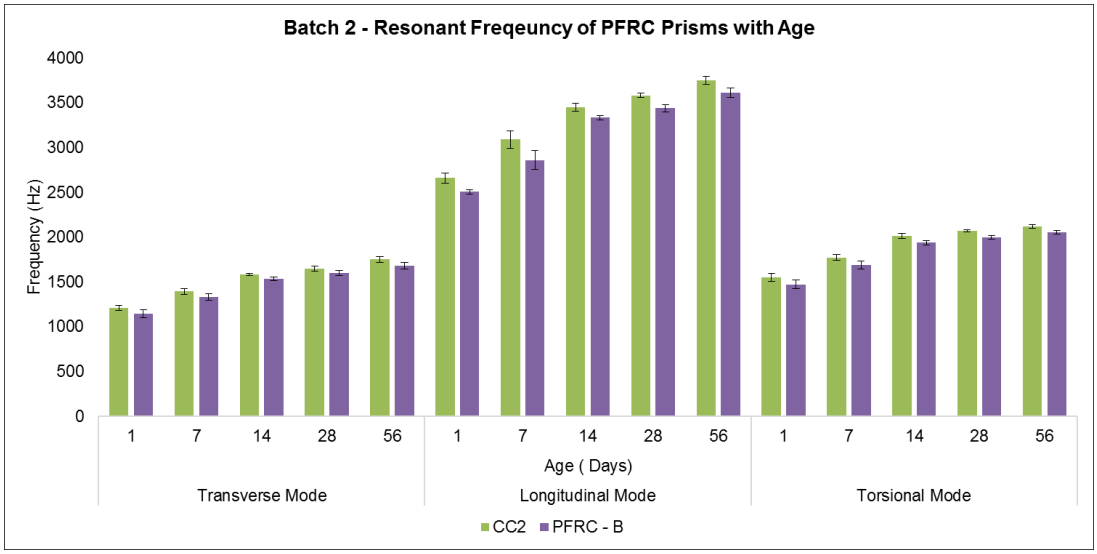

Figure 4-17: Batch 2 - Effect of age on PFRC prisms resonant frequency

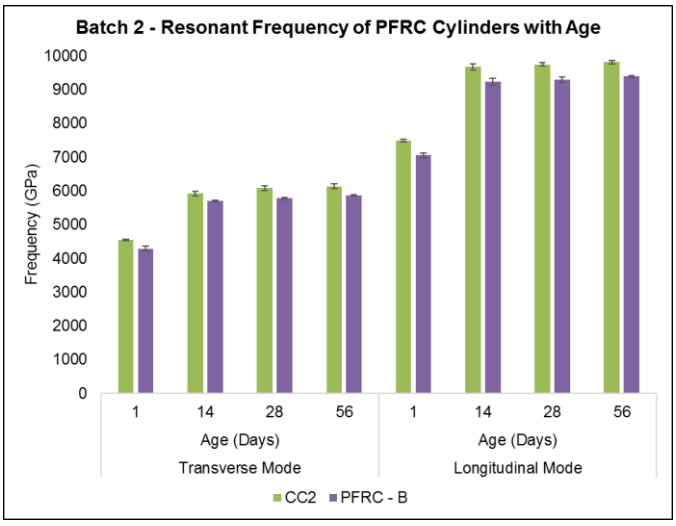

Figure 4-18: Batch 2 - Effect of age on PFRC cylinders resonant frequency

Batch 3: Concrete cylinders were cast to study the effect of adding polypropylene micro and macro fibers on the frequency response of concrete when crack induced considering wet and dry curing conditions. By developing cracks in the cylinders, outlined in Section 3.4.3, both polypropylene macro and micro fibers effectively restrained crack propagation with macro fibers having a better performance in crack width closure. The regain in dynamic elastic properties post cracking illustrates the ductility of PFRC composites. Figure 4-19 and Figure 4-20 show the detected transverse vibration and the resulting resonant frequency of water cured micro fiber PFRC cylinder. The measured original transverse resonant frequency and post-cracking frequency is 5.95 kHz and 4.11 kHz respectively.

Vibration damping can be observed through the shortening and fast decay of the time domain signal. Wave decay, or damping, can be indicated through both figures. In Figure 4-19, the wave attenuation in the cracked PFRC cylinder is indicated by the faster decay or short time span of the impulse. Correspondingly a bell width expansion indicates damping shown in Figure 4-20. The area under the highest peak magnitude increases when compared to its original frequency. As a result, IRM seems to capture the retained elastic properties of concrete, after inducing cracks, owing to the interlocking of micro fibers for cracking bridging. As the resonant frequency is proportional to its dynamic modulus, a decrease in stiffness was detected when calculating the dynamic modulus.

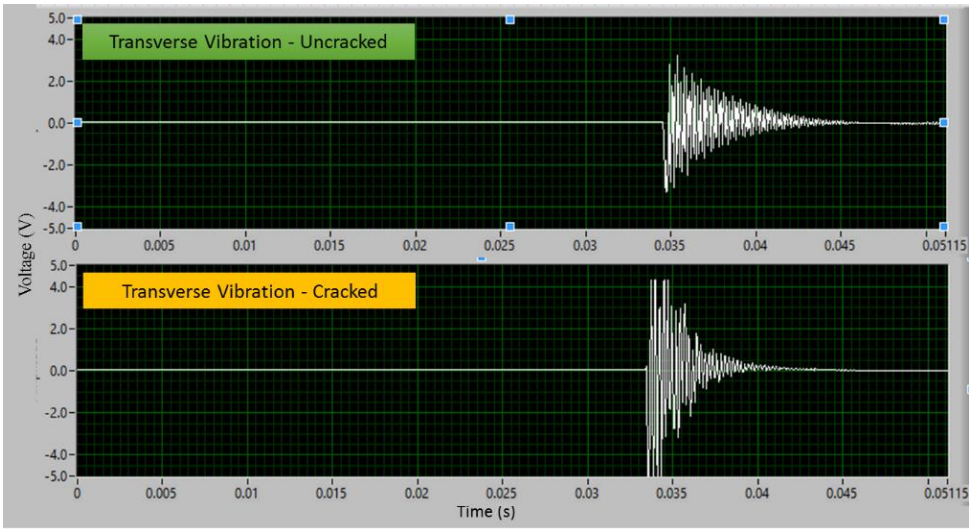

Figure 4-19: Batch 3 - Typical wave damping in transverse vibration of micro PFRC cylinder

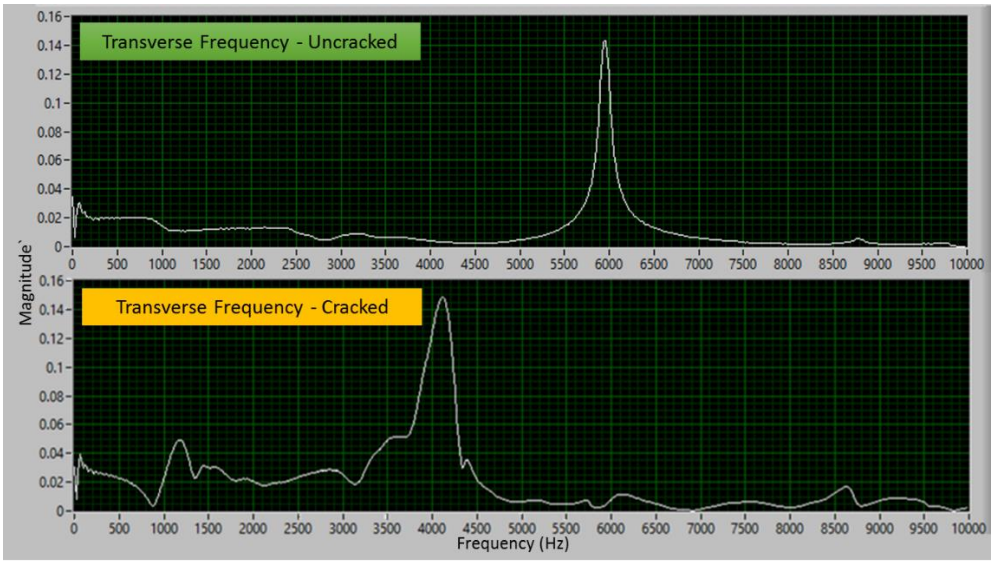

Figure 4-20: Batch 3 - Typical frequency drift of micro PFRC cylinder

As shown in Figure 4-21, the cracks relatively decreased the transverse frequency while slightly affected the longitudinal frequency. A similar response was observed for macro fibers. This is due to the direction of the applied impulse load parallel axial for longitudinal and perpendicular for transverse. Moreover, the indication that micro fibers have higher frequency responses than macro fibers is more prominent when calculating the dynamic elastic moduli. As shown in Figure 4-21, both dry and wet cured micro PFRC specimens showed ~500 Hz lower resonant frequencies when compared to macro fibers. This relates to the high-water uptake of micro fibers and greater adsorption capacity when compared to macro fibers.

Furthermore, the calculated resonant frequencies are affected by curing conditions. Dry cured PFRC cylinders samples produced ~300 Hz lower resonant frequencies when compared to water cured cylinders. Water evaporation with air curing affects the hydration rate and quality of concrete. Excess evaporation contributes to the accumulation of more voids and un-hydrated cement particles, therefore, the resonant frequency of air cured samples is lower. This aligns with the work by (Leung and Balendran, 2002); however, in this study, dry samples were air cured after 24 hours of concrete hardening for 28 days prior to test.

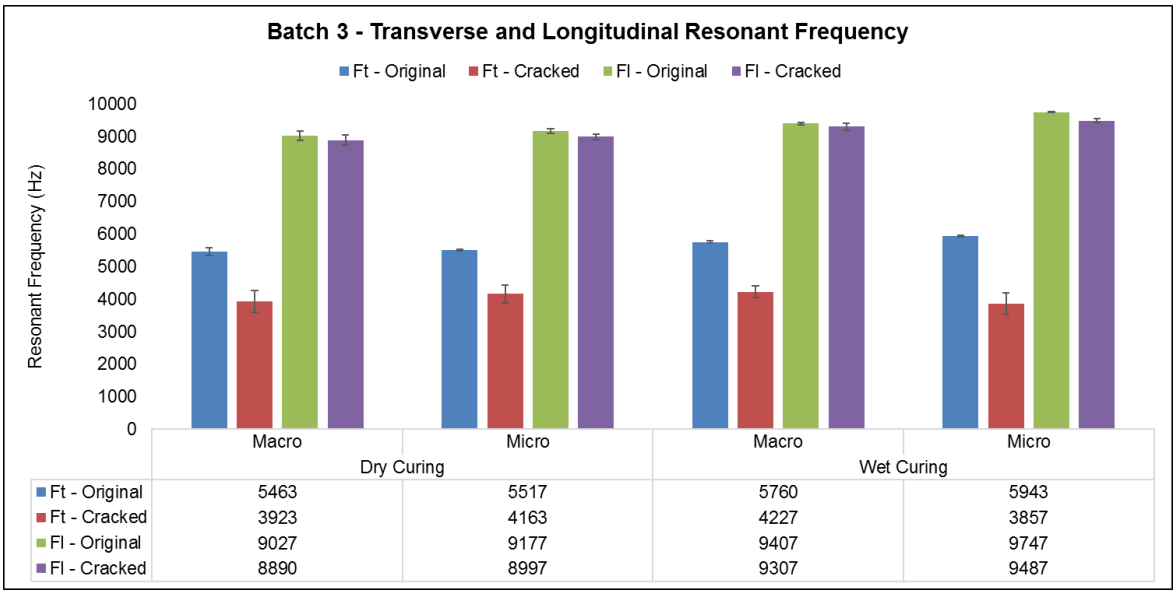

Figure 4-21: Batch 3 – Transverse and Longitudinal Resonant Frequency

Comparing Batch 3 results to Batch 1 and Batch 2, it can be concluded that presence of fly ash in the mixture slightly increases the resonant frequency of concrete. This however does not align with the study of PFRC incorporating fly ash by (Leung and Balendran, 2002). For comparative purposes, the latter authors used the forced resonance method discussed in Section 2.4.4.1 with 0.2% polypropylene fibers in PFRC, while this study investigated the impact resonance frequency instead with 0.3% micro and 0.6% macro polypropylene fibers. When fly ash is added as a supplementary cementitious material for concrete, it encounters a slow pozzolanic reaction at early age hydration (1-3 Days). Therefore, the previous authors stated that the resonant frequency of PFRC increased at early age hydration, however, they indicated that the resonant frequency of PFRC increased at later age.

Limitations

Some limitations arise from both averaging and resolution of frequency as there is a finite number of samples, or bins, to generate the frequency domain.

4.3.2 Dynamic Elastic Properties

4.3.2.1 Dynamic Modulus of elasticity and Modulus of Rigidity

The results of the elastic moduli calculated for PFRC prisms and cylinders is analyzed in this section. Generally, calculating the dynamic modulus of elasticity using the longitudinal mode showed better consistency. Moreover, since the transverse elastic modulus is dependent on correction factors, the longitudinal modulus was concsidered more consistent between the samples. The latter aligns with the investigations developed by (Kolluru et al., 2000; Malhotra and Carino, 2004; Popovics, 2008) in the relationship between the two moduli.

The following results provide the dynamic moduli empirically calculated from the IRM in transverse (E_{dt}) and longitudinal (E_{dl}) modes of vibration. Moreover, the modulus of rigidity (G) is calculated using torsional mode of vibration. The calculated modulus variations can occur if weights between samples of the same mixture are different since the weight of the sample is directly related to the modulus of elasticity of concrete as shown in Section 2.4.3. As the specimen weight increases, the dynamic modulus of elasticity proportionally increases. Table 4-9 summarizes the prism and cylinder (E_{dt}) correction factor (T), as discussed previously.

Table 4-9: T values for transverse dynamic elastic modulus calculation

Specimen Size / Type	T
100×100×350 mm / prism	1.49
150×150×550 mm / prism	1.58
Ø100×200 mm / cylinder	2.11

Through this study, dynamic properties of PFRC specimens from various batches are determined using IRM, as the values are reported in Table 4-10. Batch 1 exhibited the highest dynamic elastic properties in comparison with other batches since Batch 2 had a higher w/c ratio while Batch 3 was with no added fly ash. Fly ash is a finely pulverized powder with spherical packed particles in fresh state. By that, fly ash it is considered to improve the cement-aggregate matrix reduces porosity thus improving strength development of concrete and elastic properties. This can be deduced when comparing FRC-A cylinders of Batch 1 and Batch 3.

Batch 1: Figure 4-22 and Figure 4-23 show the dynamic moduli measured for control plain concrete (CC1), 0.6% polypropylene fiber (NFRC) and 1% polypropylene fiber (HFRC). As there is a direct relation between resonant frequency values and dynamic moduli of concrete, the calculated dynamic moduli confirm a similar relationship to results reported in Section 4.3.1. As an example, the transverse (E_{dt}) and longitudinal (E_{dl}) dynamic elastic moduli decreases by ~3GPa when adding 0.6% volume of fibers and decreases by ~6GPa when adding 1% volume of fibers. From the rule of mixtures of two phase composites, the total composite modulus of elasticity is bound by each of its component modulus and volume. Hence, when fiber volume fraction of polypropylene fibers increase, the composite PFRC elastic modulus decreased. This however, does not neglect the fact that micropore and dry shrinkage crack development in PFRC can alter the results. Yet, PFRC specimens in this study were carefully consolidated in their molds with prompt vibration. In addition, pilot investigations were considered to negate any prementioned errors. Consequently, it is apparent that the density of polypropylene fiber and increase of volume content will proportionally decrease the PFRC dynamic elastic properties when compared to plain concrete of the same mixture.

Table 4-10: Dynamic properties of PFRC specimens

Batch	ID	Dynamic Elastic Properties			
		E_{dt} (GPa)	E_{dl} (GPa)	G (GPa)	υ
Prisms: B1 (100×100×350 mm) / **B2** (150×150×550 mm)					
1	CC1	42.77±0.64	46.54±0.80	18.43±0.11	0.26±0.01
	FRC - A	40.18±0.54	44.67±1.56	17.76±0.42	0.26±0.03
	HFRC - A	37.39±1.35	44.28±0.87	16.45±1.16	0.35±0.07
2	CC2	32.04±1.84	33.71±0.58	13.31±0.29	0.27±0.01
	FRC - B	28.62±1.02	30.06±0.70	12.02±0.24	0.25±0.01
Cylinders: (Ø100×200 mm)					
1	CC1	40.4±0.47	39.2±1.69		
	FRC - A	39.0±0.34	38.1±1.35		
	HFRC - A	33.6±0.50	34.2±0.46		
2	CC2	37.3±1.02	36.1±0.54		
	FRC - B	32.9±0.53	32.1±0.74		
3	FRC - A	33.97±0.35	32.70±0.14		
	FRC - B	37.47±0.23	36.37±0.12		

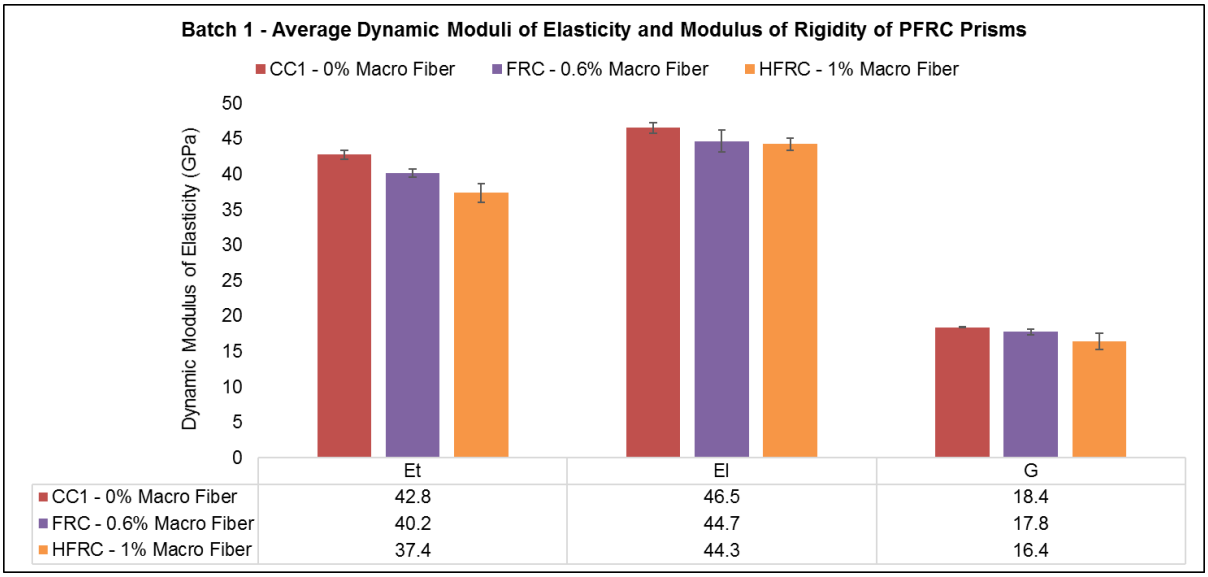

Figure 4-22: Batch 1 - Average dynamic moduli of elasticity and rigidity of PFRC prisms

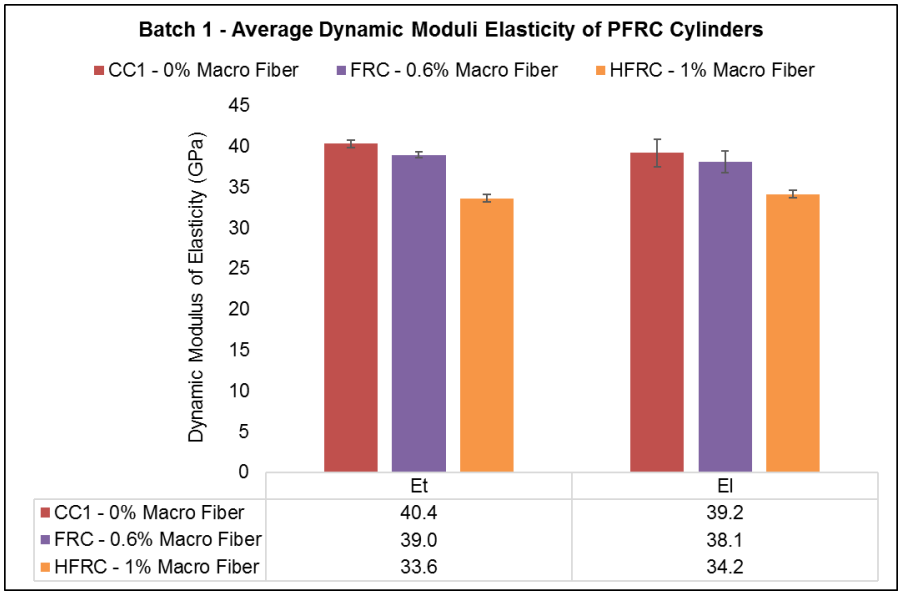

Figure 4-23: Batch 1 - Average dynamic moduli of elasticity of cylinders

Batch 2: As expected, similar trend in resonant frequency results has been observed for dynamic moduli of PFRC samples. The calculated dynamic modulus of PFRC specimens for all modes in different ages are shown in Figure 4-24 and Figure 4-25. Like concluded in Section 4.3.1., as age increases, both resonant frequency and dynamic modulus of elasticity of PFRC specimens increase. However, it is always lower when compared to the control mixture.

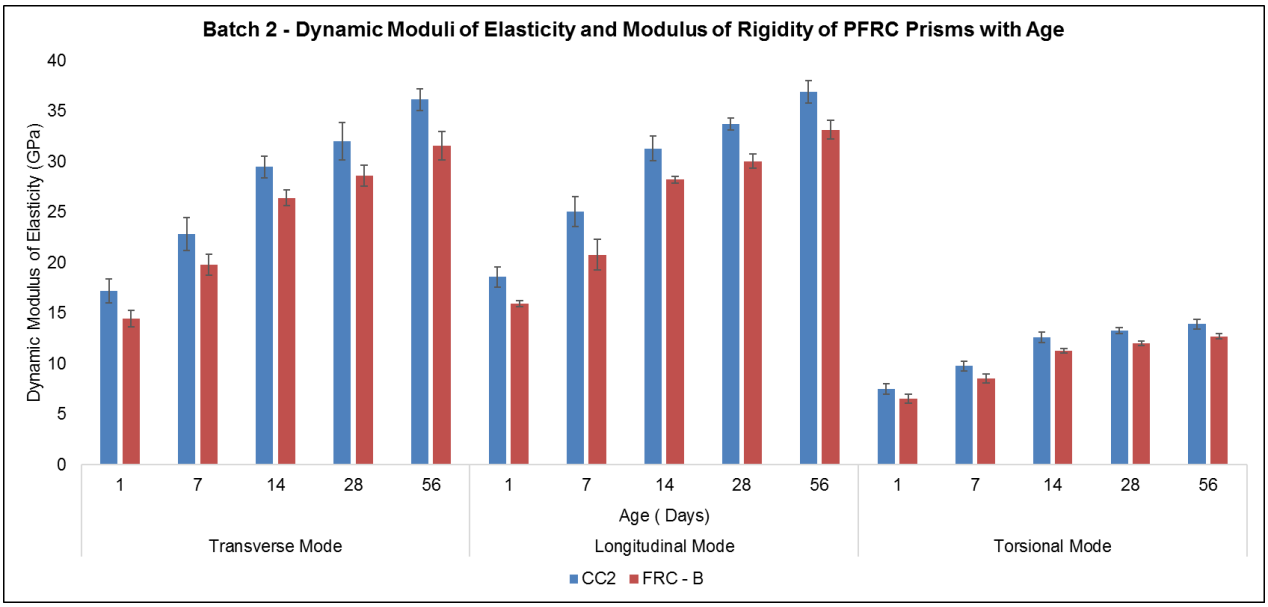

Figure 4-24: Batch 2 - Dynamic moduli of elasticity and rigidity of PFRC prisms with age

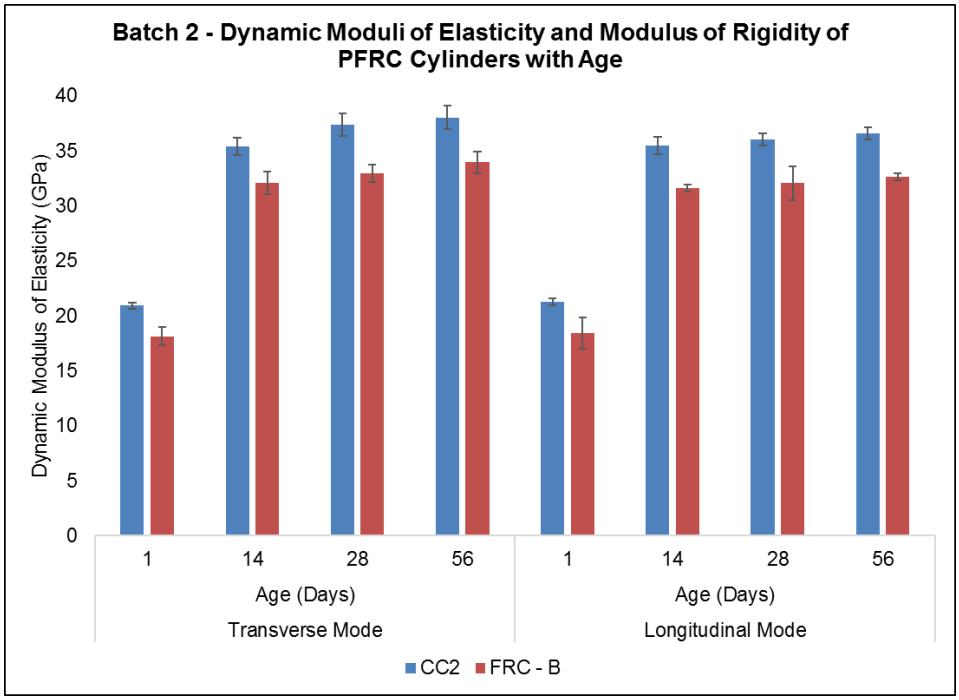

Figure 4-25: Batch 2 - Dynamic moduli of elasticity of PFRC cylinders with age

Batch 3: Figure 4-26 shows the average calculated transverse and longitudinal dynamic elastic modulus of crack induced cylinders. By applying correction factors and density correlations for each specimen using the dynamic moduli, the difference between the curing condition, post-crack dynamic modulus and fiber size is further apparent than when using the resonant frequency solely. For instance, wet cured micro fibers are shown to have a higher elastic modulus when added to concrete yet lower capability in retaining the elastic properties after cracking occurs; when compared to macro fibers. To the knowledge of the author, this is the first attempt to obtain the dynamic modulus for post cracked samples considering the self healing concept of polypropylene fiber reinforced concrete using macro and micro fibers.

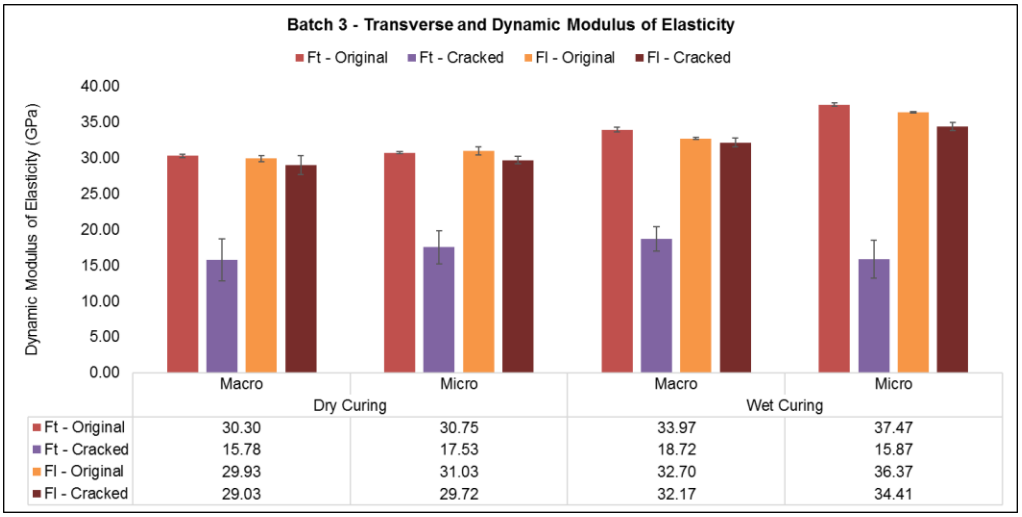

Figure 4-26: Batch 3 - Transverse and Longitudinal Dynamic Modulus

4.3.2.2 Poisson's Ratio

According to ACI 544.1R, volume percentages of fiber less than 2% are considered to have an equal Poisson's ratio similar to that of plain concrete (ACI Committee 544 and American Concrete Institute, 2008). When comparing plain concrete and fiber reinforced mixtures for all beams, the average dynamic Poisson ratio is shown in Table 4-10. From the results, Poisson's ratio indicates no practical relationship for age and volume content of PFRC. This indication is aligned with studies on the resonance frequency of standard test cylinders by (Kolluru et al., 2000).

4.3.3 Relationship between Transverse and Longitudinal Dynamic Modulus of Elasticity

A comparison of dynamic moduli values measured in this study using the transverse and longitudinal modes is shown in Figure 4-28. The transverse vibration measurements are relatively higher than the longitudinal properties. This finding is similar to (Popovics, 2008) study of the dynamic elastic properties of unreinforced concrete. Also, it is concluded that the relationship between average transverse and longitudinal elastic moduli for smaller prisms and cylinders is more unified than that of the larger prisms. Difference between the moduli increases as the specimen size increase.

Through all mixtures, the concrete cylinders and prisms result in different dynamic elastic properties for both the transverse and longitudinal modes of testing. (Popovics, 2008) validated the discrepancies in testing the resonant frequency of concrete cylinders and prisms using replicate aluminum specimens of known mechanical and elastic properties. In result, the author attributed some inconsistency in using longitudinal resonances with cylindrical specimens. This can arise from difficulty to support the cylindrical central curved surface. Thus, cylindrical specimens are recommended to be tested with prisms, of the same concrete mixture, when viable.

Appendix C shows the statistical overview of the overall prismatic and cylindrical specimens. Any outlier that affected the coefficient of skewness outside the interval (-0.5,0.5) was removed. The coefficient of variation did not exceed 0.1 which indicates good symmetry between the two factors. Note that for calculating the longitudinal elastic modulus, no correction factors were assumed. Since the transverse elastic modulus relies on the correction factor (T), any modification or misinterpretation of the value can change the results significantly. Moreover, since the Poisson's ratio of concrete is assumed, the correction factor will slightly deviate. Yet, for statistical purposes, an increase of 0.03 in Poisson's ratio will cause the correction factor to increase by 0.01 for a given radius of gyration and length ratio (K/L).

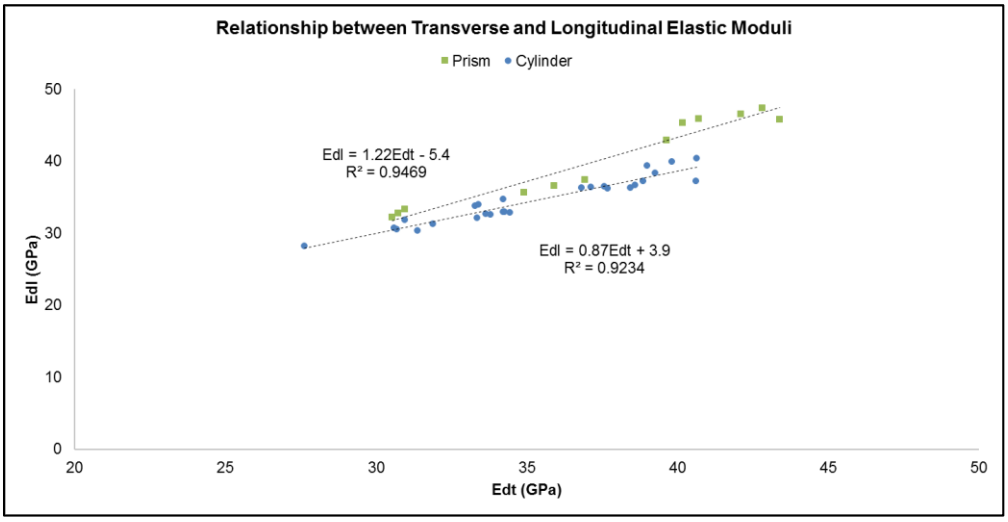

Figure 4-27: Relationship between transverse and longitudinal dynamic elasticity

4.3.4 Relationship between Dynamic Moduli of Elasticity and Modulus of Rigidity

A comparison between dynamic moduli values measured in this study using the transverse and longitudinal modes with the modulus of rigidity is shown in Figure 4-29. The results show a linear relationship between both flexural (E_{dt}) and compressive (E_{dl}) elastic moduli with the concretes dynamic modulus of rigidity (G). As mentioned in (Malhotra and Carino, 2004) and introduced by (Swamy and Rigby, 1971), the modulus of rigidity is about 40% of the modulus of elasticity. Both modal relationships provided have a G/E_d percentage of 38.1% and 41.7% for E_{dt} (R^2=0.93) and E_{dl} (R^2=0.89) respectively, indicating representable coherence.

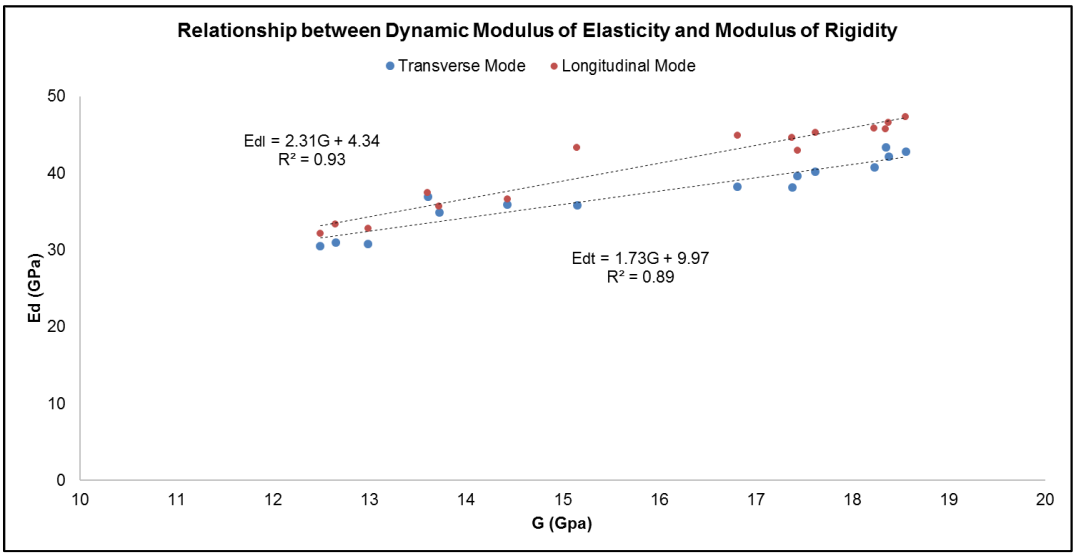

Figure 4-28: Relationship between dynamic moduli of elasticity and rigidity

4.3.5 Relationship between Dynamic Modulus of Elasticity and Compressive Strength

This section describes resulting relationship between the dynamic longitudinal modulus and compressive strength of concrete and their comparison with existing models. Figure 4-27 presents the empirical relationship between E_d and f_c by (Jin and Li, 2001) and other published works mentioned in Section 3.5.4 for sake of comparison with the obtained data in this study. To validate the calculated dynamic modulus of elasticity values, equations from studies presented in Table 3-7, were used. The calculated dynamic E_{dt} and E_{dl} elastic moduli in Figure 4-27 show a promising relation between the model established by (Jin and Li, 2001). In addition, the estimation for the static elastic modulus proposed by (Noguchi et al., 2009) was used in relationship between the static and dynamic moduli mentioned by (Neville and Brooks, 2010). Note that the model proposed by (Noguchi et al., 2009) solely relies on the measured compressive strength and density of each cylinder. Moreover, the model developed by (Jin and Li, 2001) is related between 0.5 and 0.6 w/c ratios at 28 days of wet curing conditions. In this study, having w/c ratios of 0.4 and 0.5, the model proposed by (Jin and Li, 2001) for predicting E_d from cylinder compressive strength is coherent when compared to experimental calculated dynamic moduli in this study.

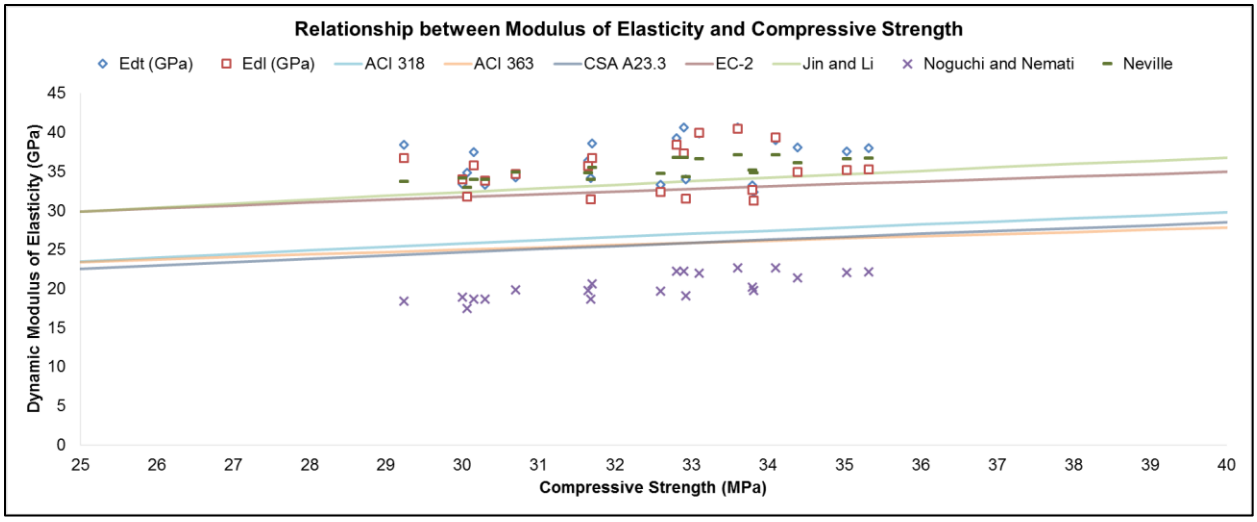

Figure 4-30: Relationship between modulus of elasticity and compressive strength

4.3.6 Relationship between Dynamic Moduli of Elasticity and Density

An attempt to establish a relationship between the dynamic moduli of elasticity and density is shown in Figure 4-29. As there are limitations of the data available, the relationship between the dynamic modulus of elasticity and density of hardened concrete is considered proportional. A linear equation was obtained for both the transverse and longitudinal modes of vibrations. Although the value of the elastic modulus is more dependent on the weight of concretes constituent aggregates, changes in concretes density due porosity should be considered. Note that other variables such compressive strength, age, properties of aggregates, rate of loading and type and size of specimen should be considered. Since density is inversely proportional to porosity of concrete, the prementioned factors including the porosity of aggregates, cement paste and interfacial transition zone would also affect the relationship.

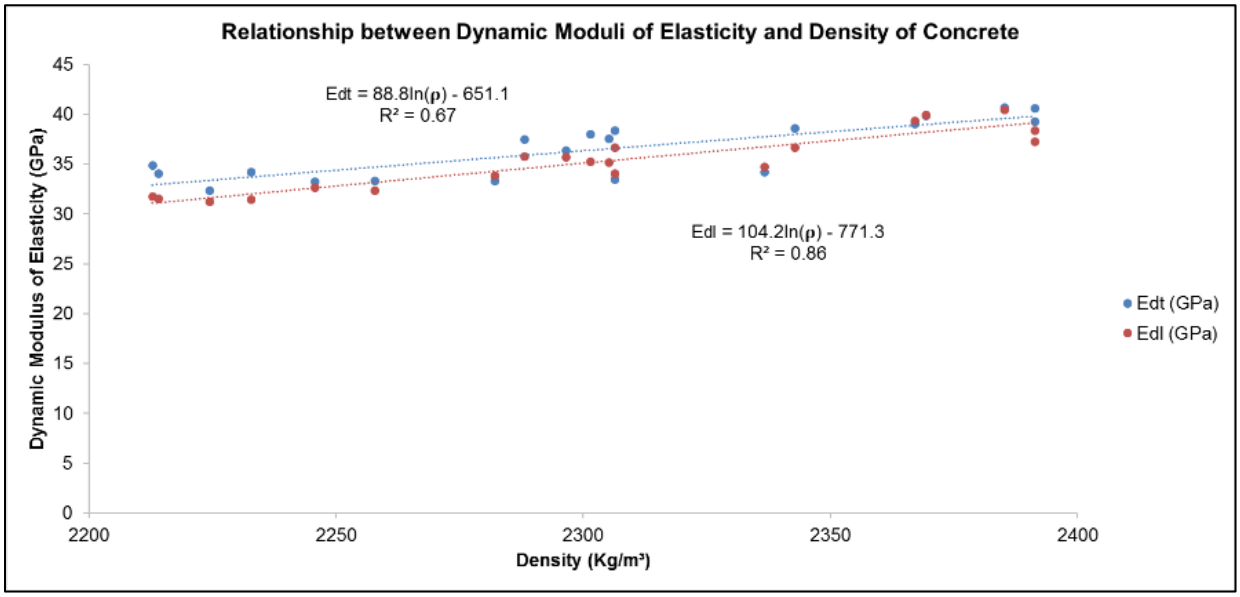

Figure 4-29: Relationship between dynamic moduli of elasticity and density

4.3.7 Summary

The impact resonance frequency method demonstrated reliable demography for assessing the dynamic elastic properties of concrete and detecting cracks present within concrete. By testing (150×150×550 mm) prisms as larger samples and (100×200mm) cylinders as smaller samples, smaller samples exhibited higher sample variation in frequency. However, these variations are statistically insignificant. The transverse elastic modulus is higher than that of the longitudinal elastic modulus. This is reliant on the correction factor (T) for calculating the elastic modulus and dimensional measurements.

From this study, it can be reasoned that a higher modulus is attributed to larger peak stresses. As the peak stresses increase, the concrete is more prone to cracking. The decrease in the dynamic modulus of PFRC, when compared to that of the relative plain concrete mixture, allows concrete to endure higher impulse stresses while maintaining crack expansion. Having a lower modulus provides concrete more flexibility to endure impact or cyclic loading and decreases the occurrence of microcracks at the interfacial transition zone between aggregates and cement. Therefore, reduced rigidity is somewhat beneficial for concrete structures susceptible to dynamic loads. As polypropylene fibers exhibit a ductile manner and high impact absorption capacity within concrete, having a lower elastic modulus is valuable.

5 Conclusion

The purpose of the presented work is to provide an overview of the dynamic elastic properties of concrete incorporating polypropylene fibers using a viable, non-destructive, and repeatable testing method. For polypropylene fiber reinforced concrete, reinforcement has an influence on the decrease in 'dynamic' modulus with increase in fiber content. Through this study, the following conclusions can be drawn as outlined below:

- From the repeatability and validation study, the longitudinal modulus shows better consistency in frequency response when compared to the transversely obtained frequencies. Moreover, effects of applied impact, accelerometer connection, position and attachment are important to consider before conducting IRM tests on amorphous or viscoelastic composites.

- By adding polypropylene fibers to plain concrete, an increase in fiber content and fiber length increases wave dampening of PFRC prisms and cylinders. Incorporating fly ash in concrete enhanced the overall dynamic elastic properties of the composite. Addition of polypropylene fiber in concrete reduces the overall composite dynamic modulus of elasticity.

- The dynamic Poisson's ratio of PFRC, calculated from the fundamental longitudinal and torsional frequencies, is considered constant and does not vary considerably with age. Besides, the addition of polypropylene fibers does not show any significant change in the ratio.

- Dry cured PFRC specimens show about a 15% decrease in the dynamic modulus of elasticity when compared to PFRC specimens cured in water. A decrease is also noted for the compressive strength.

- Micro polypropylene fibers showed higher resonant frequencies and elastic moduli in comparison to macro polypropylene fibers of the same mixture.

- Addition of polypropylene fibers improved the dynamic response of concrete post-cracking by maintaining a fraction of the original resonant and elastic properties. Macro fibers showed better improvement in crack bridging while micro fiber showed significant recovery of the elastic properties.

- Minor defects induced by tensile cracking to first peak crack shows a change in frequency for most specimens. At the same time, the extent of the defects in the sample is inversely proportional to the dynamic modulus of elasticity as the composite homogeneity and stiffness decreases.

Impact resonant frequency testing, solely, can be used as a good indicator for measuring the effect of fiber resistance to concrete degradation. By considering the aforementioned results, IRM shows great potential for monitoring cracks caused by time-independent loading in-service and external restraints in a cost-effective approach. Through this study, IRM shows a reliable and repeatable potential to monitor the extent of fiber crack bridging through flexural, compressive and shear loads of PFRC.

Recommendations for Future Studies

As a result of adding polypropylene fibers in concrete, the free vibration testing using low impulse excitation provides some indication of material damping properties and alternate elastic properties in post cracking stage. Using the impact resonance method allowed for quantifying the extent of damage through cracked cylinders and fractured prisms. Reinforcing concrete with polypropylene fibers helped retain elastic properties when defects are present and after failure occurs. However, it is important to note that the signal behaviour would likely differ with high amplitude random excitation or seismic activity. Therefore, further research in the behaviour of PFRC under seismic loads is necessary. An evaluation of the regained elastic properties of concrete should enable improved assessment of in-service structures reinforced with polypropylene. In addition, the following points are recommended to be considered in future studies:

- For FRC undergoing freeze-thaw cycles, the structure of the internal air pore system can be of interest to monitor. The resonant frequency method can be used to monitor this occurrence. The air pore distribution can be studied in relation to the amount and type of fly ash and air entraining admixtures used.
- When cracked specimens are immersed in water or present in high relative humidity environment, natural self-healing of concrete can initiate. The resonant frequency method can be used to quantify the extent of healing by monitoring water flow rate through cracks or adding a premeasured amount of self-sealing agent.
- For a more economical approach, a portable lab resonant frequency device is prototyped and can be developed to allow for immediate onsite testing while maintaining the same resolution of laboratory RFT instruments.
- Research on resonant frequency testing can be established on alternative fibers such as Kevlar and carbon nanotubes introduced to concrete. Testing polypropylene fibers in this study has shown promising results in measuring the frequency variation of different sized polypropylene fibers.

6 References

ASTM Standards

ASTM B221-14, Standard Specification for Aluminum and Aluminum-Alloy Extruded Bars, Rods, Wire, Profiles, and Tubes, ASTM International, West Conshohocken, PA, 2014, www.astm.org

ASTM C39/C39M-16b, Standard Test Method for Compressive Strength of Cylindrical Concrete Specimens, ASTM International, West Conshohocken, PA, 2016, www.astm.org

ASTM C94/C94M-16a, Standard Specification for Ready-Mixed Concrete, ASTM International, West Conshohocken, PA, 2016, www.astm.org

ASTM C138 / C138M-14, Standard Test Method for Density (Unit Weight), Yield, and Air Content (Gravimetric) of Concrete, ASTM International, West Conshohocken, PA, 2014, www.astm.org

ASTM C143/C143M-15a, Standard Test Method for Slump of Hydraulic-Cement Concrete, ASTM International, West Conshohocken, PA, 2015, www.astm.org

ASTM C150 / C150M-17, Standard Specification for Portland Cement, ASTM International, West Conshohocken, PA, 2017, www.astm.org

ASTM C618-15, Standard Specification for Coal Fly Ash and Raw or Calcined Natural Pozzolan for Use in Concrete, ASTM International, West Conshohocken, PA, 2015, www.astm.org

ASTM C215-14, Standard Test Method for Fundamental Transverse, Longitudinal, and Torsional Resonant Frequencies of Concrete Specimens, ASTM International, West Conshohocken, PA, 2014, www.astm.org

ASTM C231/C231M-14, Standard Test Method for Air Content of Freshly Mixed Concrete by the Pressure Method, ASTM International, West Conshohocken, PA, 2014, www.astm.org

ASTM C469 / C469M-14, Standard Test Method for Static Modulus of Elasticity and Poisson's Ratio of Concrete in Compression, ASTM International, West Conshohocken, PA, 2014, www.astm.org

ASTM C597-16, Standard Test Method for Pulse Velocity Through Concrete, ASTM International, West Conshohocken, PA, 2016, www.astm.org

ASTM C642-13, Standard Test Method for Density, Absorption, and Voids in Hardened Concrete, ASTM International, West Conshohocken, PA, 2013, www.astm.org

ASTM C876-15, Standard Test Method for Corrosion Potentials of Uncoated Reinforcing Steel in Concrete, ASTM International, West Conshohocken, PA, 2015, www.astm.org

ASTM C856-17, Standard Practice for Petrographic Examination of Hardened Concrete, ASTM International, West Conshohocken, PA, 2017, www.astm.org

ASTM C1064 / C1064M-12, Standard Test Method for Temperature of Freshly Mixed Hydraulic-Cement Concrete, ASTM International, West Conshohocken, PA, 2012, www.astm.org

ASTM C1609 / C1609M-12, Standard Test Method for Flexural Performance of Fiber-Reinforced Concrete (Using Beam With Third-Point Loading), ASTM International, West Conshohocken, PA, 2012, www.astm.org

ASTM C1116 / C1116M-10a(2015), Standard Specification for Fiber-Reinforced Concrete, ASTM International, West Conshohocken, PA, 2015, www.astm.org

ASTM D7508 / D7508M-10(2015), Standard Specification for Polyolefin Chopped Strands for Use in Concrete, ASTM International, West Conshohocken, PA, 2015, www.astm.org

Citations

AASHTO-AGC-ARTBA Joint Cooperation Committee, 2001. The use and state-of-the-practice of fiber reinforced concrete. Am. Assoc. State Highw. Transp. Off. Wash. DC.

ACI Committee 318, American Concrete Institute, 2014. Building code requirements for structural concrete (ACI 318-14): an ACI standard : commentary on building code requirements for structural concrete (ACI 318R-14), an ACI report.

ACI Committee 544, American Concrete Institute, 2008. Guide for specifying, proportioning, and production of fiber-reinforced concrete (ACI 544R). American Concrete Institute, Farmington Hills, MI.

Ali, M., Liu, A., Sou, H., Chouw, N., 2012. Mechanical and dynamic properties of coconut fibre reinforced concrete. Constr. Build. Mater. 30, 814–825. doi:10.1016/j.conbuildmat.2011.12.068

Aly, T., Sanjayan, J., Collins, F., 2008. Effect of polypropylene fibers on shrinkage and cracking of concretes. Mater. Struct. 41, 1741.

Bahr, O., Schaumann, P., Bollen, B., Bracke, J., 2013. Young's modulus and Poisson's ratio of concrete at high temperatures: Experimental investigations. Mater. Des. 45, 421–429. doi:10.1016/j.matdes.2012.07.070

Balendran, R.V., 1993. Building Materials Laboratory Manual 2. Department of Building and Construction: City Polytech-nic of Hong Kong.

Banthia, N., Gupta, R., 2006. Influence of polypropylene fiber geometry on plastic shrinkage cracking in concrete. Cem. Concr. Res. 36, 1263–1267. doi:10.1016/j.cemconres.2006.01.010

Banthia, N.P., Mindess, S., Bentur, A., 1987. Impact behaviour of concrete beams. Mater. Struct. 20, 293–302. doi:10.1007/BF02485926

Barragan, B., Conforti, A., Minelli, F., Moro, S., Plizzari, G.A., Toffoli, L., 2012. Shear Behavior of Shallow Beams in Polypropelene Fiber Reinfroced Concrete. BEFIB2012 – Fibre Reinf. Concr.

Beaudoin, J.J., 1990. Handbook of fiber-reinforced concrete: principles properties, developments and applications. Noyes Publications, Park Ridge, N.J., U.S.A.

Biryukovich, K.L., Biryukovich, Y.L., Biryukovich, D.L., 1965. Glass-fibre-reinforced cement.

Bischoff, P.H., Perry, S.H., 1991. Compressive behaviour of concrete at high strain rates. Mater. Struct. 24, 425–450. doi:10.1007/BF02472016

British Standard BS EN 1992-1-1, 2004. Eurocode 2: Design of Concrete Structures (No. EN 1992-1-1:2004). Bristish Standards.

Brown, M., Sellers, G., Folliard, K., Fowler, D., 2001. Restrained shrinkage cracking of concrete bridge decks: State-of-the-Art Review.

Bungey, J.H., Millard, S.G., Grantham, M., 2006. Testing of concrete in structures, 4th ed. ed. Taylor & Francis, London ; New York.

Chavan, P., Vyawahare, M., 2015. Correlation of static and Dyanmic Modulus of Elasticity for Different SCC Mixes. Int. J. Recent Innov. Trends Comput. Comun. 3, 4914–4919.

Deng, Z., Li, J., 2007. Mechanical behaviors of concrete combined with steel and synthetic macro-fibers. Comput. Concr. 4, 207–220. doi:10.12989/cac.2007.4.3.207

Dickson, R.W., Wachtman, J.B., 1971. An alumina standard reference material for resonance frequency and dynamic elastic moduli measurement. I. For use at 25 C. J. Res. Natl. Bur. Stand. Sect. Phys. Chem. 75A, 155. doi:10.6028/jres.075A.016
Gade, H., Herlufsen, S., 1994. Digital Filter Techniques vs. FFT Techniques for Damping Measurements. Bruel Kjaer 1, 1–35.
Gaidis, M., Rosenburg, J.M., 1986. New Test for Determining Fundamental Frequencies of Concrete. Cem. Concr. Aggreg. 8, 117.
Giner, V.T., Baeza, F.J., Ivorra, S., Zornoza, E., Galao, ó., 2012. Effect of steel and carbon fiber additions on the dynamic properties of concrete containing silica fume. Mater. Des. 34, 332–339. doi:10.1016/j.matdes.2011.07.068
Goens, E., 1931. Über die Bestimmung des Elastizitätsmoduls von Stäben mit Hilfe von Biegungsschwingungen. Ann. Phys. 403, 649–678. doi:10.1002/andp.19314030602
Graft-Johnson, J.W.., Bawa, N.S., 1969. Effect of mix proportion, water-cement ratio, age and curing conditions of the dynamic modulus of elasticity of concrete. Build. Sci. 3, 171–177.
Gudmarsson, A., 2014. Resonance testing of asphalt concrete. Architecture and the Built Environment, KTH Royal Institute of Technology, Stockholm.
Gupta, R., Biparva, A., 2015. Innovative Test Technique to Evaluate "Self-Sealing" of Concrete. J. Test. Eval. 43, 1091–1098. doi:10.1520/JTE20130285
Gupta, R., El-Newihy, A., 2015. Effectiveness of resonance frequency based method to predict moduli of concrete and detection flaws. JCI: International Conference on the Regeneration and Conservation of Concrete Structures.
Hamoush, 2011. Freezing and Thawing Durability of Very High Strength Concrete. Am. J. Eng. Appl. Sci. 4, 42–51. doi:10.3844/ajeassp.2011.42.51
Han, S.-H., Kim, J.-K., 2004. Effect of temperature and age on the relationship between dynamic and static elastic modulus of concrete. Cem. Concr. Res. 34, 1219–1227.
He, J., 1999. Damage Detection and Evaluation I, in: Silva, J.M.M., Maia, N.M.M. (Eds.), Modal Analysis and Testing. Springer Netherlands, Dordrecht, pp. 325–344.
Hornibrook, F.B., 1939. Application of Sonic Method to Freezing and Thawing Studies of Concrete. ASTM Bull. No. 101, 5.
Jin, X., Li, Z., 2001. Dynamic Property Determination for Early-Age Concrete. ACI Mater. J. 98, 365–370.
Jones, R., 1969. A review of the non-destructive testing of concrete. Institution of Civil Engineers.
Kakooei, S., Akil, H.M., Jamshidi, M., Rouhi, J., 2012. The effects of polypropylene fibers on the properties of reinforced concrete structures. Constr. Build. Mater. 27, 73–77. doi:10.1016/j.conbuildmat.2011.08.015
Karahan, O., Atiş, C.D., 2011. The durability properties of polypropylene fiber reinforced fly ash concrete. Mater. Des. 32, 1044–1049.
Kesler, C.E., Higuchi, Y., 1945. Problems in the sonic testing of plain concrete, in: Int. Symp. on Nondestructive Testing of Materials and Structures. RILEM, Paris, p. 45.
Kodur, V.K.R., Cheng, F.-P., Wang, T.-C., Sultan, M.A., 2003. Effect of Strength and Fiber Reinforcement on Fire Resistance of High-Strength Concrete Columns. J. Struct. Eng. 129, 253–259. doi:10.1061/(ASCE)0733-9445(2003)129:2(253)
Kolluru, S.V., Popovics, J.S., Shah, S.P., 2000. Determining Elastic Properties of Concrete Using Vibrational Resonance Frequencies of Standard Test Cylinders. Cem. Concr. Aggreg. CCAGDP 22, 81–89.
Krstulovic-Opara, N., Watson, K.A., LaFave, J.M., 1994. Effect of increased tensile strength and toughness on reinforcing-bar bond behavior. Cem. Concr. Compos. 16, 129–141.
Kurtz, S., Balaguru, P., 2000. Postcrack creep of polymeric fiber-reinforced concrete in flexure. Cem. Concr. Res. 30, 183–190. doi:10.1016/S0008-8846(99)00228-8

Lamond, J., Pielert, J. (Eds.), 2006. Significance of Tests and Properties of Concrete and Concrete-Making Materials. ASTM International, 100 Barr Harbor Drive, PO Box C700, West Conshohocken, PA 19428-2959.
Lee, B.J., Kee, S.-H., Oh, T., Kim, Y.-Y., 2015. Effect of Cylinder Size on the Modulus of Elasticity and Compressive Strength of Concrete from Static and Dynamic Tests. Adv. Mater. Sci. Eng. 2015, 1–12. doi:10.1155/2015/580638
Leung, H.Y., Balendran, R.V., 2002. Resonant frequency in polypropylene fibre reinforced concrete (PFRC) with pozzolanic materials. J. Civ. Eng. Manag. 8, 169–176. doi:10.1080/13923730.2002.10531273
Leung, H.Y., Balendran, R.V., Nadeem, A., Maqsood, T., Rana, T.M., 2003. Resonant Frequency in Fiber Reinforced Concrte: Effect of Pozzolans and Curing Condtions. ICPCM, p. 4.
Li, V., Yang, E., 2007. Self Healing in Concrete Materials. Self Heal. Mater. Altern. Approach 20 Centuries Mater. Sci. 161–193.
Maier, C., Calafut, T., 1998. Polypropylene: the definitive user's guide and databook, PDL handbook series. Plastics Design Library, Norwich, NY.
Malhotra, V.M., Carino, N.J. (Eds.), 2004. Handbook on nondestructive testing of concrete, 2nd ed. ed. CRC Press, Boca Raton, Fla.
Manolis, G.D., Gareis, P.J., Tsonos, A.D., Neal, J.A., 1997. Dynamic properties of polypropylene fiber-reinforced concrete slabs. Cem. Concr. Compos. 19, 341–349. doi:10.1016/S0958-9465(97)00030-9
Mehta, P., Monteiro, P.J.M., 2006. Concrete: Microstructure, Properties, and Materials, McGraw Hill professional. McGraw-Hill Education.
Mindess, S., Vondran, G., 1988. Properties of concrete reinforced with fibrillated polypropylene fibres under impact loading. Cem. Concr. Res. 18, 109–115. doi:10.1016/0008-8846(88)90127-5
Mindess, S., Young, J.F., Darwin, D., 2003. Concrete, 2nd ed. ed. Prentice Hall, Upper Saddle River, NJ.
Naaman, A.E., Namur, G., Najm, H., Elwan, J., 1989. Bond mechanisms in fiber reiforced cement-based composites (No. UMCE 89-9). University of Michigan, Ann Arbor, MI.
Neville, A.M., 2012. Properties of Concrete. Pearson Education.
Neville, A.M., Brooks, J.J., 2010. Concrete technology, 2nd ed. Prentice Hall, Harlow.
Noguchi, T., Tomosawa, F., Nemati, K., Chiaia, B., Fantilli, A., 2009. A Practical Equation for Elastic Modulus of Concrete. ACI Struct. J. 106. doi:10.14359/51663109
Obert, L., Duvall, W.., 1941. Discussion of the dynamic methods of testing concrete with sugesstions for standardization. Proc. ASTM 41, 1053.
Pickett, G., 1945. Equations for Computing Elastic Constants From Flexural and Torsional Resonant Frequencies of Vibration of Prisms and Cylinders. Proc. ASTM 45, 846–865.
Plachy, T., Padevet, P., Polak, M., 2009. Comparison of two experimental techniques for determination of Young's modulus of concrete specimens. Recent Adv. Appl. Theor. Mech. Puerto Cruz 14–16.
Popovics, J.., 2008. A Study of Static and Dynamic Modulus of Elasticity of Concrete (No. Final Report). University of Illinois, Urbana, IL.
Powers, T.C., 1938. Measuring Young's Modulus of Elasticity by Means of Sonic Vibrations. ASTM Proceeding 38, 460–469.
Propex Operating Company, 2016. Product Guide Specification.
Rayleigh, J.W.S., Lindsay, R.B., 1945. The theory of sound, 2nd ed. Dover Publications.
Shah, S.P., Rangan, B.V., 1971. Fiber Reinforced Concrete Properties. J. Proc. 68. doi:10.14359/11299
Sharma, B.L., Gupta, M.R., 1960. Sonic modulus as related to strength and static modulus of high strength concrete. Indian Concr. J. 34.
Shkolnik, I.E., 2005. Effect of nonlinear response of concrete on its elastic modulus and strength. Cem. Concr. Compos. 27, 747–757. doi:10.1016/j.cemconcomp.2004.12.006
Singh, S., Shukla, A., Brown, R., 2004. Pullout behavior of polypropylene fibers from cementitious matrix. Cem. Concr. Res. 34, 1919–1925.

Spinner, S., Reichard, T.W., Tefft, W.E., 1960. A comparison of experimental and theoretical relations between Young's modulus and the flexural and longitudinal resonance frequencies of uniform bars. J. Res. Natl. Bur. Stand. Sect. Phys. Chem. 64A, 147. doi:10.6028/jres.064A.014
Spinner, S., Tefft, W., 1961. A method for determining mechanical resonance frequencies for calculating elastic moduli from these frequencies. Proc. ASTM 61, 1221–1233.
Stanton, T.., 1944. Comparing the modulus of elasticity of portland cement concreteby the dynamic (sonic) and compression methods. Proc ASTM 17.
Swamy, G., Rigby, N., 1971. Dynamic properties of hardened paste, mortar and concrete. Mat Constr 4, 13–40. doi:10.1007/bf02473927
Thomson, W.., 1940. Measuring changes in physical properties of concrete by the dynamic method. Proc ASTM 1113.
Thorton, H., Alexander, A., 1987. Development of impact and resonant vibration signature for inspection of concrete structures. ACI Spec Publ SP 100 667.
Timoshenko, J.N., StephenGoodier, 1970. Theory of elasticity. McGraw-Hill.
Timoshenko, S.P., 1922. On the transverse vibrations of bars of uniform cross-section. Philos. Mag. Ser. 6 43, 125–131. doi:10.1080/14786442208633855
Toutanji, H., McNeil, S., Bayasi, Z., 1998. Chloride permeability and impact resistance of polypropylene-fiber-reinforced silica fume concrete. Cem. Concr. Res. 28, 961–968.
Ward, C., Rattanawangcharoen, N., Gheorghiu, C., 2008. Impact resonance method for damage detection in carbon-fibre-reinforced polymer–strengthened reinforced concrete beams subjected to fatigue and thermal cycling. Can. J. Civ. Eng. 35, 1251–1260. doi:10.1139/L08-066
Whitehurst, E.A., 1967. Evaluation of Concrete Properties from Sonic Tests, ACI monograph. American Concrete Institute.
Yew, M.K., Mahmud, H.B., Shafigh, P., Ang, B.C., Yew, M.C., 2015. Effects of polypropylene twisted bundle fibers on the mechanical properties of high-strength oil palm shell lightweight concrete. Mater Struct 49, 1221–1233. doi:10.1617/s11527-015-0572-z
Yildirim, O., HasanSengul, 2011. Modulus of elasticity of substandard and normal concretes. Constr. Build. Mater. 25, 1645–1652. doi:10.1016/j.conbuildmat.2010.10.009
Zhang, P., Li, Q., 2013. Effect of polypropylene fiber on durability of concrete composite containing fly ash and silica fume. Compos. Part B Eng. 45, 1587–1594. doi:10.1016/j.compositesb.2012.10.006
Zheng, Z., Feldman, D., 1995. Synthetic fibre-reinforced concrete. Prog. Polym. Sci. 20, 185–210. doi:10.1016/0079-6700(94)00030-6
Zhou, Y., Gao, J., Sun, Z., Qu, W., 2015. A fundamental study on compressive strength, static and dynamic elastic moduli of young concrete. Constr. Build. Mater. 98, 137–145. doi:10.1016/j.conbuildmat.2015.08.110

Appendix A Material and Equipment Specifications

A. Materials

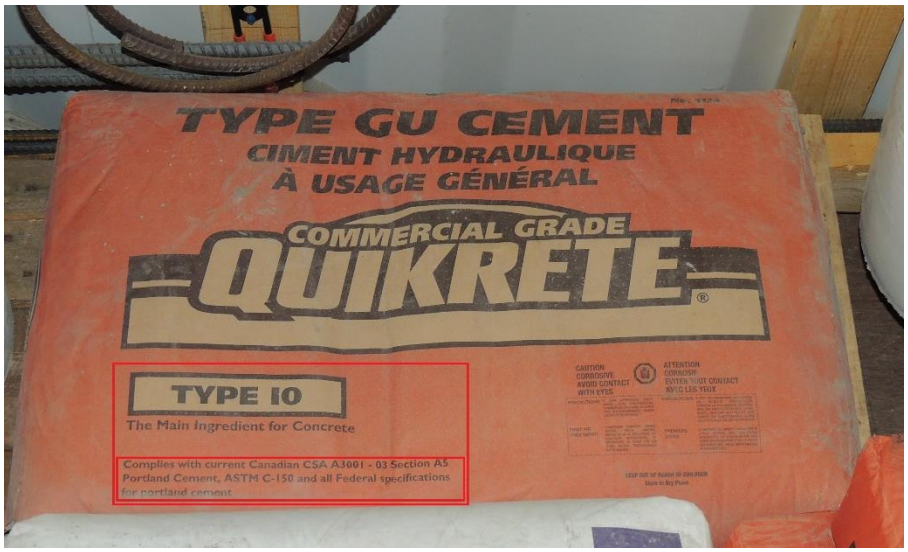

QUIKRETE® Portland Cement is used for making high strength repair mortars, concrete and for any other applications requiring Type I

Aluminum 6061-T6 Cylinder Properties

Material Property	Value
Density	2700 kg/m^3
Tensile Strength	310 MPa
Yield Strength	270 MPa
Modulus of Elasticity	68 GPa
Modulus of Rigidity	26 GPa
Poisson's Ratio	0.33

Element	Composition (%)
Silicon	0.4 – 0.8
Iron	0 – 0.7
Copper	0.15 – 0.4
Manganese	0 – 0.15
Magnesium	0.8 – 1.2
Chromium	0.04 – 0.35
Zinc	0 – 0.25
Titanium	0 – 0.15
Aluminum	95.85 – 98.55

RELATIVE DENSITY AND ABSORPTION OF COARSE AGGREGATE

CSA A23.2-12A

January 12, 2016
Project Number: 1530704/7000

LEHIGH MATERIALS, DIVISION OF LEHIGH HANSON MATERIALS LTD.
P.O. Box 1790
Sechelt, BC
V0N 3A0

ATTENTION: Mr. Nick Sawchuk

PROJECT: CSA Concrete Aggregate Testing, December 2015

Sample:	**Coarse Aggregate**
Source:	**Sechelt Pit**

Date sampled: December 2015
Date tested: January 12, 2016

Sampled by: Client
Tested by: DC

Trial No.	Mass (g)	Relative Density (Dry Basis)	Relative Density (SSD Basis)	Apparent Relative Density	Absorption (%)
1	3483.4	2.699	2.717	2.748	0.66
2	3808.0	2.690	2.709	2.743	0.72
AVERAGE		**2.695**	**2.713**	**2.746**	**0.69**

Reported by: I. Chung

Reviewed by: [redacted]
L. Hu, M.Sc.E., P.Eng.

GOLDER ASSOCIATES LTD., 300 - 3811 North Fraser Way, Burnaby, BC Canada V5J 5J2 Tel: 604-412-6899 Fax: 604-412-6816

RELATIVE DENSITY AND ABSORPTION OF FINE AGGREGATE

CSA A23.2-6A

January 12, 2016
Project Number: 1530704/7000

LEHIGH MATERIALS, DIVISION OF LEHIGH HANSON MATERIALS LTD.
P.O. Box 1790
Sechelt, BC
V0N 3A0

ATTENTION: Mr. Nick Sawchuk

PROJECT: CSA Concrete Aggregate Testing, December 2015

Sample:	**Fine Aggregate**
Source:	**Sechelt Pit**

Date sampled: December 2015
Date tested: January 7, 2016

Sampled by: Client
Tested by: DC

Trial No.	Mass (g)	Relative Density (Dry Basis)	Relative Density (SSD Basis)	Apparent Relative Density	Absorption (%)
1	500.5	2.649	2.669	2.705	0.79
2	500.8	2.652	2.672	2.708	0.78
AVERAGE		**2.651**	**2.671**	**2.707**	**0.79**

Reported by: I. Chung

Reviewed by: [redacted]
L. Hu, M.Sc.E., P.Eng.

GOLDER ASSOCIATES LTD., 300 - 3811 North Fraser Way, Burnaby, BC Canada V5J 5J2 Tel: 604-412-6899 Fax: 604-412-6816

Golder Associates

SIEVE ANALYSIS OF FINE AND COARSE AGGREGATE

CSA A23.2-2A

LEHIGH MATERIALS, DIVISION OF LEHIGH HANSON MATERIALS LTD.
P.O. Box 1790
Sechelt, BC
V0N 3A0

January 12, 2016
Project Number: 1530704/7000

ATTENTION: Mr. Nick Sawchuk

PROJECT: CSA Concrete Aggregate Testing, December 2015

Sample:	Fine Aggregate
Source:	Sechelt Pit

DATE SAMPLED: December 2015
DATE TESTED: January 6, 2016

SAMPLED BY: Client
TESTED BY: RZ

SIEVE ANALYSIS					MATERIAL SPECIFICATION: CSA FA1	
Sieve Size (mm)	% Retained	% Passing	Individual % Retained (Split values)			
			+ 5	- 5		
10	0.0	100.0	0.0		100	100
5	0.0	100.0	0.0		95	100
2.50	10.3	89.7		10.3	80	100
1.25	17.7	72.0		17.7	50	90
0.630	21.9	50.2		21.9	25	65
0.315	28.6	21.5		28.6	10	35
0.160	16.2	5.3		16.2	2	10
0.080	4.1	1.2		4.1	0	3
PAN	1.2	0		1.2		
Total	100.0		0.0	100.0		

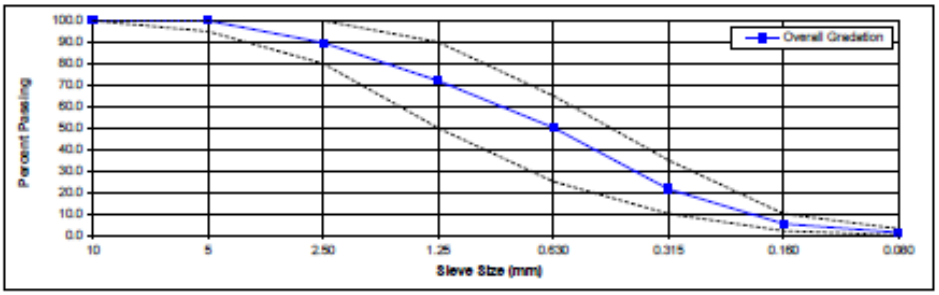

Remarks: Fineness Modulus: 2.61

Reported by: I. Chung

Reviewed by: [redacted]
L. Hu, M.Sc.E., P.Eng.

Notice: The test data given herein pertain to the sample provided, and may not be applicable to material from other production zones/periods. This report constitutes a testing service only. Interpretation of the data given here may be provided upon request.

Fiber Supplier

Propex Operating Company, LLC
PO Box 22788-
Chattanooga, Tennessee 37422
Phone 800-621-1273
Website www.fibermesh.com
E-mail fibermesh@propexglobal.com

Propex™ Fibermesh®

B. Resonant Frequency Apparatus

Model Number 003	STANDARD LOW NOISE COAXIAL CABLE	Revision B ECN #: 27379

Performance	ENGLISH	SI	
Number of Conductors	1	1	
Cable Style	Coaxial - Low Noise	Coaxial - Low Noise	
Environmental			
Temperature Range	-320 to +500 °F	-196 to +260 °C	
Pull Strength	75 lb	330 N	[1]
Electrical			
Impedance (±2 Ohm)	50 Ohm	50 Ohm	
Capacitance (±2 pF/ft) (conductor to conductor @ 70 °F (21 °C))	30 pF/ft	90 pF/m	
Insulation Resistance (@ 50 V @ 68 F)	>1 Tohm	>1 Tohm	
Noise Level (pk - pk)	≤3 mV	≤3 mV	
Physical			
Cable Jacket Diameter	.079 in	2.01 mm	[1]
Cable Jacket Material	TFE	TFE	
Cable Jacket Color	Blue	Blue	
Conductor Style	Solid	Solid	
Conductor Material	Nickel Plated Copper Covered Steel	Nickel Plated Copper Covered Steel	
Conductor Diameter (29 AWG)	.011 in	.279 mm	
Insulation Material Over Conductor(s)	Extruded TFE	Extruded TFE	
Shield Type Over Conductor(s)	Braid: 90% Minimum Coverage	Braid: 90% Minimum Coverage	
Shield Material Over Conductor(s)	Nickel Plated Wire	Nickel Plated Wire	
Low Noise Barrier Material (Over Conductor)	Liquid Graphite	Liquid Graphite	
Low Noise Barrier Material (Over Insulator)	Graphite Impregnated PTFE Tape	Graphite Impregnated PTFE Tape	
Bend Radius (minimum)	1 in	25.4 mm	
Weight	.1 oz/ft	9.5 gm/m	[1]

All specifications are at room temperature unless otherwise specified.
In the interest of constant product improvement, we reserve the right to change specifications without notice.
ICP® is a registered trademark of PCB group, Inc.

Optional Versions (Optional versions have identical specifications and accessories as listed for standard model except where noted below. More than one option maybe used.)

Notes
[1] Typical.

Entered: GLB	Engineer: WDC	Sales: BAM		Spec Number:
Date: 09/24/2007	Date: 09/24/2007	Date: 09/24/2007		**31605**

PCB PIEZOTRONICS ELECTRONICS DIVISION
3425 Walden Avenue
Depew, NY 14043
UNITED STATES
Phone: 800-828-8840
Fax: 716-684-0987
E-mail: info@pcb.com
Web site: www.pcb.com

Appendix B Compressive Strength

The following tables contain the properties of concrete cylinders tested for compressive strength including the maximum load at fracture and density of cylinders. Tests were performed on Ø100×200 concrete cured in a water-bath set at 23±1˚C for each batch. Batch 3 includes the compressive strength of air dry specimens at an ambient temperature 22±2˚C with a relative humidity of 50%.

Water-saturated Curing

Batch	Mixture ID	Cylinder #	Mass *(Kg)*	Density *(Kg/m^3)*	Load (KN)	Compressive Strength *(MPa)*
1	CC1	1	3.93	2385	274.59	33.6
		2	3.90	2369	270.50	33.1
		3	3.94	2391	268.87	32.9
	FRC - A	1	3.90	2367	278.68	34.1
		2	3.94	2391	268.05	32.8
		3	3.86	2343	259.06	31.7
	HFRC - A	1	3.85	2337	250.89	30.7
		2	3.76	2282	247.62	30.3
		3	3.80	2308	245.17	30.0
2	CC2	1	3.80	2306	238.93	29.7
		2	3.78	2296	236.79	29.4
		3	3.77	2288	246.42	30.6
	FRC - B	1	3.72	2258	256.41	31.9
		2	3.66	2224	266.38	33.1
		3	3.70	2246	276.22	34.3
3	FRC - A	1	3.58	2172	244.89	31.7
		2	3.54	2152	235.67	30.1
		3	3.55	2153	239.11	32.9
	FRC - B	1	3.69	2238	248.65	35.3
		2	3.70	2242	226.25	35.0
		3	3.67	2230	251.05	34.4

Ambient Curing

Batch	Mixture ID	Cylinder #	Mass *(Kg)*	Density *(Kg/m^3)*	Load (KN)	Compressive Strength *(MPa)*
3	FRC - A	1	3.56	2222	211.64	26.9
		2	3.55	2206	211.86	27.0
		3	3.51	2210	200.24	25.5
	FRC-B	1	3.58	2246	236.32	30.1
		2	3.552	2217	228.18	29.0
		3	3.556	2241	224.60	28.6

Appendix C Resonant Frequency Study Results

All frequency values are measured to the nearest 10 Hz according to ASTM C215. Dynamic Poisson's ratio values where calculated using the longitudinal resonant frequency. Crack widths were measured at 15 consecutive points along the crack. Cracks developed at cylinder edges due to contact with SCIJ were not included in the averages.

Cylinders

	Sample #	Mass (Kg)	Density (Kg/m³)	Ft (Hz)	Fl (Hz)	Et (GPa)	El (GPa)
Batch 1	CC1	3.93	2462	6030	9970	40.65	40.43
	CC2	3.9	2446	6000	9950	39.82	39.92
	CC3	3.94	2468	6020	9560	40.61	37.27
	LFRC - A1	3.9	2443	5930	9870	39.01	39.32
	LFRC - A2	3.94	2468	5920	9700	39.28	38.37
	LFRC - A3	3.86	2418	5930	9580	38.61	36.66
	HFRC - A1	3.85	2412	5590	9330	34.22	34.68
	HFRC - A2	3.76	2356	5580	9320	33.30	33.80
	HFRC - A3	3.8	2381	5560	9300	33.41	34.01

	Curing Age (Days)			1	14	28	56	1	14	28	56
	Sample #	Mass (Kg)	Density (Kg/m³)	Transverse Frequency (Hz)				Longitudinal Frequency (Hz)			
Batch 2	CC1	3.8	2306	4580	5900	6150	6190	7540	9760	9810	9880
	CC2	3.78	2296	4540	6000	6010	6050	7480	9690	9710	9790
	CC3	3.77	2288	4540	5870	6100	6180	7460	9580	9730	9800
	LFRC - B1	3.72	2258	4210	5710	5790	5870	6990	9270	9310	9400
	LFRC - B2	3.665	2224	4350	5680	5750	5840	7120	9120	9220	9350
	LFRC - B3	3.7	2246	4310	5720	5800	5890	7060	9320	9380	9420
				Transverse Modulus of Elasticity, Edt (GPa)				Longitudinal Modulus of Elasticity, Edl (GPa)			
				21.28	35.31	38.37	38.87	21.66	36.29	36.66	37.19
				20.74	36.22	36.34	36.82	21.18	35.55	35.70	36.29
				20.74	34.68	37.45	38.44	21.03	34.69	35.78	36.30
				17.60	32.38	33.29	34.22	18.22	32.05	32.33	32.95
				18.51	31.56	32.35	33.37	18.63	30.56	31.24	32.12
				18.35	32.32	33.23	34.26	18.49	32.22	32.64	32.92

	Condition		Curing	Sample #	Mass (Kg)	nsity (Kg/	Ft (Hz)	Fl (Hz)	Et (GPa)	El (GPa)
Batch 3	Original		Dry	LFRC - A1	3.56	2222	5580	9190	31.90	31.24
				LFRC - A2	3.55	2206	5500	9050	31.38	30.37
				LFRC - A3	3.51	2210	5310	8840	27.62	28.19
			Wet	LFRC - A4	3.58	2233	5730	9360	33.81	32.57
				LFRC - A5	3.55	2213	5810	9450	34.45	32.90
				LFRC - A6	3.55	2214	5740	9410	33.64	32.64
			Dry	LFRC - B1	3.58	2246	5520	9270	30.95	31.82
				LFRC - B2	3.55	2217	5480	9090	30.70	30.49
				LFRC - B3	3.56	2241	5550	9170	30.61	30.76
			Wet	LFRC - B4	3.69	2302	5950	9760	37.58	36.50
				LFRC - B5	3.69	2305	5910	9740	37.13	36.41
				LFRC - B6	3.67	2293	5970	9740	37.69	36.21
	Crack Width (mm)	0.4	Dry	LFRC - A1	3.56	2220	4030	9110	16.63	30.68
		0.33		LFRC - A2	3.55	2206	4270	8840	18.92	28.98
		0.4		LFRC - A3	3.51	2210	3470	8720	11.80	27.43
		0.45	Wet	LFRC - A4	3.57	2205	4150	9170	18.21	31.48
		0.25		LFRC - A5	3.54	2196	4050	9440	16.94	32.90
		0.45		LFRC - A6	3.53	2184	4480	9310	21.02	32.14
		0.2	Dry	LFRC - B1	3.57	2241	4500	9060	20.53	30.33
		0.25		LFRC - B2	3.55	2213	3820	8880	14.89	29.05
		0.2		LFRC - B3	3.53	2227	4170	9050	17.17	29.78
		0.4	Wet	LFRC - B4	3.68	2297	4110	9500	17.89	34.51
		0.5		LFRC - B5	3.69	2302	4070	9560	17.58	35.02
		0.4		LFRC - B6	3.67	2290	3390	9400	12.14	33.69

Prisms

	Sample #	Mass (Kg)	Density (Kg/m³)	Ft (Hz)	Fl (Hz)	Fto (Hz)	Et (GPa)	El (GPa)	G (Gpa)	v
Batch 1	CC1	8.94	2474	2770	6150	3540	42.81	47.34	18.55	0.28
	CC2	8.88	2410	2840	6180	3570	42.12	46.55	18.38	0.27
	CC3	8.5	2353	2860	6200	3610	43.39	45.74	18.35	0.25
	LFRC - A1	8.4	2325	2750	6040	3540	39.65	42.90	17.43	0.23
	LFRC - A2	8.98	2390	2840	6120	3510	40.19	45.28	17.62	0.28
	LFRC - A3	9.38	2404	2960	6140	3560	40.72	45.84	18.23	0.26
	HFRC - A1	9.42	2483	2740	5960	3420	38.13	44.62	17.38	0.28
	HFRC - A2	9.24	2459	2730	6010	3380	38.21	44.93	16.81	0.34
	HFRC - A3	8.64	2354	2640	6030	3280	35.83	43.29	15.15	0.43

	Curing Age (Days)			1	7	14	28	56	1	7	14	28	56	1	7	14	28	56
	Sample #	Mass (Kg)	Density (Kg/m³)	Transverse Frequency (Hz)					Longitudinal Frequency (Hz)					Torsional Freqeuncy (Hz)				
Batch 2	CC1	28.31	2291	1200	1370	1570	1630	1790	2670	3020	3450	3560	3790	1550	1770	2000	2060	2100
	CC2	28.1	2289	1190	1380	1590	1640	1730	2600	3200	3410	3610	3700	1510	1740	2000	2070	2110
	CC3	28.54	2341	1240	1430	1590	1680	1740	2710	3050	3500	3580	3760	1600	1810	2050	2080	2140
	LFRC - B1	27.81	2236	1150	1340	1530	1590	1670	2510	2900	3310	3440	3620	1480	1690	1920	2000	2050
	LFRC - B2	27.55	2230	1100	1290	1520	1580	1650	2480	2740	3340	3400	3560	1420	1640	1930	1980	2040
	LFRC - B3	27.86	2211	1190	1360	1560	1630	1720	2530	2940	3350	3480	3660	1520	1730	1960	2020	2080
				Transverse Modulus of Elasticity, Edt (GPa)					Longitudinal Modulus of Elasticity, Edl (GPa)					Torsional Modulus of Elasticity, G (GPa)				
				16.60	21.63	28.41	30.62	36.93	18.59	23.78	31.04	33.05	37.45	7.41	9.66	12.34	13.09	13.60
				16.52	22.22	29.50	31.38	34.92	17.61	26.68	30.29	33.95	35.67	7.03	9.33	12.33	13.21	13.72
				18.59	24.72	30.56	34.12	36.60	19.56	24.78	32.63	34.14	37.66	8.07	10.32	13.24	13.63	14.43
				14.68	19.93	25.99	28.06	30.96	16.03	21.40	27.88	30.11	33.35	6.59	8.60	11.10	12.04	12.65
				13.57	18.66	25.91	28.00	30.53	15.61	19.05	28.31	29.33	32.16	6.05	8.07	11.18	11.77	12.49
				15.15	20.74	27.29	29.80	33.18	16.24	21.93	28.48	30.73	33.99	6.94	8.98	11.53	12.25	12.99
									Poisson ratio, v									
									0.25	0.23	0.26	0.26	0.38					
									0.25	0.43	0.23	0.29	0.30					
									0.21	0.20	0.23	0.25	0.30					
									0.22	0.24	0.26	0.25	0.32					
									0.29	0.18	0.27	0.25	0.29					
									0.17	0.22	0.23	0.25	0.31					

Transverse and Longitudinal Dynamic Moduli Relationship - Statistics

Component	***Prism***		***Cylinder***	
Modulus of Elasticity	Transverse (E_{dt})	Longitudinal (E_{dl})	Transverse (E_{dt})	Longitudinal (E_{dl})
Mean	37.005	40.861	35.272	34.531
Standard Error	1.150	1.459	0.681	0.614
Median	38.127	43.290	34.265	34.013
St. Dev.	4.454	5.651	3.536	3.192
Variance	19.841	31.931	12.505	10.191
Kurtosis	-1.476	-1.742	-0.872	-0.760
Skewness	-0.073	-0.437	-0.174	0.081
Range	12.767	14.915	13.023	12.241
Minimum	30.625	32.424	27.623	28.187
Maximum	43.391	47.339	40.646	40.428
Sum	555.073	612.911	952.352	932.333
Count	15	15	27	27
95% Confidence	2.467	3.129	1.399	1.263
RSD	0.031	0.036	0.019	0.018

Appendix D Repeatability Study

Force Variation

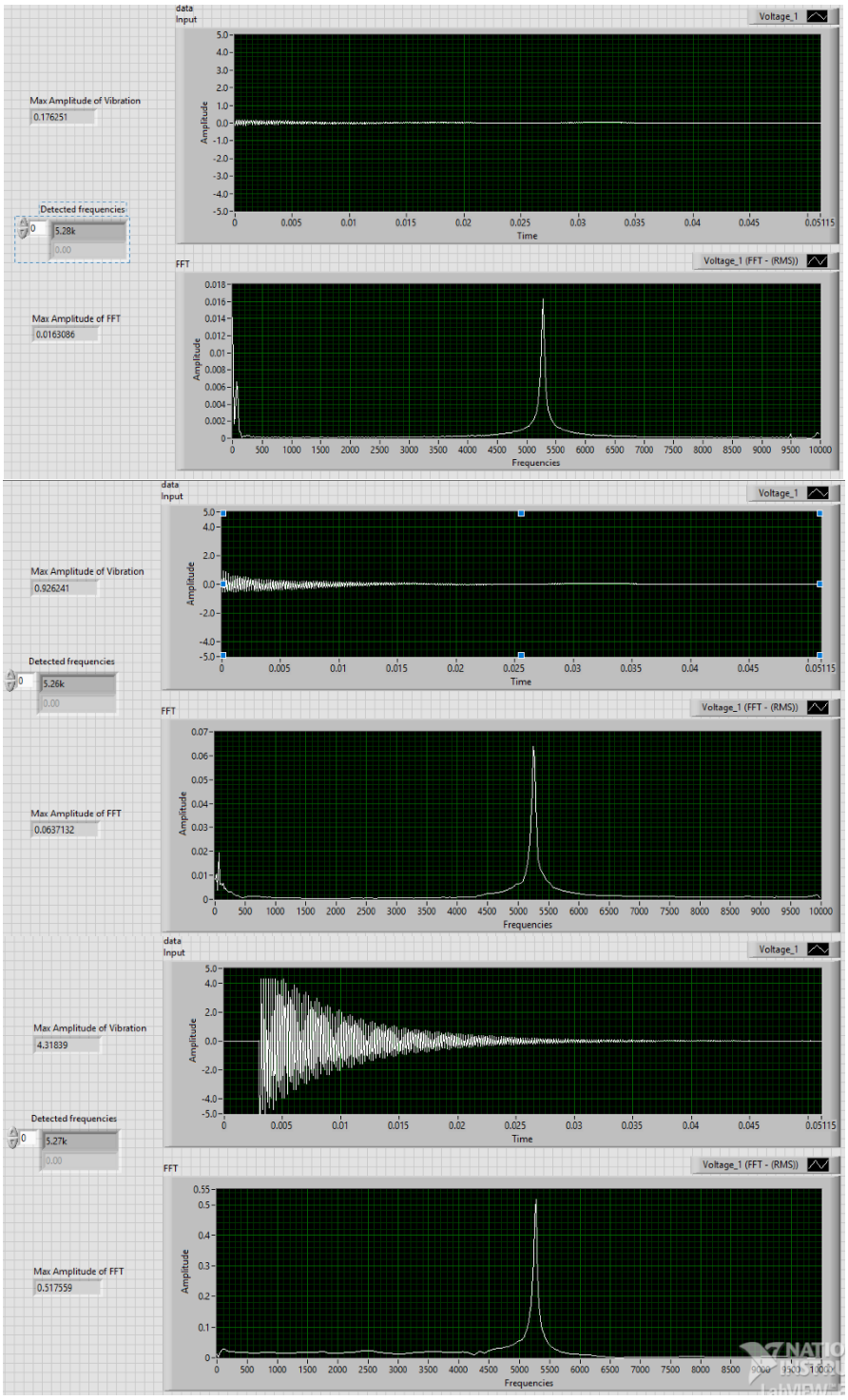

Force Variation – Statistics

Component	Magnitude	Frequency (Hz)
Mean	0.186	5264.757
St. Error	0.074	3.431
Median	0.070	5273.438
St. Dev.	0.222	10.294
Variance	0.049	105.964
Kurtosis	0.060	-2.571
Skewness	1.299	-0.271
Range	0.571	19.531
Minimum	0.016	5253.906
Maximum	0.588	5273.438
Sum	1.676	47382.813
Count	9	9
95% Confidence	0.170	7.913

Accelerometer Connection Type – Statistics

Component	Magnitude	Frequency (Hz)
Mean	0.126	5277.344
Standard Error	0.040	35.156
Median	0.090	5312.500
St. Dev.	0.090	78.612
Variance	0.008	6179.810
Kurtosis	4.445	5
Skewness	2.082	-2.236
Range	0.219	175.781
Minimum	0.067	5136.719
Maximum	0.285	5312.500
Sum	0.631	26386.719
Count	4	4
95% Confidence	0.112	97.609